ABSTRACT

Title of thesis: AN INVESTIGATION OF CONCENTRATED AND DISTRIBUTED STRAIN INDUCING CONSTRAINTS FOR TRAINING SHAPE MEMORY ALLOYS

Pauline M. Parent, Master's of Science, 2012

Thesis directed by: Professor Alison Flatau, PhD.
Department of Aerospace Engineering

This research explores concentrated and distributed strain inducing constraints for Two Way Shape Memory (TWSM) training of cantilevered NiTiNOL shape memory alloy strips via the constrained thermal cycling of deformed Martensite training method. The goal is to evaluate the performance of a tip-moment trained sample actuator, which is characterized by constant strain along the sample length, and compare it with the performance of tip-force trained sample actuators, which have root concentrated strain. The shape and net tip displacement of trained specimens is expected to vary with training constraint type and training load magnitude, rendering it uncertain which sample will have greater work potential. A training structure and systems for introducing thermal and mechanical loads were developed to provide the explored training constraints and induce TWSM. The work performance was evaluated by measuring vertical displacement of tip weights. The experimental results indicate that samples subject to strain distributing constraints during training have higher work potential than samples subject to concentrated strain inducing constraints.

AN INVESTIGATION OF CONCENTRATED AND DISTRIBUTED STRAIN INDUCING CONSTRAINTS FOR TRAINING SHAPE MEMORY ALLOYS

by

Pauline Marie Parent

Thesis submitted to the Faculty of the Graduate School of the
University of Maryland, College Park in partial fulfillment
of the requirements for the degree of
Master's of Science
2012

Advisory Committee:
Professor Alison Flatau, Chair/Advisor
Professor Norman Wereley
Professor Sung Lee

Dedication

Pour ma famille qui m'inspire à toujours continuer et pour qui,

je n'abandonnerai jamais.

Acknowledgments

First and foremost, I'd like to thank my advisor, Professor Alison Flatau, for her continued support and encouragement throughout my journey towards becoming an engineer. She has always taken the time to help me overcome any challenge that graduate school or my research have presented me with, and has continually encouraged me to push further and reach achievements I did not think were possible. I am extremely grateful to her for having allowed me the opportunity to do such challenging and interesting research.

I would also like to thank my mentor, Dan Clingman, without whom this research project and thesis would not be possible, for his continued guidance throughout the course of my research. He has sacrificed his invaluable time to be present via teleconference at weekly meetings and has always made himself available to answer questions. I would also like to thank Professor Norman Werely and Professor Sung Lee for agreeing to serve on my thesis committee and for taking the time to review this thesis. Their efforts in helping me graduate with my master's degree are very much appreciated.

My colleagues in the aerospace engineering undergraduate and graduate programs and my friends have made my time at the University of Maryland an experience of a lifetime. I would like to thank Michael Godana for his help with setting up and running experiments and for being such a wonderful assistant. His eagerness to learn and achieve great results made him a pleasure to work with. I owe many thanks to Eric Avadikian and Panagiotis Koliais for their assistance in building and

modifying the training structure used for this research, and Mor Gilad and Siddarth Kolluru for sharing their technical expertise and graduate experience with me, supporting me, and helping me stay motivated. I'd also like to thank Benjamin King Sutton Woods, Robert Vocke, Ganesh Raghunath, William Staruk, Lina Castano, Zohaib Hasnain, Oscar Alvarado, Aaron Sassoon, Levi DeVries, and Ananth Sridharan for letting me bounce ideas off of them and for being so willing to teach me new things. Special thanks must go to Chen Friedman and Cyrus Abdohalli for making my first experience with LaTex software a pleasant one.

I would also like to express my gratitudes towards Chris Sutton, for his friendship and support throughout the completion of my thesis, and for helping me write Matlab code well beyond my experience level. He has been more kind and patient with me than I could ever ask for and has helped me keep a level head during the stressful times. I am also extremely grateful towards my best friend, Michael Papavizas, who supported me and helped me over the last three years through both the good times and the bad times.

I am very grateful for my incredible friends who have stuck by my side, even though I wasn't always able to be by theirs: Nichelle Nguyen, Rachel Champlain, Anna Finch, Lauren Holder, Scott Sacks, Aaron Smith, and my many other wonderful friends.

I would also like to acknowledge support from some of the staff members in the lab. Dr. Suok-Min Na's technical help is highly appreciated, as is that from Dr. Jin-Hyeong Yoo.

Most of all, I owe my deepest thanks to my family, without whom I would not have had the courage to embark on a new academic and career path, nor to complete my master's degree. Their undying love and continuous support have constantly motivated me to do the best that I can and to never give up. I owe my success and all that I have accomplished in my life to them.

I would like to extend my gratitude towards anyone else that has contributed ideas or allowed me to discuss my research with them. I am grateful for the colleagues that guided me through the unfamiliar breed of homework assignments that engineering classes introduced me to. They not only taught me how to approach technical assignments, but also taught me how to "think like an engineer".

Lastly, I would like to acknowledge financial support from the Nation Science Foundation (NSF) and the Women In Engineering department at the University of Maryland, College Park.

Table of Contents

List of Tables

List of Figures

Nomenclature

SMA	Shape Memory Alloy
NiTiNOL	Nickel Titanium Naval Ordinance Laboratory
TWSME	Two-Way Shape Memory Effect
TWSM	Two-Way Shape Memory
SME	Shape Memory Effect
OWSME	One-Way Shape Memory Effect
A_s	Austenite Start Transformation Temperature
A_f	Austenite Finish Transformation Temperature
M_s	Martensite Start Transformation Temperature
M_f	Martensite Finish Transformation Temperature
σ_s	Critical Stress
SIM	Stress-Induced Martensite
TIM	Thermal-Induced Martensite
σ_{Ds}	De-twinning Start Stress
σ_{Df}	De-twinning Finish Stress
CAD	Computer-Aided Design
NI	National Instruments
DAQ	Data-Acquisition Device

Chapter 1

Background and Motivation

1.1 Introduction

As the technology and manufacturing of smart materials becomes more advanced, there is an increased interest within the aerospace community in the development of morphing and adaptive structures using Shape Memory Alloys (SMAs) [1, 5]. The family of Nickel based alloys known as NiTiNOL (Nickel Titanium Naval Ordinance Laboratory) is a smart material that has numerous aerospace applications. It's additional properties of corrosion resistance and high fatigue strength make NiTiNOL a suitable choice for many applications across the aerospace industry and other fields outside of engineering [3]. NiTiNOL is also biocompatible and has been used extensively in the medical field [3]. These unique properties combined with the Shape Memory Effect (SME) greatly expand the possibilities for its use beyond aerospace and biocompatible dependent applications. SMAs have also made it into the hands of everyday consumers through the form of eye-glasses, in which the pseudo-elastic properties of NiTiNOL are put to use.

The property of particular interest to the aerospace industry is that SMAs exhibit the Two-Way Shape Memory Effect (TWSME). This effect is the ability to move between two distinct shapes or displacement profiles in response to an easily varied input such as temperature. This ability, also referred to as strain recovery, makes

SMA alloys a candidate for use in vibration isolation and noise reduction [1, 6]. The growing use of smart materials in the development of morphing structures has led scientists and engineers to take a closer look at the ability of SMAs to do work through Two-Way Shape Memory (TWSM) actuation. There are currently a number of commercial applications in engineering fields employing NiTiNOL wire. Little research, however, has been found where experiments are conducted using bars, beams, or high-aspect ratio plates of SMA materials. The use of flat beams in general is relatively scarce, yet plate-like structures and beams are known to be significantly more robust [7] and are capable of a larger TWSM actuation stroke [8] than wires. For these reasons, high-aspect-ratio plates, rectangular bars, or beams of NiTiNOL have been suggested for use in morphing airfoils. To this end, this thesis presents a study of two approaches to training cantilevered NiTiNOL samples.

Previous work has been done in training SMA wires to exhibit the TWSME. Various loading methods for TWSM cold-shape setting are available [9], but the most common entails the use of a tip-force on a cantilevered specimen to induce bending deformation. The research presented in this thesis focuses on the use of a constant tip-moment training constraint that is intended to increase the volumetric efficiency and energy conversion within SMAs relative to what can be achieved with a tip-force training constraint. Use of the phrase "tip moment" throughout this thesis is intended to convey a load that produces a moment throughout a cantilevered sample, inducing distributed strain throughout the length of a cantilevered specimen. Use of the phrase "tip force" is intended to convey a load that produces concentrated strain at the root of a cantilevered specimen that reduces towards the tip of the

specimen. The tip-moment constraint approach should activate stress and strain throughout the length of the sample during activation of the TWSME. A sample trained to induce the TWSME in a more efficient manner should increase a sample's ability to produce work. The experiments devised provide a method of comparing the performance of a tip-moment trained sample against that of a tip-force trained SMA specimen when acting as an actuator.

1.2 Background on Shape Memory Alloys

1.2.1 History and Applications of Shape Memory Alloys

Research experimenting with the SME dates back to as early as the 1940s when scientists were first exploring the properties of metallic compounds capable of exhibiting reversible martensitic transformation, e.g. between a twinned and de-twinned state [3]. Chang and Read first discovered the remarkable property that allows a material to remember its Austenitic shape in the Au-Cd alloy [10]. The major breakthrough, however, introducing SMAs to the field of engineering, was when NiTiNOL surfaced as a shape memory alloy [8]. Buehler *et al.* [11] discovered the shape memory effect in the Ni-Ti alloy in 1963 and it quickly became the most popular commercial SMA due to it's properties of combining SME and pseudo-elasticity with high recoverable strain, excellent damping ability, and very good biocompatibility [2, 8, 11]. Since then, many other alloys such as In-Ti, Cu-Zn, and Cu-Al-Ni and other third element infused Cu-Al alloys, have been identified that exhibit the

SME. NiTiNOL remains, however, the most commonly used SMA due to exhibiting higher ultimate tensile strengths and easier processibility [8, 10].

NiTiNOL was first used as a commercial product in the aerospace industry as the material chosen for pipe couplings in the U.S. Navy F-14 fighter aircraft [3]. Since then, its commercial applications have turned to numerous other engineering fields [12] and industries, such as the automotive industry [13]. SMAs have been widely used for applications in the biomedical and medical fields in making devices such as state of the art surgical tools [2]. NiTiNOL's wide-spread popularity is fueled additionally by the fact that some of its unique properties can be fine tuned to create a customized actuator. One can control the shape of deformation, target strain activated and recovered within the material during the SME, and even manipulate phase transformation temperatures by varying alloy composition and material stress [8, 10]. In the most recent two decades, experimentation with alloy composition has led to SMA use in every day household applications such as air conditioning vents, eyeglasses, cell phone antennas, and even women's brassieres under-wiring [3, 6].

It is important to note that the grand majority of these common commercial uses for SMAs employ their ability to exhibit pseudo-elasticity with the super-elastic effect. SMAs can generally be used for three categories of applications. These include:

1. Pseudo-elasticity, where the material acts like a very strong spring;

2. One-Way Shape Memory Effect (OWSME) coupled with shape or strain

recovery, where the material can be deformed in the cold state and then will return to the parent shape upon heating;

3. Two-Way Shape Memory Effect (TWSME) coupled with

   - shape or strain recovery, which entails inducing a stress within the material as it attempts to recover strain under physical constraints preventing displacement; and
   - work production, requiring the material to do work in order to recover strain.

Commercial applications falling under the first and second category are currently the more successful and more prevalent applications in the aerospace industry [1]. The pipe couplings used on the F-14 aircraft mentioned earlier, otherwise known as Cryofit [6], are an example of the second category, i.e. of a OWSM-induced shape recovery application of NiTiNOL. The third category, TWSM coupled with strain recovery and/or work-production, has always been of interest to aerospace engineers and is gaining increasing attention as a result of advances in the use of TWSM for bending actuation.

Engineers and scientists have utilized the TWSM phenomenon for various air and space operations, such as release mechanisms in spacecraft and actuators in morphing and adaptive structures [1]. NASA explored the use of SMA cable actuators lined around F-15 jet engine inlet cowlings [1] for noise mitigation and performance optimization. The concept called for different levels of actuation of the SMA cables to rotate the inlet cowling as needed to maximize aircraft performance in different

flight regimes. Similar experiments were performed on the aft cowling of the fan portion of a high-bypass ratio engine so that the changes in exhaust temperatures would actuate the SMA cables, causing the exhaust cowling diameter to change in such a way that optimized engine performance. More recently, the Boeing company has experimented with embedded strips of NiTiNOL in the engine cowling composite skin of their aircraft [1]. They explored the concept of variable geometry chevrons lining the circumference of the engine bypass exhaust cowlings (see figure 1.1). The chevrons are typically used statically as a means of mixing the exhaust flow to assist in noise reduction [1]. The embedded SMA strips were trained to bend inwards and stiffen during high-temperature exhaust operations on the ground, and soften and straighten during air operations to maximize noise reduction for both ground and air operations. Preliminary results were promising and research development utilizing this concept is still underway [1].

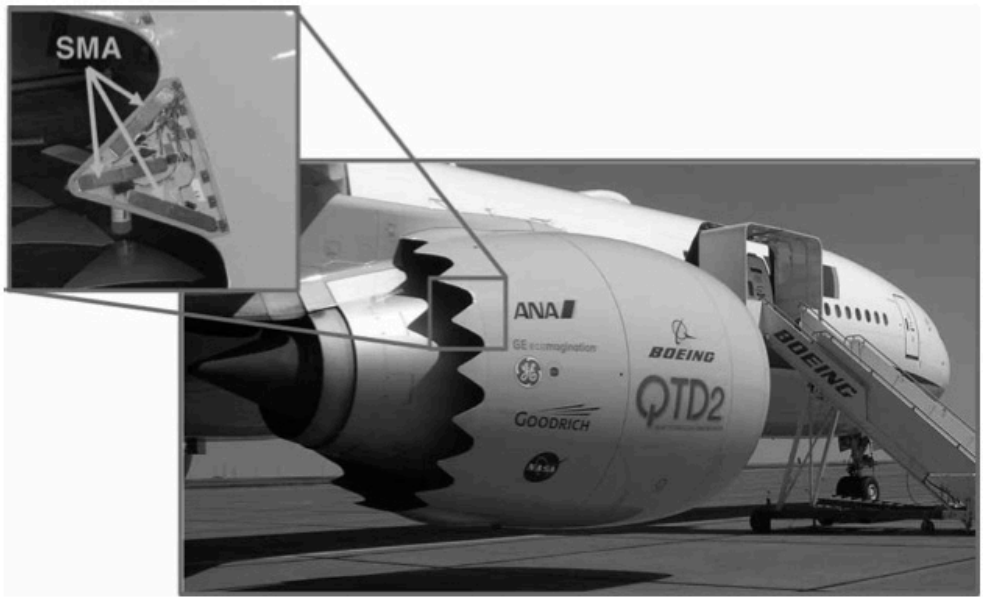

Figure 1.1: Flow mixing chevrons on Boeing aircraft engine exhaust cowling [1]. SMA bars are either activated or allowed to passively bend chevrons as exhaust temperatures vary for noise mitigation.

1.2.2 SMA Properties and the Shape Memory Effect

Phases and Transformation Temperatures

NiTiNOL is a SMA that typically consists of 50% Nickel and 50% Titanium. As described briefly in section 1.2.1, this alloy is capable of exhibiting both shape memory and pseudo-elasticity. These properties are the result of NiTiNOL being an intermetallic compound in which the atoms can be arranged in specific lattice structure configurations induced by different thermal and mechanical conditions. A change in condition causes a reorientation in the lattice structure, leading to phase transformation [2, 3]. This phase change is of the diffusionless type, in that

the atoms do not have to move long distances to rearrange into a different lattice structure and the original chemical nature of the compound remains intact [9, 14].

The two primary phases exhibited during the SME are the Austenite and Martensite phase. Austenite is the material's "parent phase" and occurs at higher temperatures. The Martensite phase occurs at lower temperatures, and is characterized by a lower Modulus of Elasticity. The molecules in the Martensite phase are arranged in a monoclinic fashion as depicted in the middle and right sketches of figure 1.2. The Austenitic atomic structure has a higher Modulus of Elasticity [15] and has a cubic lattice structure, shown in the left sketch in figure 1.2. An SMA in Martensite phase is roughly four times softer than when it is Austenitic. A sample can be easily deformed during this phase and can endure up to 8% recoverable strain [9] as it moves between its twinned and de-twinned shapes. Mizar and Hartl *et al.* [1, 9] describe the atomic lattice structure of the Martensite phase as one composed of what are known as lattice variants. These variants represent the specific arrangement that every Martensitic unit cell of atoms has in the lattice structure with respect to its corresponding unit cell of atoms within the cubic lattice structure characterizing the Austenite phase [3, 9].

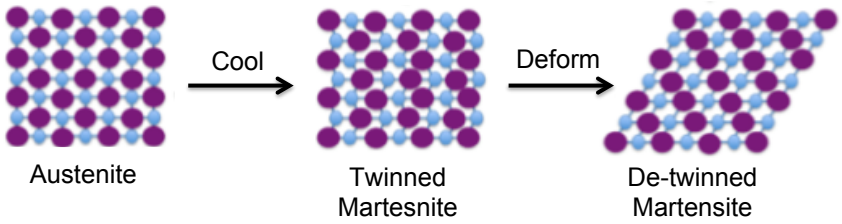

Figure 1.2: NiTiNOL phase lattice structure [2]. Hot Nitinol is cubic and Austenite. Cooled Austenite becomes Twinned Martensite, retaining original Austenite shape. Deformation of twinned Martensite results in de-twinned Martensite and must be heated to return to original cubic Austenite shape.

A sample undergoing an Austenite to Martensite transformation is said to be demonstrating a forward transformation, which occurs through two processes known as Bain Strain and Lattice Invariant Shear [2, 9]. Bain Strain refers to the movement of atoms within the lattice structure of the Austenitic material required in order to cause the solid-state phase transformation to Martensite. The second part of the transformation process, the Lattice Invariant Shear, refers to the self-accomodation that the atoms exhibit when transforming into the twinned Martensite phase [1]. This is the process by which SMAs are able to maintain the same volume in all phases. Hartl *et al.* [1] describe this self-accomodation as the process that occurs when the atoms orient themselves in such a manner that strain energy required for the phase change is minimized.

Martensitic atoms are able to accommodate the former Austenitic structure using one of two different methods, slip and twinning. Slip is a permanent structure

change accommodation process. Twinning is the dominant process. It is the reversible structural change transformation mechanism that allows for the material to exhibit the SME. With twinning, a structure under stress will move its lattice variant boundaries to accommodate the applied stress [9]. In other words, twinning allows for the inner monoclinic structure to adapt to the surrounding Austenite shell, so the overall shape is still the parent Austenite shape until deformed. When in the Martensite phase, a SMA is much more malleable and can undergo a certain amount of recoverable strain. This causes de-twinning of the structural lattice, which leads to a macroscopic shape change. Figure 1.2 provides a visual description of the lattice structure in the Austenite phase and that of the Martensite phase in both the twinned and de-twinned state.

In some Ni-rich alloys as well other compounds enriched with Fe, Al, or Pd, a phase known as the R-phase can be observed between the Austenite and Martensite phases. This intermediate phase is characterized by a rhombohedral lattice structure and is said to be caused by stress fields associated with Ti_3Ni_4 precipitates introduced during the cold-working and heat-treating of the enriched alloy [3]. This phase can be triggered additionally through manipulation of heat treatment temperatures and thermo-mechanical cycling [2]. The research described in this thesis, however, employs the use of roughly equiatomic NiTiNOL, in which the R-phase is not observed.

Each of the two primary phases exhibited by NiTiNOL has a start transformation temperature at which a SMA specimen commences transformation into that phase, and a finish temperature at which the sample has completely undergone transfor-

mation. [15]. At A_s, the sample begins its transformation from Martensite to the Austenite, rigid phase, and the atomic structure is fully Austenitic at A_f. Likewise, at M_s, the Austenite to Martensite transformation commences and is complete at M_f, at which point the material is fully Martensite. Figure 1.3 demonstrates the affect of changing temperature through the various transformation temperatures and their affect on the total Martensite volume fraction of a SMA specimen.

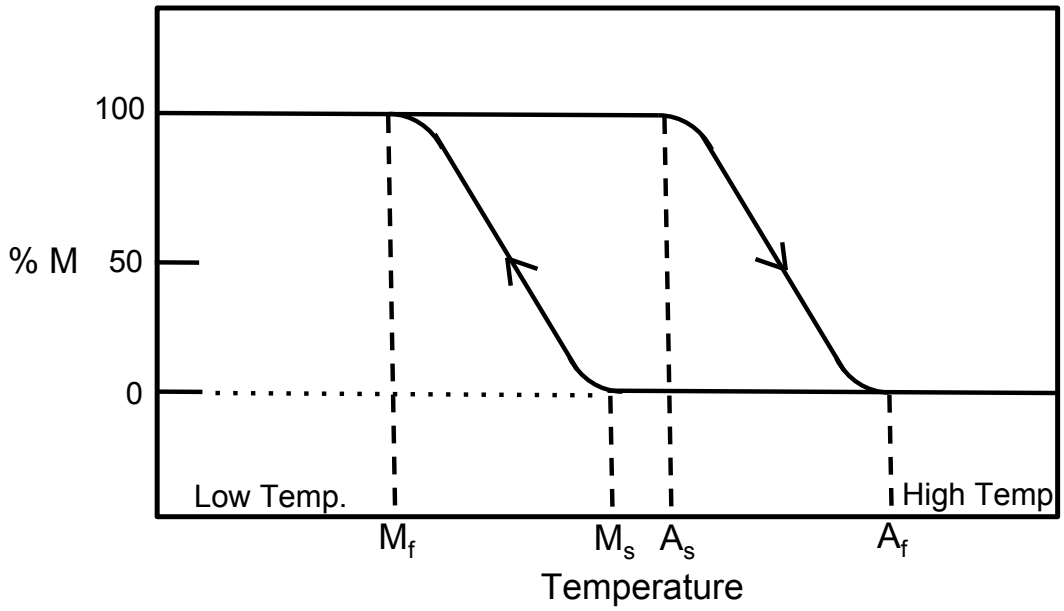

Figure 1.3: Temperature vs. Martensite Volume Fraction [2]: Martensite volume fraction increases as SMA cools, transforming into 100% Martensite. Martensite volume fraction decreases as temperature increases and specimen becomes more Austenitic.

An Austenitic (rigid) sample that is cooled below M_s will begin to transform to the Martensite twinned monoclinic structural state and be considered fully Martensitic once the M_f temperature is reached. As a load is applied, de-twinning occurs.

Figure 1.4 demonstrates the process by which Thermal-Induced Martensite (TIM) is formed as temperature is cycled. The stress level marked as σ_{Ds} marks the point at which de-twinning commences when a stress-inducing load is applied. De-twinning of TIM is fully complete at σ_{Df}. It is important to note that the transformation temperatures rise with an increase in stress but σ_{Ds} and σ_{Df} do not. Above σ_{Df}, a specimen will automatically transform into deformed, de-twinned Martensite upon cooling from Austenite. Transformation temperatures also vary widely across different alloy compositions and can be altered by heat treatment as well as TWSM training. This unique property has been a significant factor in the adoption of SMA applications across different fields.

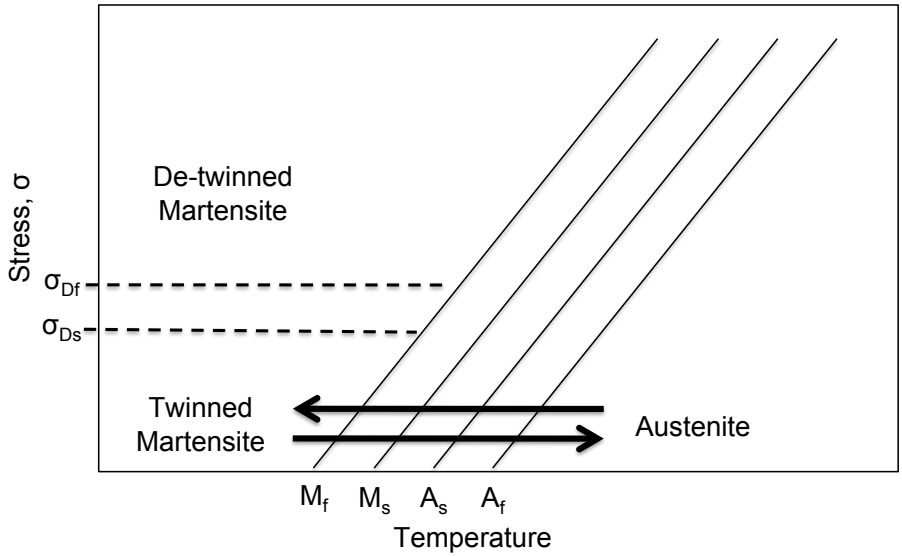

Figure 1.4: Temperature vs. Stress: Formation of TIM [3, 4]. Arrows represent phase change path followed with thermal cycling only. An increase in temperature results in reverse transformation from twinned Martensite to Austenite and a decrease in temperature results in forward transformation from Austenite to twinned Martensite. TIM is independent of load change.

Pseudo-elasticity and the Shape Memory Effect

The super-elastic effect occurs at temperatures above A_f, where a value of stress exceeding what is known as the critical stress (σ_s) value induces a phenomenon called Stress-Induced Martensite (SIM) [2, 10, 15]. SIM is independent of temperature, unlike Thermal-Induced Martensite (TIM), and is responsible for the pseudo-elastic property that made NiTiNOL popular in a wide spread of commercial applications early on. When a stress is applied above σ_s at temperatures higher than A_f, a macroscopic shape change can result. Once the stress has fallen below σ_s, however,

the material reverts back to the cubic lattice structure associated with the Austenite phase and becomes fully Austenitic again, thus leading to a very interesting and useful elastic effect. There exists, however, a limit in the temperature over which the pseudo-elastic effect is no longer present and permanent deformation can occur. This temperature is known as M_d, representing the temperature at which the stress required to form SIM exceeds the stress required to move variants within the lattice structure [2, 15]. Due to the unique thermo-mechanical properties of SMAs, SIM can also occur when a specimen is at a temperature just above the M_s temperature. An increase in stress affects the electrical resistance within the alloy, leading to a drop in temperature below M_s [10]. As previously observed in figure 1.4, transformation temperatures also rise with an increase in stress. Similarly, as the stress is removed, the resistance changes again such that the temperature of the material rises above M_s, which also decreases slightly and the material is fully Austenitic again [10]. This phenomenon and the pseudo-elasticity SIM loading path are illustrated in Figure 1.5

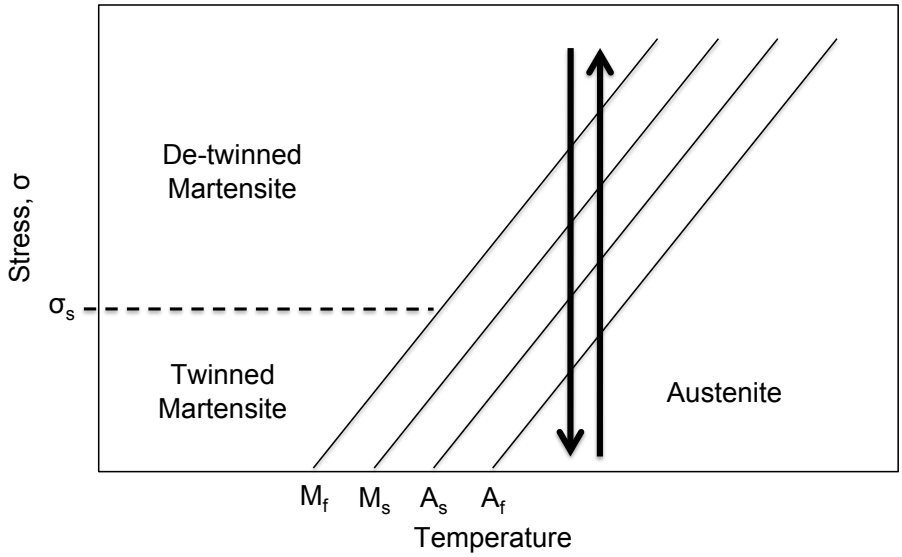

Figure 1.5: Temperature vs. Stress: Formation of SIM [3, 4]. Arrows represent phase change path followed with load cycling only. A decrease in stress results in reverse transformation from de-twinned Martensite to Austenite and an increase in stress results in forward transformation from Austenite to de-twinned Martensite. SIM is independent of temperature change.

The OWSME and TWSME are exhibited at temperatures between M_f and A_f. As a specimen cools from Austenite to Martensite, it becomes softer and transforms into the twinned monoclinic structure described in the *Phases and Transformation Temperatures* part of this section. A sample in Austenite will remain in the Austenite shape as it cools to twinned Martensite. Upon physical deformation, the material is now de-twinned and the deformation remains. Once the material is heated again to a temperature beyond A_f, it will recover its original trained hot shape, provided it was not strained beyond its maximum recoverable strain limit. This process is what is known as the OWSME. A NiTiNOL sample in Martensite has a recover-

able strain limit of roughly 8% and can be strained at any percentage up to its limit and still recover its shape upon transformation to Austenite. This process of forward (Austenite to Martensite) and reverse (Martensite to Austenite) phase transformation is visually described by the illustration in figure 1.6.

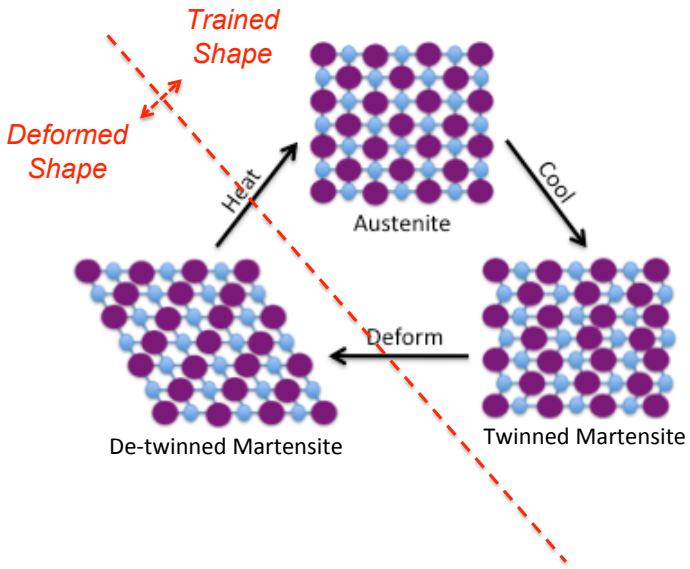

Figure 1.6: The OWSME [2]. Austenitic SMA is cubic in trained parent shape and is achieved at elevated temperatures. Cooled SMA transforms to monoclinic twinned Martensite and retains parent shape until deformed into de-twinned Martensite. De-twinned Martensite must be heated to transform to Austenite to recover trained parent shape.

The OWSME itself is a remarkable discovery and the phenomenon has been studied, characterized, and modeled extensively by scientists and engineers [10, 16–18]. The TWSME is an even more complex phenomenon. In addition to remembering a hot parent shape in the Austenite phase, SMAs can be trained in such a way that they remember a cold shape in the Martensite phase. This means that Austenitic

Nitinol transforms into de-twinned, deformed Martensitic Nitinol when cooled and returns to the parent shape upon heating. This is shown in figure 1.7.

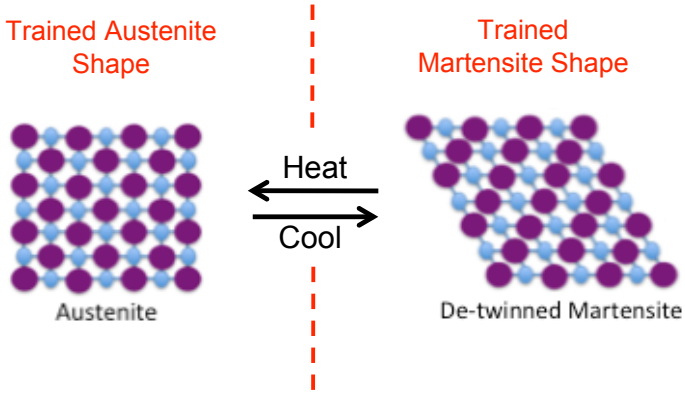

Figure 1.7: The TWSME [2]. Austenitic SMA is cubic in trained parent shape (see figure 1.6). Cooled SMA transforms directly to deformed, de-twinned Martensite. De-twinned Martensite must be heated to transform to Austenite to recover strain and trained parent shape.

The TWSME is induced through a process known as training [9], that exposes the SMA to thermo-mechanical fatigue. This thermo-mechanical fatigue leads to a gradual change in the microstructure of the material, resulting in the stabilization of a hysteretic response and allowing the material to remember both a hot and cold shape. As the lattice variant boundaries reorient themselves to accommodate an applied load, they create an elastic stress field in the direction of the strain applied [19]. Each additional cycle further "plows" [19] the path for variants to stabilize in the direction of that particular stress field. This stabilized stress field then acts as a guide for the displacement of variants with transformation from

Austenite to Martensite. With the stabilization of the stress field, the stress level required for de-twinning decreases, resulting in earlier onset of visible deformation and shape change [19]. This redirection of the stress field is the hysteretic response that is responsible for the TWSME. With the creation of a direction-oriented stress field however, there is an increase in the resistance in reverse transformation and return to the cubic structure upon heating. This phenomenon is known as creep and results in the sample's original Austenite shape structure being different from that upon the completion of TWSM training. Stated alternately, both the Martensite and Austenite shape displace a small and roughly equal amount further in the direction of the deformed lattice structure orientation with each additional training thermal cycle.

The strain recovery limit in TWSM is lower than for the OWSME and transformation strains are lower in forward transformation (Austenite to Martensite) than for reverse transformation (Martensite to Austenite). However, the TWSM material transformation depends solely on temperature and the cycle can be repeated extensively, as opposed to having to re-deform the material upon cooling in order to repeat the cycle of the OWSME [3, 9]. The TWSME is the property that provides the means for repeated actuation, a critical component in the development of adaptive structures.

Training Methods

The OWSME can be induced in SMAs very easily using a procedure known as heat-treatment or annealing. This process is primarily used to set the parent shape that the material is to return to upon heating to A_f. Heat-treating can also be used to free the material of any residual strains. The procedure entails deforming a specimen into the desired hot shape, and then heating it to the shape setting temperature. The typical temperature range for heat-treatment of Ni-Ti alloys of different compositions is 300°C - 600°C [2, 3]. Samples can be treated in as little as 10 minutes for smaller sized samples. Larger samples may require annealing time on the order of hours. Samples are typically water quenched following the heat-treatment to avoid unnecessary aging of the material [3, 20](i.e. unnecessary formation of precipitates and transformation characteristic changes). Care should be exercised when choosing parameters for heat-treatment of SMA so as not to negatively affect fatigue life.

As mentioned earlier, TWSM training is done through a thermo-mechanical fatigue process. Unlike the training method used to induce the OWSME in a SMA specimen, there are numerous methods by which a sample can be trained to exhibit the TWSME. Mizar [9] describes the various common methods that can be used to subject the specimen in training to thermo-mechanical fatigue. The common methods include:

- Pseudo-elastic load cycling, calling for repeated loading of the material while in the temperature range for the super-elastic effect (above A_f but below M_d);

- Excessive deformation beyond the recoverable strain limit in the Martensite state;
- Constrained thermal cycling of deformed Martensite, which involves constraining the sample into the desired remembered cold shape and cycling thermal load by heating above A_f, cooling to temperatures below M_f;
- OWSM cycling where the sample is deformed after being cooled to Martensite and then heated to repeat the shape memory cycle; and
- Cycling a load through the super-elastic effect and SME, which consists of loading the specimen to the desired shape in the pseudo-elastic region and cooling the sample to a temperature below M_f while maintaining the constrained state, followed by heating the sample. This cycle is then repeated a number of times (number of cycles varies with sample dimensions, thickness, and composition and ranges anywhere from 10 to 500).

Constrained thermal cycling of deformed Martensite is the most commonly used method today and is the chosen method by which the samples in this research are trained to exhibit the TWSME.

These methods of inducing thermo-mechanical fatigue in SMAs have been studied extensively with emphasis on the effect of the thermo-mechanical training itself. Wang and Yu *et al.* [21, 22] have largely explored the residual effects of varying thermo-mechanical treatments on SMA springs of varying composition. There has also been some work exploring and modeling the thermo-mechanical effects of various types of loading [4, 15, 23]. Little research, however, has been done on the effect

of material loading in TWSM training on specimen performance. The majority of these experiments focus on the behavioral response of samples subject to a load in the pseudo-elasiticity range of temperatures. Furthermore, existing experiments usually employ the use of samples in the form of a spring [21, 22], tube [15], thin film ribbon [9], small diameter fibers, or wire [2]. Many bulk SMAs have been successfully fabricated but remain unpopular as opposed to their wire or other thin-form counterparts due to their slower response time [8]. A thicker sample requires a significantly longer amount of time to cool and complete a forward transformation [8]. Likewise, more time is needed for a reverse transformation to occur. Aside from this downfall, however, bulk SMAs have a larger actuation stroke and increased ability to produce work, making them a suitable candidate for adaptive structure applications.

To the best of the author's knowledge, little research has been conducted investigating TWSM training of bulk SMA samples, and no experimentation has been done to explore the effect of using moment inducing loads to induce bending deformation. Existing studies employ loading types that involve wrapping samples around mandrels, or subjecting a root cantilevered specimen to a tip force, in order to achieve a bending response.

1.3 Summary

NiTiNOL's (Nickel-Titanium Naval Ordinance Laboratory) discovery in 1973 marked a huge breakthrough in the field of SMAs (Shape Memory Alloys). NiTiNOL is an inter-metallic compound composed of roughly 50% Nickel and 50% Titanium. It's unique properties combining shape memory and pseudo-elasticity with high tensile strength, corrosion resistance, and biocompatibility, introduced SMAs to a large variety of commercial applications. It spurred a particular interest within the aerospace community for use in adaptive structures.

It exhibits two primary solid state phases known as Austenite and Martensite. Transformation between these phases is defined by four transformation temperatures: A_s (Austenite Start Transformation Temperature), A_f (Austenite Finish Transformation Temperature), M_s (Martensite Start Transformation Temperature), and M_f (Martensite Finish Transformation Temperature).

The OWSME (One-Way Shape Memory Effect) is induced when a sample is heat-treated to assume a desired parent shape, which if mechanically deformed, it will recover upon reverse transformation induced by heating above A_s. TWSM (Two-Way Shape Memory) occurs when the specimen is trained to remember a shape at both the Austenite and Martensite state. The most common TWSM training method and that used for this research is constrained cycling of deformed Martensite. The super-elastic effect is observed at temperatures above A_f when a stress level is applied that exceeds the critical stress value (σ_s) and SIM (Stress-Induced Martensite) forms.

Existing studies focus on the constitutive modeling of the super-elastic effect and TWSM in SMA springs, wires, and tubes, as well as the effects of various training methods on this form of specimen. In comparison, bulk SMA specimens are capable of providing larger actuation stroke but have slower response time. There has been significant research investigating the thermo-mechanical behavior of SMAs under various types of loading. Little experimentation has been done, however, in comparing the effects of various types of loading during TWSM training on the performance of bulk SMAs.

1.4 Outline of Thesis

The research described in this thesis explores the possibility of increasing TWSM work performance of a SMA specimen through the use of a training load that induces strain throughout the entirety of the specimen. The history of the SME as well as the sample material used for these experiments is described in this chapter. Background on the SME and super-elastic effect as well as the methods by which these phenomenon are induced have been discussed. A review of the existing studies and literature on SMAs and the motivation for the present work described in this thesis have also been presented in this chapter. Chapter 2 provides a detailed description of the experimental setup, equipment, and SMA specimens used to conduct this research. The challenges faced as well as changes made to accommodate these unique issues in the structural and electrical design of the experimental setup are explained. Chapter 3 provides a comprehensive description of the experimental

techniques and methodology used to induce the TWSME and investigate the effects of tip-moment and tip-force type TWSM training on specimen performance. The analytical methods and fundamental principles used to evaluate sample behavior are discussed in detail. The test matrices developed and followed to analyze the effect of tip-moment and tip-load application and training are also presented. Chapter 4 presents a discussion of the results of all analytical studies conducted in preparation for TWSM training and provides a detailed evaluation of the overall effectiveness of each type of load used in TWSM training. The thesis concludes with Chapter 5 in which the significance of the findings are discussed and suggestions for future experimentation to further evaluate the change in SMA TWSM actuation performance with use of the explored training method.

Chapter 2

Experimental Setup

2.1 Overview

Thin rectangular SMA samples of various dimensions were trained via the constrained thermal cycling of deformed Martensite method in order to provide a study of the efficacy of the two constraint approaches explored in this research. This chapter describes the training concept and the design and development of the experimental setup used to train the specimens and evaluate the behavior in specimens resulting from the two constraint methods investigated. The motivation behind the training structure design, as well as the hardware used to bring the designs to life, are discussed in detail. An explanation of the challenges faced in the development of the setup as well as the solutions implemented are provided. A description of the setup used to analyze the trained behavior of the specimens is outlined and a description of the test matrix used to characterize the results of the two training protocols and the motivation for said matrix is also provided in this chapter.

2.2 Overview of Constraint Concepts

The goal of this research requires the ability to be able to produce a tip force and a tip moment on a cantilevered strip of material. Sketches depicting the na-

ture of these two types of loads and the resulting internal strain distribution in a cantilevered beam subjected to the loads are shown in figure 2.1.

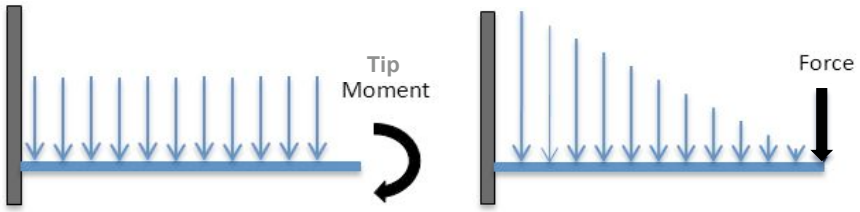

(a) (b)

Figure 2.1: Strain distribution in a cantilevered beam with load application. (a) Arrows drawn represent trend in strain magnitude induced throughout length of beam by tip moment application. Strain is constant throughout beam. (b) Arrows drawn represent trend in strain magnitude induced at various points along the beam by tip force application. Strain is concentrated towards the root.

Implementing a tip force is readily achieved by suspending weights from a clamp attached to the free end of the cantilevered sample. Implementing a tip moment, however, required development of a method for loading the sample. The first step towards the design of a structure with this end goal in mind was to come up with a method to apply forces on the tip of a sample in such a way that a couple is produced, resulting in a moment. The initial concept entailed the use of two pulleys mounted on an axel with its axis aligned along the free end of a cantilevered specimen. This design depended on the concept that applying a force couple would cause the pulleys to rotate while allowing its axel to move with the free end of the sample. This would create a moment at the end of the specimen and cause displacement of the specimen in the direction of the moment.

A demonstration model was developed and fabricated to visualize this idea and assist with conceiving a suitable experimental test-bed design. A large aluminum 0.25 m (10 in) diameter pulley was fixed at its rotation axis to the tip of a 0.8 m×0.01×0.004 m (32 in×0.5 in×0.14 in) aluminum beam. The base was held firmly as a force couple was applied by hand at opposing points on the outer diameter of the pulley. The pulley was allowed to move freely with the beam as a turning moment was induced. Figure 2.2 shows photos of this demonstration showing the beam displacement induced by the applied moment. It also illustrates how the tip force-couple is related to the moment produced in the beam.

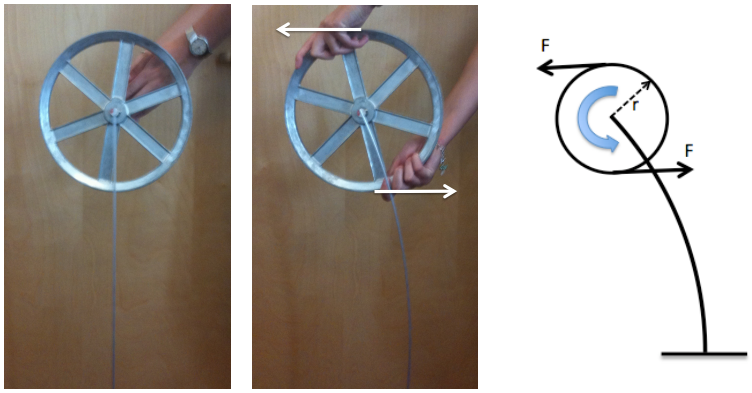

(a) (b) (c)

Figure 2.2: Demonstration of Concept: (a) Large pulley is fixed at center axis of rotation to tip of cantilevered beam. (b) Equal and opposing forces are applied to produce a moment. (c) A moment M where $M{=}2{\cdot}F{\cdot}r$ is created with application of forces F on a pulley of radius r.

2.3 Structural Setup

2.3.1 Training Structure Development and Construction

The structural setup described here was designed with the ability to implement both a tip force and a tip moment to a cantilevered SMA specimen. The option to vary certain parameters, such as load quantity and sample length, while keeping the force couple applied to the tip pulleys relatively constant as the beam deflects, was kept in mind during the conceptualization of this structure. The structure was built out of wood 0.05 m×0.1 m (2 in×4 in) beams. The constructed wooden frame is roughly 1.22 m (4 ft) long, 0.61 m (2 ft) wide, and 1.22 m (4 ft) tall. The size of the structure was determined with the intent of the 4 ft width minimizing changes in the angles at which the force vectors sketched in figure 2.2 act on the pulley as the beam deflects while accommodating lab space constraints.

All experiments entail the sample being clamped at the root. To set up for this, a wood beam was placed across the lower half of the frame in the center. A bench vise was clamped to the center of the beam such that a cantilevered sample would be mounted upright with the axis of an axel on which two pulleys would be mounted located directly above the vise at a distance equal to sample length. Figure 2.3 provides a visual description of this setup.

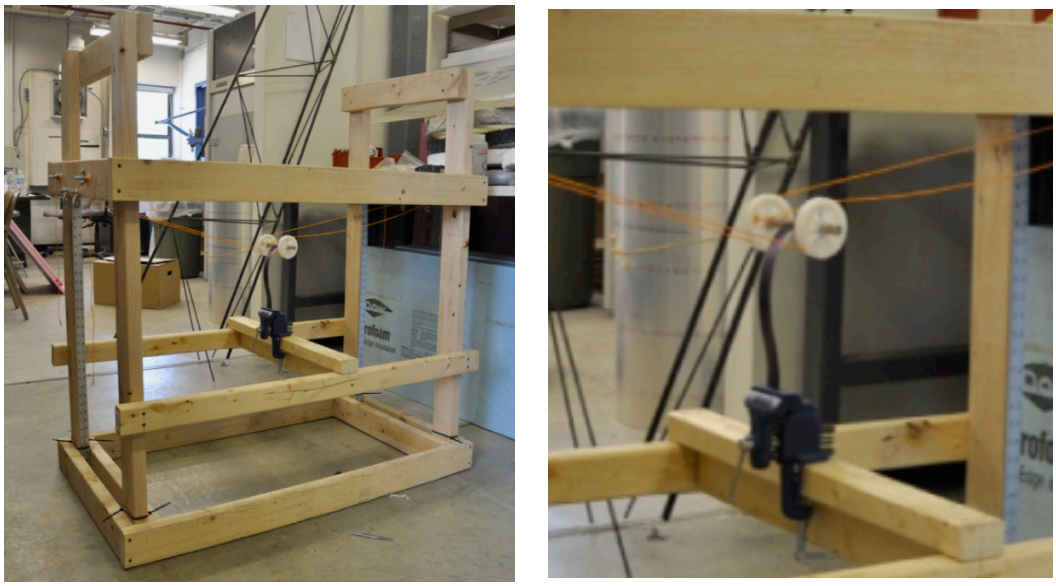

(a) (b)

Figure 2.3: Structural Setup: (a) Sample is clamped in center of wooden training structure with center pulleys fixed on an axel at it's free end. (b) Zoomed view of center axel with pulleys attached when clamped on free end of cantilevered specimen.

A center clamp was designed and fabricated in order to fix two pulleys to the tip of a cantilevered sample. The clamp is composed of two half-moon stainless steel rods, 20.3 cm (8 in) long and 1.3 cm (0.5 in) in diameter. The half moon rod pictured in figure 2.4 has tapped screw holes at 2.54 cm (1 in), 6.35 cm (2.5 in), and 8.89 cm (3.5 in) from the center of the rod. Screw holes were drilled at the same distances along the length of the other half moon rod to compliment the tapped rod. The rods can then be screwed together tightly to properly clamp a specimen. Two set screws are used to place the pulleys symmetrically on the rod with respect to the center of the sample.

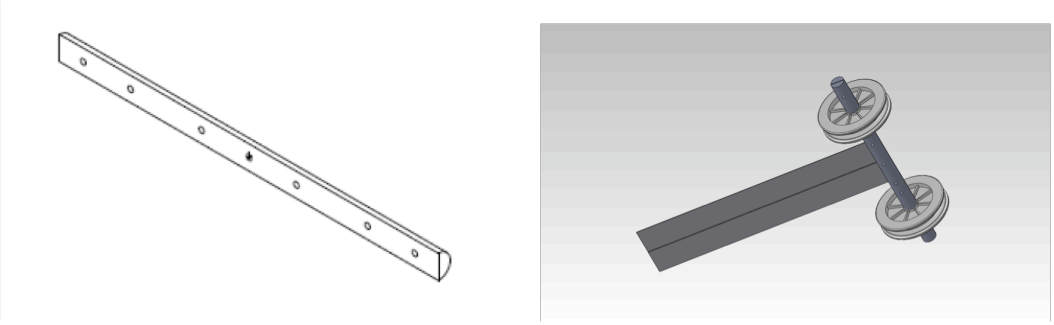

(a) (b)

Figure 2.4: CAD illustrations of tip pulley clamp setup: (a) Stainless steel half-moon rod used to clamp pulleys to tip of sample. (b) Solidworks depiction of center pulley and tip clamp setup.

Samples used in this research were provided by Boeing Research and Technology Flight Sciences. Initial samples had dimensions of $0.2286\,\mathrm{m}\times0.0254\,\mathrm{m}\times0.000508\,\mathrm{m}$ ($9\,\mathrm{in}\times1\,\mathrm{in}\times0.02\,\mathrm{in}$). After initial studies, a need for thicker samples was identified, and samples with dimensions of $0.1778\,\mathrm{m}\times0.0314\,\mathrm{m}\times0.00188\,\mathrm{m}$ ($7.\,\mathrm{in}\times1.24\,\mathrm{in}\times0.074$ in) were obtained.

Two 5.23 cm (2.06 in) outer diameter acetal pulleys were modified with a new inner diameter of 1.29 cm (0.5075 in) to fit over the two half-moon rods when clamped around the tip of the thinner samples. Two more 5.23 cm outer diameter acetal pulleys were modified with a new inner diameter of 1.43 cm (0.5625 in) to accommodate the clamping of the thicker samples. Small holes were drilled through the sides of each pulley perpendicular to the axis of rotation to accommodate set screws. Two more holes were drilled through the sides of each pulley at locations directly opposing each other, as a place to fix strings to pulleys for use with load application.

The complete setup of the acetal pulleys fitted over the half-moon rods clamping around a specimen can be viewed in part (b) of figure 2.4. Applying a force couple on the two pulleys fitted on either side of the sample tip creates a moment at the free end of the beam, i.e. along the axis formed through the center of the pulleys.

Wooden crossbars with two centrally located pulleys were made for the shorter ends of the wooden frame. The crossbars could be raised and lowered so that the two pulleys were perfectly aligned with the pulleys on the free end of the cantilevered SMA sample. For a longer sample, the wood frame is moved up vertically, away from the ground and vice versa for a shorter sample. Figure 2.5 shows a zoomed in view of the pulleys attached to the wooden crossbars.

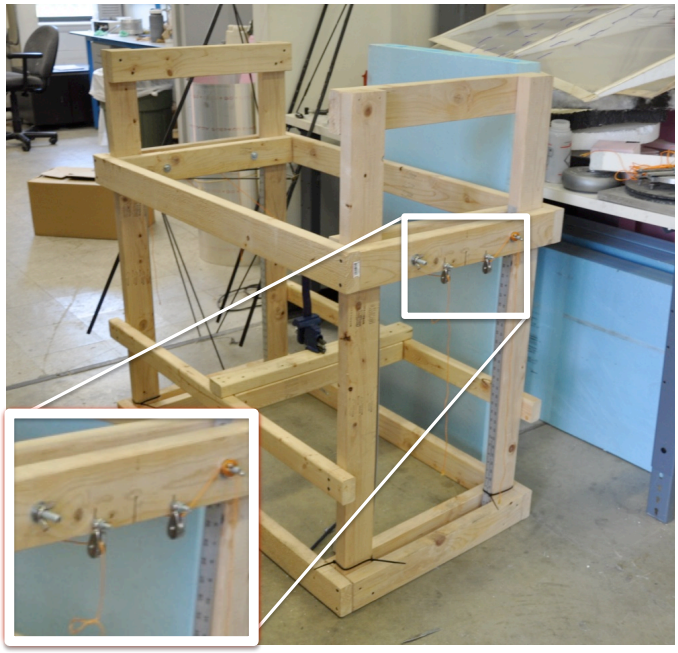

Figure 2.5: The wooden structural frame with two small pulleys centrally located on crossbars. Crossbar height is adjustable for variation in sample size where height adjustment may be necessary to keep outer pulleys level with center pulleys.

Two strings were attached on opposite sides of each center pulley and wound around the pulleys three times before extending out to the two side pulleys on either side of the structure. Four thin steel rods 0.61 m (2 ft) in length were bent to form large hooks that can be tied to the end of each string. Small aluminum washers with masses of approximately 25 or 35 grams each were threaded over the hooks and used as weights to apply the load intended to induce a tip moment on the cantilevered sample. When a load is applied equally on all four outer frame pulleys, a force couple is produced on the pulleys attached to the tip of the sample, resulting in a moment at the tip of the cantilevered specimen. A tip force is induced on the cantilevered sample when weights are applied to the strings on only one side of the test fixture.

2.3.2 Training Structure Modifications

When a 0.2286 m×0.0254 m×0.000508 m (9 in×1 in×0.02 in) NiTiNOL sample was placed in the vice with the stainless steel clamp and center pulley system attached at the tip, it was visually apparent that the weight of the clamp and center pulleys caused the sample to deflect in unwanted directions (shown in figure 2.6).

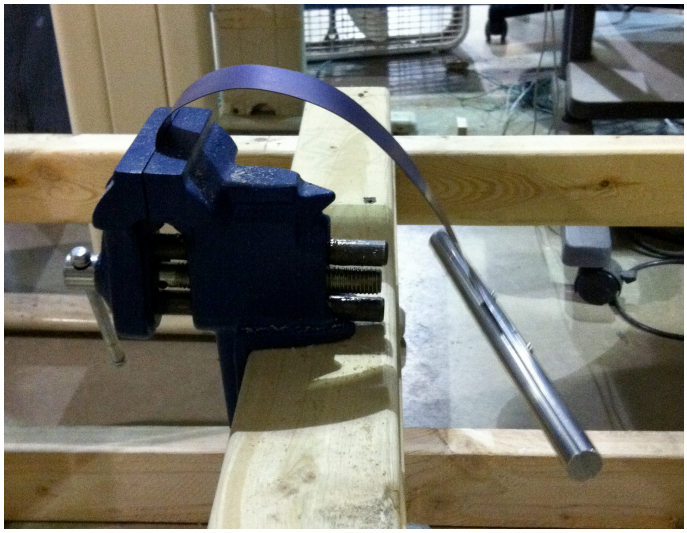

Figure 2.6: Thin NiTiNOL sample deflecting due to weight of stainless steel clamp.

Various methods were devised to solve the problems associated with the weight of the stainless steel rod and pulley tip clamp. The first solution explored entailed compensation of the weight with an upwards force created by an elastic cord attached to the clamp and suspended from a rod laid across the top of the frame. Due to the slight horizontal displacement with bending deformation of the sample during training, the elastic cord was attached to hooks equipped with roller bearings to allow for movement along the horizontal rod used to suspend the cord with negligible friction. Figure 2.7 provides photos of the elastic cord suspension method and a zoomed in image of the roller bearings used.

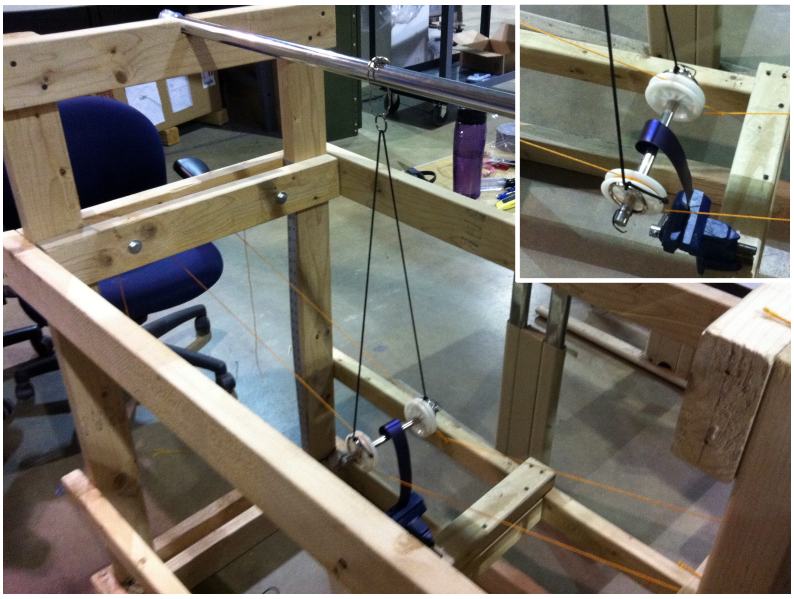

(a)

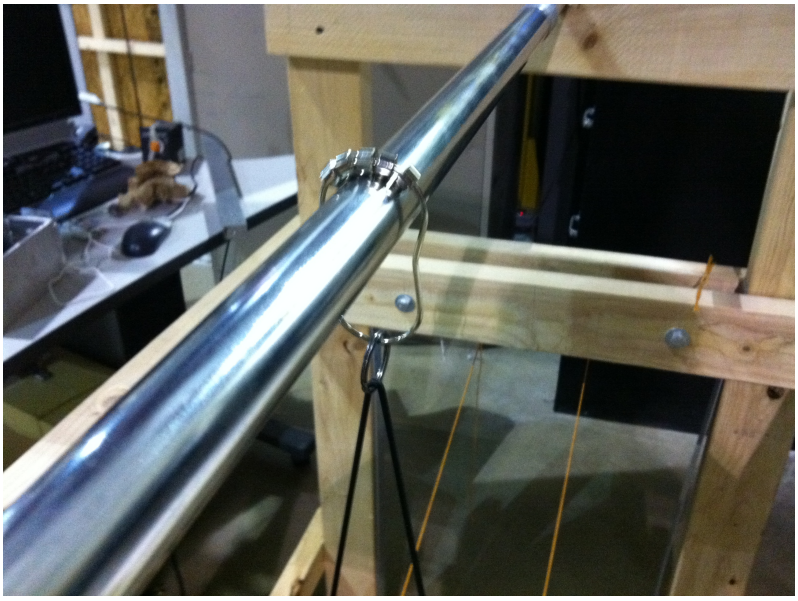

(b)

Figure 2.7: Bungee clamp weight compensation system. (a) Bungees attached to either side of center pulley axel and hung from rod laid across wooden frame are used to support weight of clamp. (b) Close up of bungees fixed to roller bearings that roll along rod as tip of sample displaces horizontally upon load application.

Although the weight of the clamp was offset by the bungee cord attachment, the upwards force created by the bungee exceeded the weight of the clamp. With the bungee cord pulling upwards on the center pulley axel fixed to the tip of the sample, the specimen was not able to displace freely in the horizontal direction as a moment was applied. This resulted in the tip curling phenomenon that can be viewed in the sample in image (a) of figure 2.7. Since the frame was built with the intention to induce a pure tip moment with no additional tip forces of any kind, the bungee chord idea was determined to be unsuccessful. This method of weight compensation was abandoned and a second solution was devised.

In an effort to increase the flexural stiffness, the product of Modulus of Elasticity, E, and Area Moment of Inertia, I, (equation 2.1a), with I defined using b for beam width, h as beam thickness (equation 2.1b) [7], two samples were centrally placed side by side. The weight vector of the tip clamp, however, was still too large and other methods of increasing the stiffness were then explored.

$$Stiffness = E \cdot I \tag{2.1a}$$

$$I = \frac{b \cdot h^3}{12} \tag{2.1b}$$

In an attempt to dramatically increase the area moment of inertia, the frame structure was modified to accommodate horizontal placement of the sample. This involved rotating the vice ninety degrees as well as repositioning the outer pulleys. Prior to the modification, two pulleys were attached in the same horizontal plane on either side of a wooden frame that moves up and down around the wooden structure

to allow for change in sample length. They were placed at a distance apart equal to the distance between the two inner acetal pulleys when placed on the clamping rod at the tip of the sample. Since the clamping rod was now located in a position that is perpendicular to its previous placement, the plane of the outer pulleys also had to be rotated to be parallel to the clamping rod. To accommodate for various sized samples, the two pulleys on either side were each fixed to a screw which can be clamped at any point horizontally along the length of an 80/20 aluminum beam using the head of the screw to slide within the rail of the beam and a bolt to secure it in a specific location. The 80/20 beams were fixed to the outer frame of the wooden structure. The ability for the outer pulleys to be positioned at any point along the length of the 80/20 beams attached to the outer frame allows for various types of loading configurations as well. The outer frame was also fixed in a position that was level with the plane in which the sample is clamped since the ability to move the frame up and down for sample length was no longer required. Figure 2.8 provides a CAD illustration of the modified structural setup with a sample placed horizontally in the center of the training structure and a close up view of the 80/20 aluminum rail modification. A further increase in stiffness was induced by, again, placing two samples side by side in the clamp.

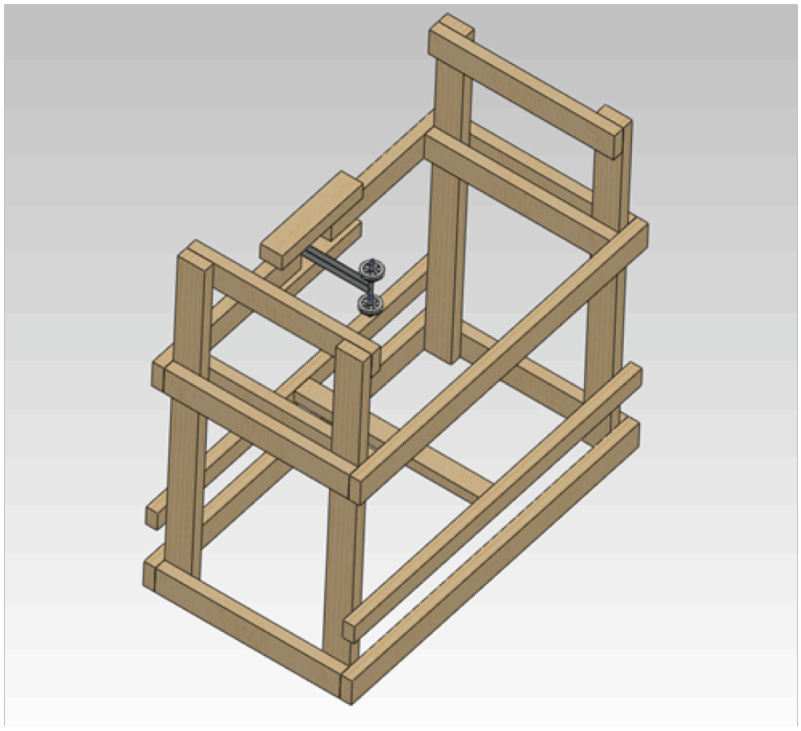

(a)

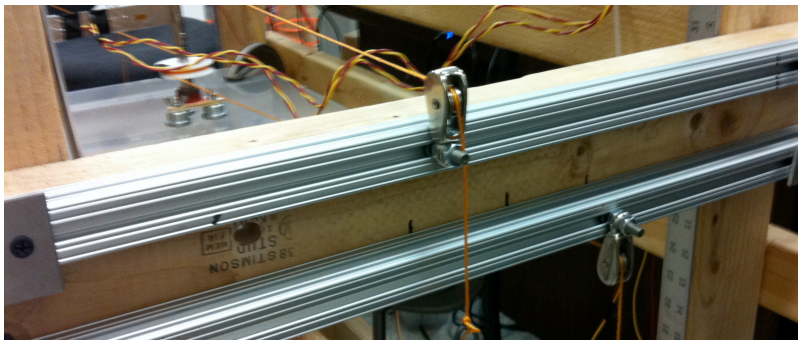

(b)

Figure 2.8: Training structure: (a) Solidworks depiction of training structure modified for horizontal sample placement. (b) 80/20 beams fixed to outer frame used as rails for outer pulley position variance.

This ninety degree setup modification proved to be a great improvement in that the sample was now able to sustain the weight of the tip clamp without a lot of displacement in the direction of the clamp weight. The stiffness was not large enough, however, to fully eliminate additional unintended displacement and twisting of the sample under the weight of the clamp.

To minimize twisting of the sample as the tip loads were applied, a triangular ball transfer platform and shelf setup was designed to both support the weight of the clamp system and to constrain tip motion to only horizontal displacement. Three small ball transfer bearings were fixed at the corners of a triangular piece of a balsa wood. A bolt with a diameter slightly larger than that of the circular area created by the two half moon rods screwed together was glued to the center of the balsa wood triangle and intended to cup the bottom of the stainless steel rod when a sample is cantilevered horizontally in position for training. The stainless steel clamp rods fit into the bolt and the clamp then rests on the platform, which moves freely on a plexiglass shelf, preventing any twisting or unwanted displacement to occur, aside from in the intended horizontal plane of movement. Hardening clay was placed around the rod and top of the bolt where the half moon rods rest in order to secure the clamp rod to the platform and to keep it perpendicular to the platform at all times. This clamp weight compensation mechanism and shelf are pictured in figure 2.9. The clay used to keep the clamp upright can be seen in figure 2.10.

(a)

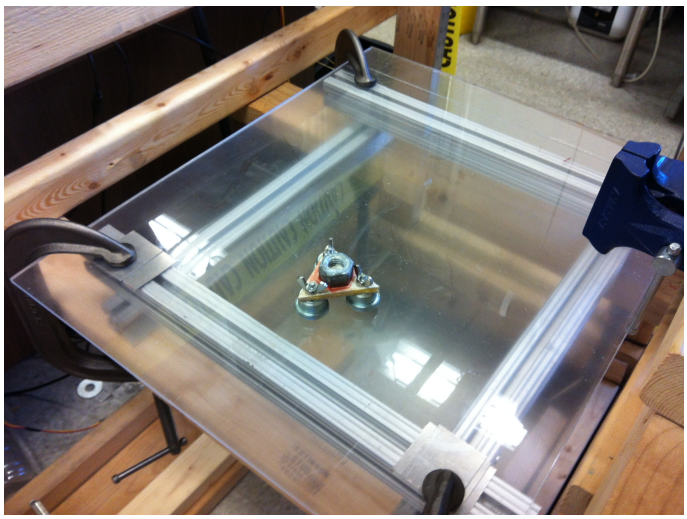

(b)

Figure 2.9: Clamp weight compensating system: (a) Close up view of compensating ball transfer platform used to offset clamp weight. (b) Weight compensation system: Ball transfer platform and negligible friction surface.

Figure 2.10: Hardening clay wrapped around meet point between stainless-steel half-moon rod clamp and ball transfer platform base.

2.3.3 Strain Gauge Setup

A strain study was conducted to investigate the strain distributions in the cantilevered beams under different loads. Aluminum samples of similar dimensions (25.4 cm×2.5 cm×0.051 cm and 19.1 cm×3.2 cm×0.2 cm) as the NiTiNOL samples to be used in the experiments were instrumented with Vishay Micro-Measurements strain gages with a grid resistance of 350 ohms (models 301181 and 2549). The thinner sample was instrumented with two 1.36 cm×0.59 cm (0.5345 in×0.231 in) strain gauges. One strain gauge was placed 8.9 cm (3.5 in) from the root of the sample. Its location is such that the strain reading can be assumed to reflect the general trend

in root strains. The second was placed 20.3 cm (8 in) from the root (2.5 cm from the tip) and assumed to reflect the general trend in tip strains. A depiction of the two strain gauge set up can be seen in figure 2.11.

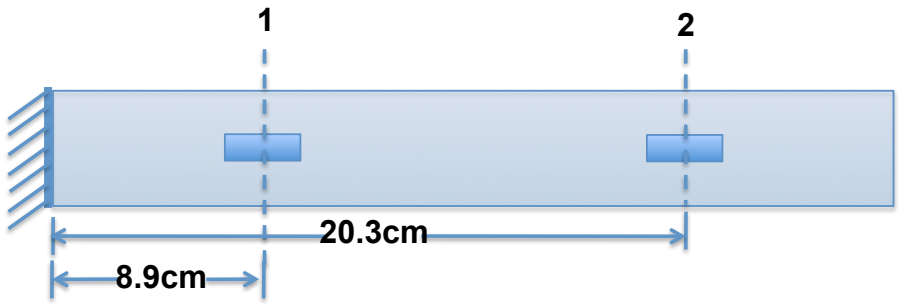

Figure 2.11: Double strain gauge layout on thinner aluminum sample.

An aluminum sample representing the sample with a thickness of 0.19 cm (0.074 in) was also equipped with strain gauges. The layout for this particular specimen includes four evenly spaced strain gauges. The strain gauges used are 0.0193 m×0.004 m (0.76 in×0.1575 in) in dimension. They were placed at 3.3 cm (1.23 in), 7.4 cm (2.9 in), 12.1 cm (4.8 in), and 15.7 cm (6.2 in) from the root along the length of the thicker aluminum sample. A visual depiction of this layout is provided in figure 2.12. The protocol followed to perform the strain reading experiments as well as the results of the strain tests are presented in chapter 3.

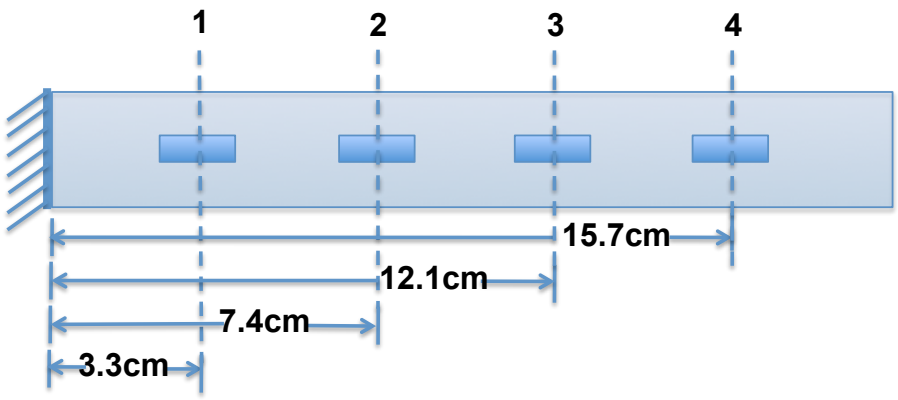

Figure 2.12: Strain Gauge Layout on Thicker Aluminum Sample

2.3.4 Characterization Testing Setup

This section describes the experimental setup used to evaluate the success of the TWSM training performed on the specimens such that the work potential of each specimen could be calculated. Once training of each sample had been completed, the vice used to clamp the samples at the root was rotated 90 degrees. With the repositioned vice, the samples were cantilevered with their tip bending towards the ground so they would do work against gravity and displace upwards when heated to Austenite. To measure work, various weights were fixed to the tip of the samples using Kapton polyimide tape. The weights were composed of 25 g and 35 g washers. The specimens performed work and lifted the weights when transforming from Martensite to Austenite upon heating. The vertical displacement of each sample was tracked with a backdrop constructed using cardboard. A printed protractor was taped to a large piece of paper and a large grid was hand drawn on the paper with its origin coinciding with the origin of the protractor. The large paper was

taped to the cardboard backdrop and placed behind the sample if looking from the side of the frame, such that the origin was positioned directly behind the point at which the root of the sample is clamped. A photo of this setup is provided in figure 2.13.

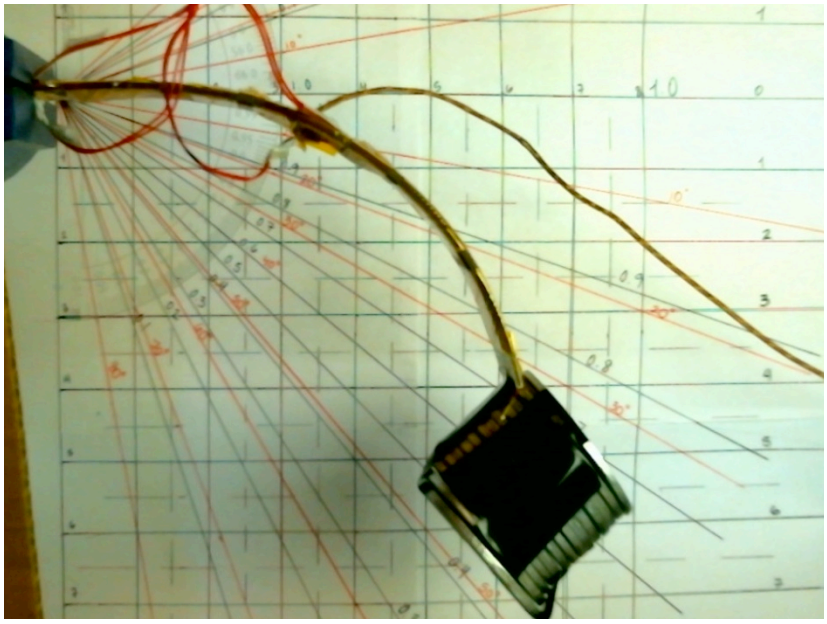

Figure 2.13: Combined tip moment and tip force trained NiTiNOL sample transforming to Austenite while lifting a weight composed of washers.

2.4 Electrical Setup

2.4.1 Training Electrical System Design

The following paragraphs describe all the hardware and equipment used to provide the heating required to induce the OWSME as well as the heating and cooling portions of the training protocol used to induce the TWSME on each SMA sample.

All heat treatments were conducted using a Lindberg/Blue M programmable box furnace. This type of furnace is capable of reaching temperatures as high as 1200°C. The cooling associated with the OWSM process was achieved by quenching the samples in a container of cold water. Heavy weights were used to flatten the specimens while in the furnace. No other equipment was used (with the exception of tongs for handling of hot specimens) in the OWSM training process.

All electrical wiring for the TWSM training was done using 22 AWG gauge insulated wire. For these experiments, the samples were heated using MINCO model 5165 rubber silicone resistance strips with pressure sensitive adhesive backing. To thermally isolate the samples and improve heat distribution, two 2.54 cm×2.54 cm× 0.254 cm (1 in×1 in×0.1 in) square pieces of G-10 plastic were placed on either side of the clamped root of the specimen such that no part of the SMA is in direct contact with the vice to which it is cantilevered. Heat resistant Kapton polyimide tape was used to ensure adhesion of the strip heaters to the SMA samples throughout the entire training process. All Kapton tape used for the purpose of strip heater adhesion was placed in a band like manner such that bands of tape surrounded the entire sample wrapping over the sample and strip heater at intervals along the sample length. Strip heaters were chosen as the preferred heating method due to the size of the training structure being too large to be placed within any of the ovens available. Modification to the ovens available for placing only portions of the experimental structure within an oven was not feasible. It should be noted that strip heaters are used for training purposes only. Typically, heating of the specimens to induce the TWSME is done passively by external temperature changes. As mentioned in

chapter 1, the transformation temperatures of the specimens can be altered through heat-treatment, loading, and alloy composition. They can, therefore, be changed to remain within a certain range of temperature and suit the needs of the application for which they are being used.

Three type K calibrated Omega fiberglass insulated stripped lead termination thermocouples were used to measure both sample and strip heater temperature during the entire training process. Each was hand soldered to ensure proper contact between the thermocouple point of measure and the surface of the sample. One thermocouple was placed on one side of the sample in contact with the alloy. Two thermocouples were placed on the other side with one on the strip heater surface, and one in contact with the alloy as shown in figure 2.14. They were adhered to the surfaces of the specimen and strip heaters using Kapton polyimide tape.

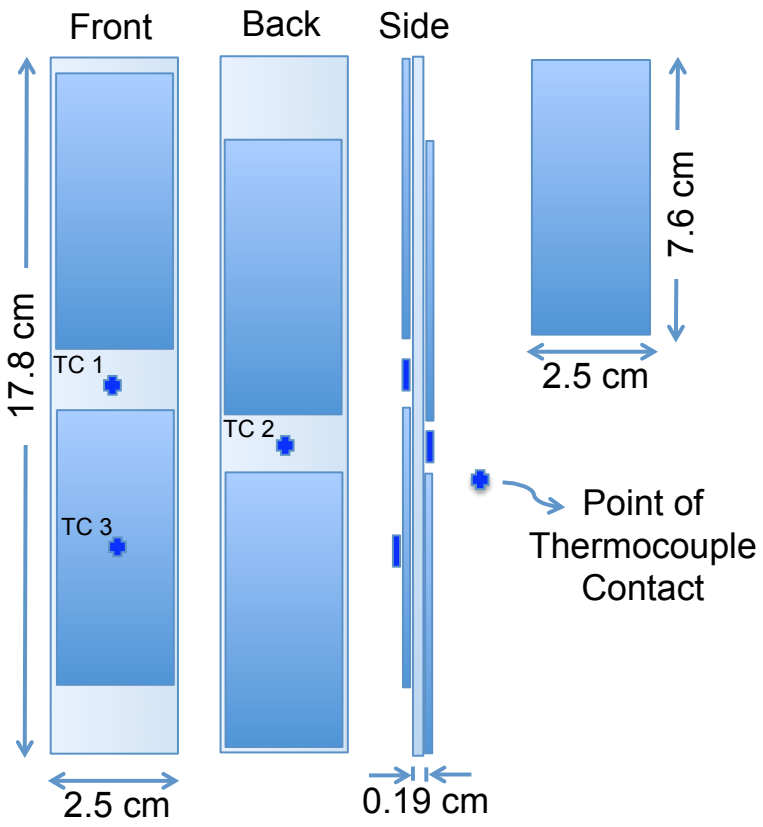

Figure 2.14: Strip heater and thermocouple layout on training sample.

The power to the strip heaters was provided by an AE Techron LV 3620, 120/230V AC, 15A, 50-60 Hz, dual channel amplifier. Output voltage was provided using an AO02 model analog output module inserted into a National Instruments (NI) brand SC-2345 model signal conditioning unit. A NI USB-6251 data acquisition (DAQ) interface sends signals from a Dell Latitute E6510 model laptop computer to the signal conditioning unit and acts a medium between the computer and the signal conditioning unit, where all hardware is connected. Three TC02 model analog input modules (also inserted in the SC-2345 signal conditioning unit) were used for the readings of the three thermocouples. A standard Honeywell three-speed desk fan was used to aid in cooling the samples during the Austenite to Martensite transformation portion of each training cycle. All cooling of the samples was done at the fastest fan speed to expedite the cooling process. The same NI-DAQ set up with the USB-6251 interface and SCC-2345 signal conditioning unit was used in conjunction with an AO-02 analog output module to control the fan. The fan was powered by a standard 120V power wall outlet with it's power chord spliced and interrupted by a 5V-DC Omron relay. The relay was used to directly control the open and close of the circuit allowing power to the fan. A custom circuit was developed for the support of the relay system. The DAQ system sends a voltage to a transistor acting as a switch controlling the current allowed to flow through the relay coil. Current to the relay was supported by a 5V-DC power supply. The power supply and transistor are separated in the circuit by a small resistor which limits current flowing into the base of the transistor to prevent damage.

Other alternative control methods were considered when choosing options for turning the fan on and off during the training process. Several opto-isolators were purchased and tested, but were found to be too fragile and unable to handle the current required to control the fan. The relay proved to be most robust and able to handle the task at hand. A high-pass and low-pass filter were also constructed and tested in an attempt to eliminate the use of two analog output modules and condense the system down to one output module controlling both the strip heaters and fan. Although the filters were successful in filtering out the appropriate signals, separate modules were chosen as the preferred method in an effort to minimize room for error or unintentional overload with the use of such delicate equipment. Use of two separate modules also reduced the chances of failure due to faulty wiring and/or circuit component failure. The dual module method also proved to be easier to troubleshoot.

2.4.2 System Control Algorithm Development

A control algorithm using a graphical coding program was designed and developed to automatically and autonomously conduct the thermal cycles required for TWSM training. The control algorithm was implemented using graphical coding in LabView. Design of the program was based on the necessity to vary temperature between a high and low state using the strip heaters and fan for 500 cycles, with each cycle being roughly 7 minutes in duration. The custom control design is described by the flow chart provided in figure 2.15. The LabView program is installed on a

Dell Latitude E6510 Laptop computer that was used for all operations associated with this project.

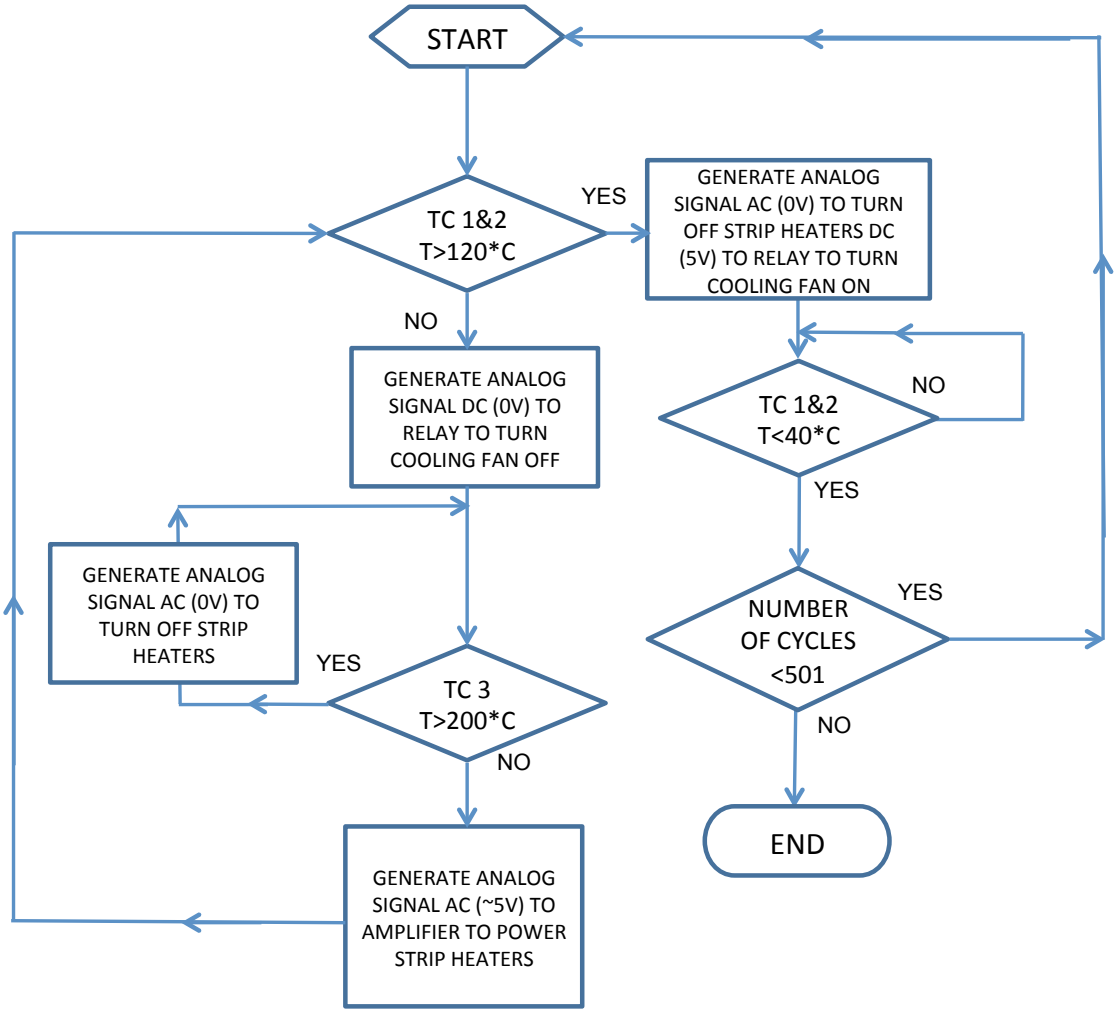

Figure 2.15: Flow Chart of Control Program Used to Train SMAs

The LabView program utilizes a case structure approach where separate cases control separate states within the system and a shift register determines which case is active based on a certain variable of the user's choice. For this particular system, a case is defined for both the heating and cooling states. Temperature was used as the variable controlling the shift registers. The starting case is the

"heat" case, within which a second shift register leads to two separate sub-cases. Case 1 sends power to the amplifier and, therefore, to the strip heaters coupled with a 0 voltage signal to the fan relay system, keeping the fan off during heating. Two thermocouples adhered to the surface of the sample (TC 1 & 2 in figure 2.15 using Kapton polyimide tape constantly verify that the temperature is still below the preselected "hot" temperature. A third thermocouple (TC 3 in figure 2.15 monitors the temperature of the strip heaters. If the maximum allowable strip heater temperature is reached, 0V is sent to the strip heaters until the temperature has dropped below the maximum allowable temperature. Power only returns to the strip heater once the temperature measured by the third thermocouple drops below the maximum temperature. There is no allowance for overshoot of this maximum temperature. This third thermocouple and maximum temperature limit serves as a safety measure preventing the strip heaters from burning out.

When the preselected "hot" temperature is reached by both thermocouples monitoring the temperature of the specimen, the shift register tells the system to switch to the "cool" case. Due to the thermal conductivity properties of the material, heating is distributed but not 100% uniform. The thermocouples monitoring the temperature of the specimen are strategically placed in locations where a strip heater is not present. Under the assumption that the thermocouples are monitoring the coolest portion of the specimen on either side, the temperature in the surface regions of the specimen that are in direct contact with the strip heaters are presumably hotter than the temperature of the surface underneath the two thermocouples, ensuring that the cooling phase of the cycle does not commence until all regions of

the specimen have presumably reached the pre-selected hot temperature. In addition, the preselected "hot" temperature is 10°C above the temperature necessary for the specimen to reach the fully Austenite state. Overshoot of the "hot" temperature is allowed but is typically minimal due to the two thermocouples consistently measuring temperatures within 8 degrees of each other.

During the cooling portion of the cycle, 0 V is sent to the strip heaters and a 5 V signal is sent to the fan relay system, turning on the fan to assist in cooling the samples. Again, the first two thermocouples adhered to the specimen surface constantly monitor the temperature of the specimen. The shift register only reinitiates the "heat" case once the temperature measured by both thermocouples drops below the preselected "cold" temperature. The preselected "cold" temperature is also 10°C below the temperature necessary for the specimen to reach the fully Martensitic state and, like in the "heat" case, overshoot is minimal. Figure 2.16 shows the LabView program with the heat and cool case structure displayed. More figures of the structure of the LabView program are provided in appendix A.

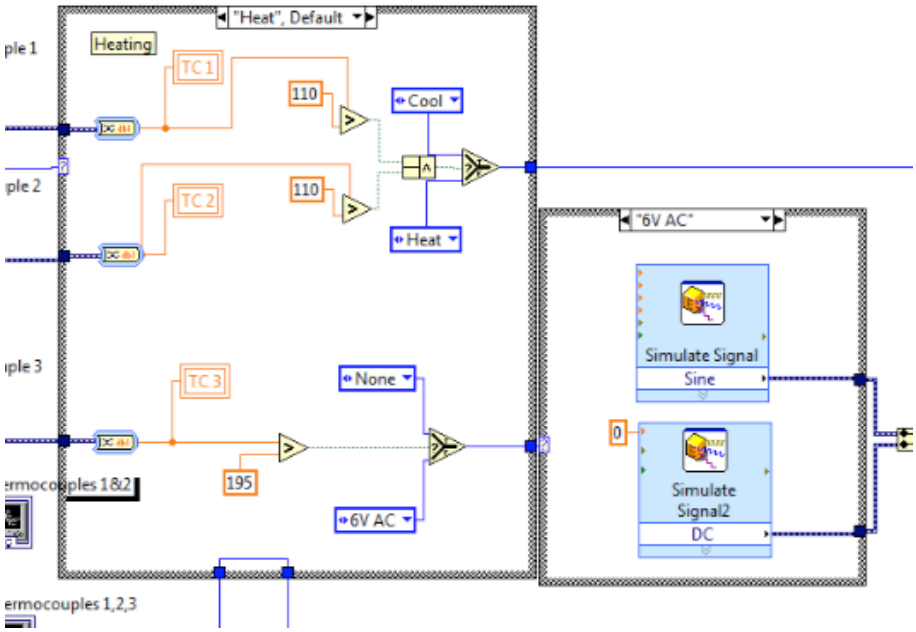

(a)

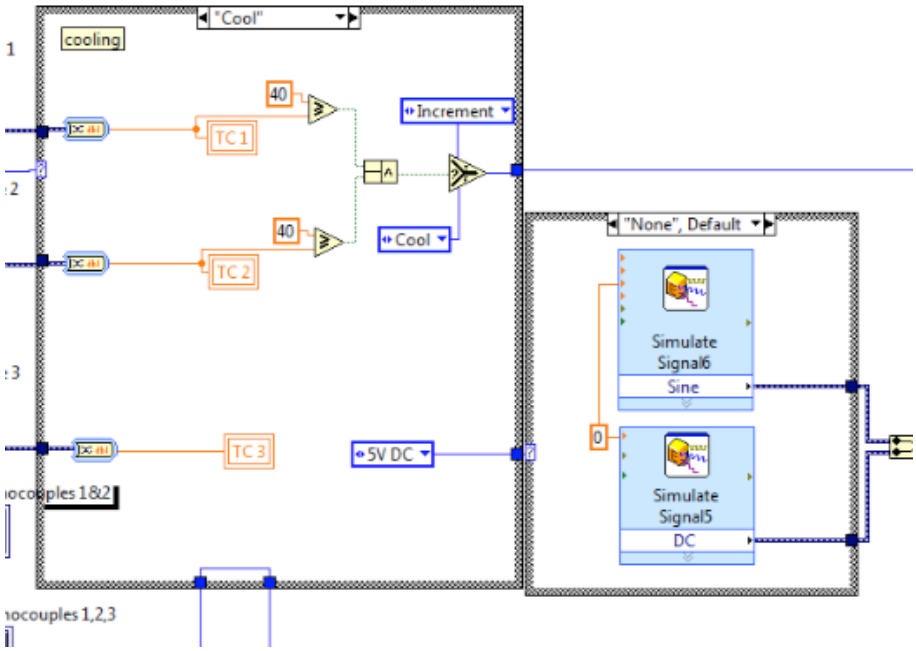

(b)

Figure 2.16: Screenshots of the LabView heat and cool case structures used to autonomously train SMA samples: (a) Training system heat case structure. (b) Training system cool case structure.

A Logitech HD Webcam model C615 was installed directly above the setup in order to monitor the training process. A time lapse video can be created from photos taken at an increment of 2 seconds during the entire period of training. A program called Flix was used to capture images at preselected intervals. All photos and videos were saved on a 1TB Western Digital Passport portable external hard drive.

2.4.3 Strain Testing Electrical Setup

All strain measurements were conducted through the NI-DAQ system consisting of the USB-6251 Terminal Device and SCC-2345 Signal Conditioning Box. SCC-SG02 analog input quarter-bridge configuration strain gauge modules were used in the SCC-2345 to provide a wheat-stone bridge for gathering the strain information. Strain readings were taken through a custom LabView program designed to directly read the local strain exerted within the sample upon deformation. Each strain gauge, regardless of size used, was connected separately to its own individual SG02 module. All electrical wiring was done using the same 22 AWG gauge insulated wire used for the rest of the electrical setup, with the exception of 28 AWG gauge copper wire used as a transition medium between the larger gauge wire and the very delicate wire leads of the strain gauges. The LabView program was designed to automatically save all strain data upon termination of the run of the code. The data was saved into text files and the information in the text files located on the WD external hard-drive was post-processed using Matlab.

2.4.4 Sample Characterization Testing Electrical Setup

Testing the samples for training success and for characterization of their ability to perform work required that the sample be heated and cooled repeatedly, as during training. Heating and cooling of the samples was done using the same heaters, fan, and thermocouple setup as that for the training of the specimens. Heating and cooling of the samples was done independently and manually by operating separately designed LabView codes. The thermocouples were used to monitor the temperature of both the sample and strip heater to determine when to initiate both heating and cooling portions of the thermal cycles and ensure that the strip heaters did not overheat. All physical electrical wiring to the heating and cooling components remained the same as that used for training.

The same Logitech HD webcam used to monitor the training of the specimens was used to evaluate the success of the training as well as record the results from the characterization tests. Regular video recordings were taken of the sample training tests and saved directly on the WD hard drive. In order to evaluate specimen performance, the camera had to be relocated to accommodate the 90 degree rotation of the vice and root cantilevered specimen position. The webcam was placed such that the image was aligned with the grid printed background origin located directly behind the cantilevered root of a trained specimen. Images were captured manually using the software included with the webcam installation to record the displacement data of each sample.

2.5 Summary

The experimental system developed for training and evaluation of cantilevered SMA samples is described in this chapter. The system was constructed with the ability to vary parameters including sample size, loads for training the sample under a tip force or a tip moment, the temperatures at which training was conducted, and the number of training cycles. A description of the control system used to autonomously train the samples is presented. Included is a description of the heaters, fan, thermal, and electrical components used to cycle temperature loads on a specimen in training for a fixed number of cycles. The equipment and programs used to evaluate the success of training and the performance of a trained specimen are described. The physical setup used to identify strain within the samples is also depicted and discussed in this chapter. The methods and protocols by which the samples were trained and tested using the physical setup described here are presented in chapter 3. The results of the training sessions and evaluation experiments are provided and discussed in chapter 4.

Chapter 3

Development of TWSM Training System

3.1 Overview

In order to induce the TWSME in a SMA specimen, a training protocol has to be followed. This chapter describes the protocols by which the specimens used in this research were trained to "remember" both a hot (Austenitic) shape and a cold (Martensitic) shape. The thermal and mechanical loads to which the specimens were subjected are described. The analytical studies and mathematical equations used to determine the mechanical loads are presented. Strain tests were performed on various samples to gain insight into the strain distribution induced on a cantilevered specimen by the training protocols. The test matrices used to perform these strain tests on the aluminum samples are discussed. The experimentation procedure used to evaluate the effectiveness of a training method and the test matrices developed to record test data are also discussed.

3.2 Strain Studies

Multiple strain measuring experiments were performed throughout the duration of this research project. Strain readings were essential to understanding the types of loading the specimens were subjected to. Strain readings were also used to provide

confirmation regarding whether or not a tip-force and tip-moment constraint as applied using the training structure introduced concentrated (tip force) root strain and distributed uniform strain throughout a cantilevered specimen (tip moment). The samples were subject to a range of loads for the two targetted loading configurations and strain readings for each case were read using the graphical Labview program and strain gauges described in chapter 2. Test matrices were structured for each set of strain testing and are described in the following paragraphs.

Initial strain tests were conducted on the $0.254\,\mathrm{m} \times 0.0254\,\mathrm{m} \times 0.000508\,\mathrm{m}$ ($10\,\mathrm{in} \times 1\,\mathrm{in} \times 0.02\,\mathrm{in}$) aluminum sample that was instrumented with two strain gauges. The size of the aluminum sample was chosen to closely resemble the size of the thinner NiTiNOL samples intended for testing the experimental setup. Structural loading strain readings were taken for two types of loading configurations. The first of the tests involved inducing a tip-force load on the sample. Figure 3.1 shows the strain measured as a tip force is applied to the cantilevered specimen. The initial strain test indicates that the training structure can be used to successfully induce a tip-force load on a cantilevered sample, such that the majority of the strain induced in the sample remains concentrated at the root.

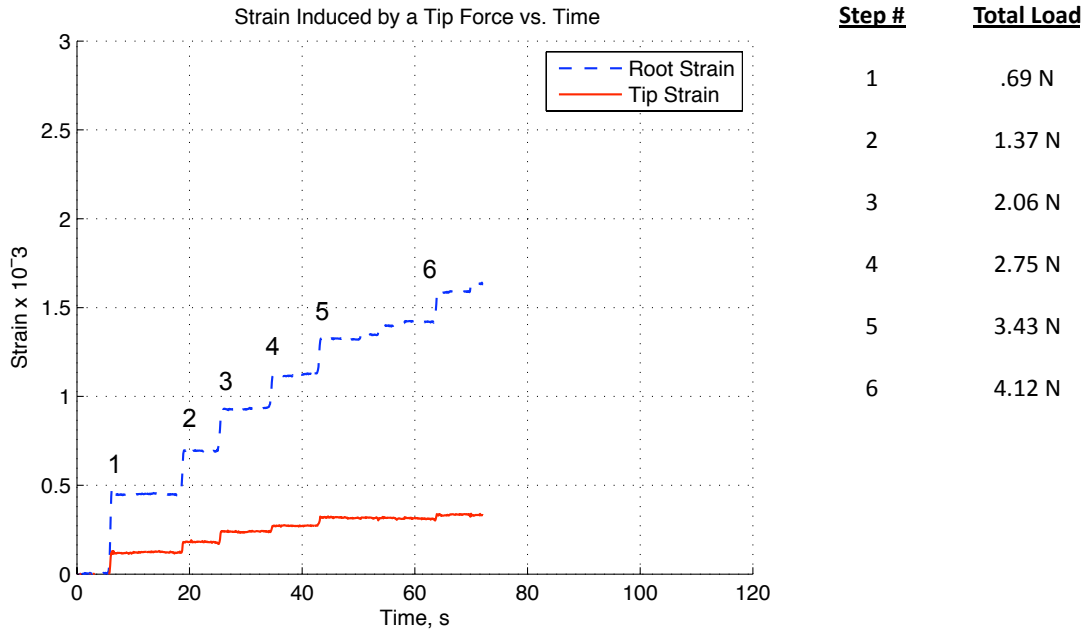

Figure 3.1: Root and tip strain induced in cantileverd sample by tip-force load. Tip force was incrementally increased in steps, which are numbered in the figure. The legend to the right of the figure provides details on the total tip force applied on the specimen after each step. Strain is highest near the root of the sample.

Next, a tip moment was applied to the cantilevered sample by placing equal weights on the strings attached to the two center pulleys, shown in part (b) of figure 2.4 (two strings per pulley). The resulting strain distribution, shown in figure 3.2, indicates that as the beam deflects, more strain was induced near the tip of the sample than near the root, instead of expected near equal magnitude of strain near the tip and root. Although application of equal forces (weights) on the strings attached to the center pulleys will initially produce a tip moment as intended, additional force components act on the tip of the sample once it begins to deflect.

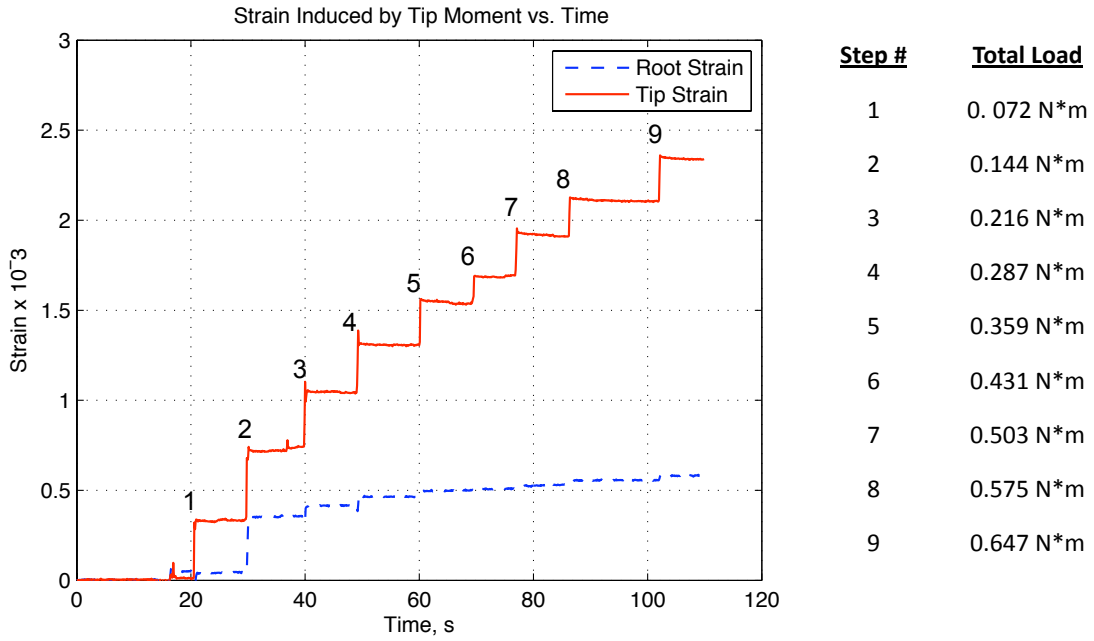

Figure 3.2: Root and tip strain induced in a cantileverd sample by initial training configuration for introducing a tip moment to undeformed sample. Tip moment was incrementally increased in steps, which are numbered in the figure. The legend to the right of the figure provides details on the total tip moment applied on the specimen after each step. Strain at the tip of the sample is roughly five times greater than strain near the root of the sample. Applying a tip moment to an undeformed sample with the test structure fails to produce only a tip moment as the cantilevered sample deflects.

Since the tip-force and intended tip-moment loads as produced by the training structure produced concentrated strain at opposite ends of the cantilevered sample, the strain resulting from a superposition of a tip-moment and tip-force load as applied by the training structure was investigated to see if combined tip-force

and tip-moment application using the structure would produce relatively uniform strain along the length of the sample such as successful application of a constant tip moment during deflection of the sample would produce. It should be noted that the tip-moment load applied by the training structure does not produce strain consistent with that expected to be produced by a constant moment, but that the phrase "tip-moment load" in reference to the load applied by the experimental setup conveys the load that is induced by equal weights applied on either side of the training structure with the intention of producing a constant tip moment. Figure 3.3 illustrates that the approach of a superposition of both types of loads results in the desired even distribution of strain throughout the sample.

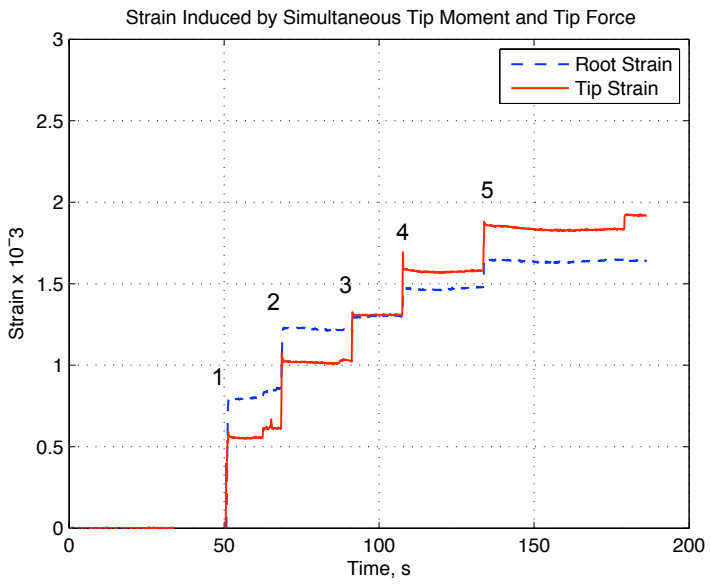

Step #	Total Moment	Total Tip Force
1	0.026 N*m	0.491 N
2	0.051 N*m	0.981 N
3	0.077 N*m	1.472 N
4	0.103 N*m	1.962 N
5	0.128 N*m	2.453 N

Figure 3.3: Simultaneous application of tip-moment and tip-force load on cantilevered sample leads to more similar increase in strain throughout sample as it deflects. Tip moment and tip force were incrementally increased in steps, which are numbered in the figure. The legend to the right of the figure provides details on the total tip force and tip moment applied on the specimen after each step.

In order to get a more comprehensive understanding of the strain induced within a cantilevered sample subject to a tip force, tip moment, as well as the simultaneous application of a tip moment and tip force, another aluminum sample was instrumented with four evenly spaced strain gauges. As mentioned in chapter 2, the aluminum sample used was thicker and was similar in dimension to the thicker $0.1905\,\mathrm{m}\times0.0318\,\mathrm{m}\times0.002\,\mathrm{m}$ ($7.5\,\mathrm{in}\times1.25\,\mathrm{in}\times0.07\,\mathrm{in}$) NiTiNOL samples used for training.

A test matrix was constructed for the strain readings taken from the aluminum sample with the quad gauge setup. In addition to the various loading combinations observed, two different loading protocols were followed for combination tip moment and tip force application. The first of these protocols involved applying a moment load first followed by a prescribed tip force. The second protocol called for simultaneous application of a tip force on one side as a load is applied on both sides of the structure to induce a tip moment. Table 3.1 provides information regarding which loading protocol was followed for each test. Table 3.2 provides the testing matrix used to determine which of these two simultaneous tip force and tip moment protocols yielded the most even increase in strain throughout the entire specimen (i.e. provide the best approximate of a sustained tip-moment load as the sample deflected in response to the load).

The matrix is divided into two main columns containing the specifics pertaining to type, number, and order in which the washers used as loads are applied on either side of the training structure to induce either a tip force or tip moment. A set implies that the specified number of washers in that particular set were applied all at once. If two sets were applied and there are four washers in a set, four washers were applied all at once, followed by another four all at once for a total of eight washers. The order in which the sets are applied is prescribed by the position within the test matrix. The washers that were first applied to either set are listed first, followed by the washers applied immediately afterwards and so forth. A "-" implies that no washers were placed and is displayed in tip force tests where washers are only applied on one side of the structure. In some tests, small washers were applied

on one side of the structure at the same time that large washers were applied on the other side. This is denoted by a displaced horizontal line separating the small washer sets and the large washer sets.

Table 3.1: Loading protocol followed for 4 strain gauge test on $0.1905\,\mathrm{m} \times 0.0318\,\mathrm{m} \times 0.002\,\mathrm{m}$ aluminum sample to determine most suitable protocol for tip-force and tip-moment combination loads.

Test #	1- 3	4-7
Loading Protocol	Tip moment followed by tip load.	Simultaneous tip moment and tip load.

Table 3.2: Strain testing for 0.1905 m×0.0318 m×0.002 m aluminum sample instrumented with four strain gauges to determine most suitable protocol for tip-force and tip-moment combination loads.

		Training Structure Side A			Training Structure Side B		
Test #	Washer Mass	# in Set	# of Sets	Total	# in Set	# of Sets	Total
1	35g	2	6	12	2	6	12
	25g	2	5	10	2	5	10
		2	4	8	-	-	-
2	35g	4	4	16	4	4	16
	25g	4	2	8	4	2	8
		6	1	6	-	-	-
3	35g	4	4	16	4	4	16
	25g	4	2	8	4	2	8
		4	2	8	-	-	-
4	35g	6	2	12	4	2	8
	25g	6	1	6	4	1	4
5	35g	6	2	12	4	2	8
		4	1	4	4	1	4
	25g	6	1	6	4	1	4
		6	1	6	4	1	4
		2	1	2	4	1	4

Table 3.3: Strain testing for 0.254 m×0.0254 m×0.000508 m aluminum sample instrumented with four strain gauges to determine most suitable protocol for tip-force and tip-moment combination loads con't.

		Training Structure Side A			Training Structure Side B		
Test #	Washer Mass	# in Set	# of Sets	Total	# in Set	# of Sets	Total
6	35g	6	1	6	4	1	4
		4	2	8	4	2	8
		2	1	2	4	1	4
	25g	4	4	16	2	4	8
7	35g	6	2	12	4	2	8
		4	1	4	4	1	4
		2	1	2	4	1	4
	25g	6	1	6	4	1	4
		6	1	6	2	1	2
		4	1	4	2	1	2

Although application of a tip moment followed by a compensating tip force can result in even distribution of strain throughout a cantilevered specimen and should give the same result as simultaneous application of the tip moment and tip force, the latter proved to be the preferred method. With simultaneous load application, the strain at each point along the sample rises evenly together as the loads are

applied, as opposed to an abrupt rise of strain in one part of the beam followed by an abrupt rise of strain in the other parts. This is also much more practical for implementation of an autonomous training protocol. Figure 3.4 shows the strain distribution with a cantilevered aluminum specimen subject to a combination load composed of a 0.3 N· m tip moment simultaneously applied with a 1.4 N tip force. The strain gauges are numbered increasing from root to tip as described in chapter 2. This is the combination load used to train the combination load trained NiTiNOL specimen that approximated training with a constant tip moment. The tip-force load applied compensates for the increase in tip strain caused by the degrading tip moment as the beam deflects due to the geometry of the training structure. This plot demonstrates how a tip moment used in combination with a tip-force load as applied by this training structure can induce a relatively evenly distributed strain throughout a sample.

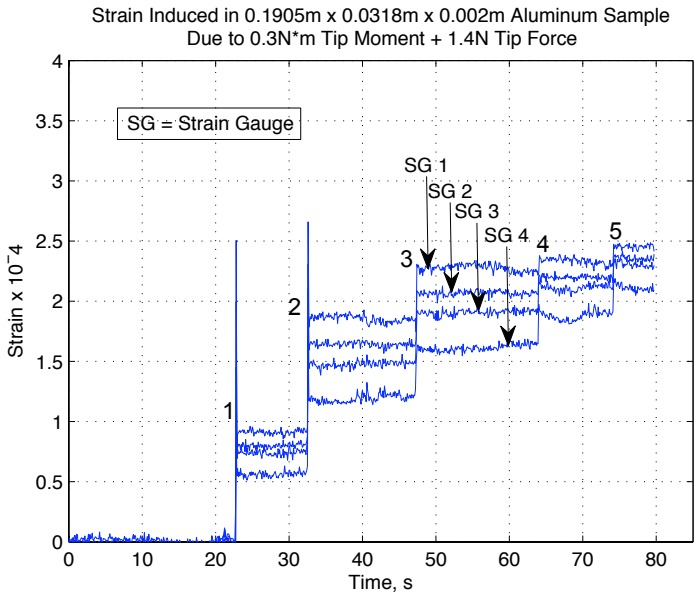

Step #	Total Moment	Total Tip Force
1	0.07 N*m	0.69 N
2	0.14 N*m	1.4 N
3	0.22 N*m	1.4 N
4	0.27 N*m	1.4 N
5	0.3182 N*m	1.4 N

Figure 3.4: Strain induced in 0.1905 m×0.0318 m×0.002 m aluminum sample subject to 0.3 N· m tip-moment load and 1.4 N tip-force load. Tip moment and tip force were incrementally increased in steps, which are numbered in the figure. The legend to the right of the figure provides details on the total tip force and tip moment applied on the specimen after each step.

In addition to the the simultaneous tip-force and tip-moment loading protocol, several strain readings were taken on a specimen subject to a tip-force load as well as just a tip moment induced by the training structure. These were used as supporting evidence that the training structure was inducing the expected similar associated strain within a thicker sample just as in the thinner sample. Table 3.4 indicates which test was conducted under which of the three loading protocols. The test matrix used to perform these various strain readings on the thicker aluminum sample is provided in tables 3.5 and 3.6.

Table 3.4: Loading protocol followed for 4 strain gauge test on $0.1905\,\mathrm{m} \times 0.0318\,\mathrm{m} \times 0.002\,\mathrm{m}$ aluminum sample .

Test #	1- 3	4-6	7-10
Loading Protocol	Tip Force	Tip Moment	Simultaneous tip moment and tip force.

Table 3.5: Strain testing for 0.1905 m×0.0318 m×0.002 m aluminum sample instrumented with four strain gauges.

		Training Structure Side A			Training Structure Side B		
Test #	Washer Mass	# in Set	# of Sets	Total	# in Set	# of Sets	Total
1	35g	4	3	12	-	-	-
		2	1	2	-	-	-
2	35g	4	3	12	-	-	-
		2	1	2	-	-	-
3	35g	6	3	18	-	-	-
		4	1	4	-	-	-
		6	3	18	-	-	-
4	35g	6	2	12	6	2	12
		4	1	4	4	1	4
	25g	8	3	24	8	3	24
5	35g	4	4	16	4	4	16
	25g	6	4	24	6	4	24
6	35g	4	4	16	4	4	16
	25g	6	4	24	6	4	24

Table 3.6: Strain testing for 0.1905 m×0.0318 m×0.002 m aluminum sample instrumented with four strain gauges con't.

		Training Structure Side A			Training Structure Side B		
Test #	Washer Mass	# in Set	# of Sets	Total	# in Set	# of Sets	Total
7	35g	6	2	12	4	2	8
	25g	8	3	24	4	3	12
8	35g	6	2	12	4	2	8
		4	1	4	4	1	4
	25g	4	2	8	4	2	8
9	35g	6	2	12	4	2	8
		4	1	4	4	1	4
	25g	4	2	8	4	2	8
10	35g	6	2	12	4	2	8
		4	1	4	4	1	4
	25g	6	3	18	4	3	12

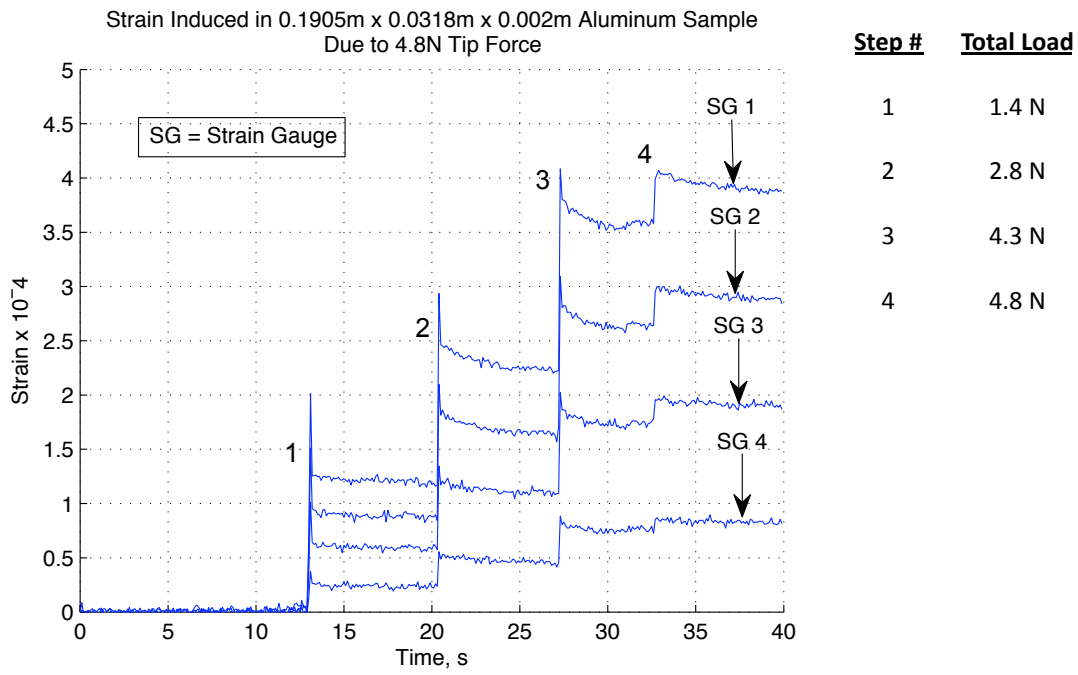

Figure 3.5: Strain induced in a 0.1905 m×0.0318 m×0.002 m aluminum sample subject to a 4.8 N tip-force load. Tip force was incrementally increased in steps, which are numbered in the figure. The legend to the right of the figure provides details on the total tip force applied on the specimen after each step. Strain is highest and most concentrated towards the root of the sample, as expected.

Multiple tip-moment strain tests suggested that as the sample displaces when subjected to a tip moment, a force vector and a force couple are created in the forces applied to the sample tip, just as in the thinner sample. The thicker sample, however, is much stiffer than the thinner aluminum samples. Due to this increase in stiffness, the sample displaces less for a specific initial tip moment, leading to less degradation of the tip moment induced as the beam deflects. Figure 3.6 shows how an incremental increase in tip moment slowly results in higher strain at the

tip of the sample. As the sample starts to displace, a force vector appears and results in tip strain that is greater than root strain and not the desired constant strain distribution along the length of the sample that a constant tip moment with deflection of the sample would produce.

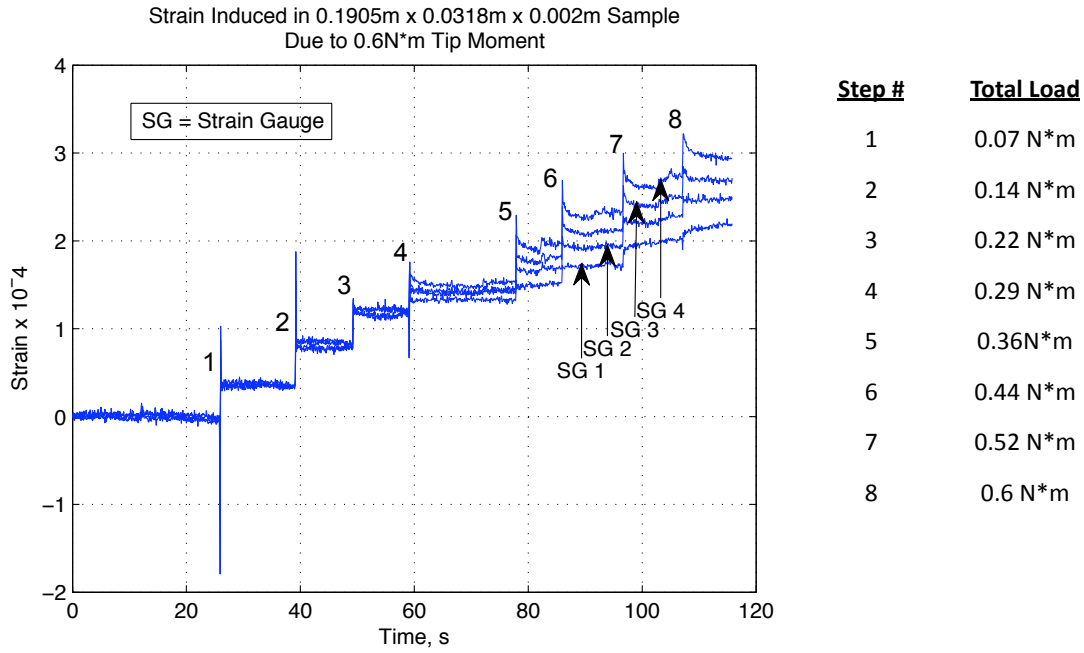

Figure 3.6: Strain induced in $0.1905\,\mathrm{m} \times 0.0318\,\mathrm{m} \times 0.002\,\mathrm{m}$ aluminum sample subject to $0.6\,\mathrm{N \cdot m}$ moment load. Tip moment was incrementally increased in steps, which are numbered in the figure. The legend to the right of the figure provides details on the total tip moment applied on the specimen after each step. Strain increases at a constant rate throughout sample until loads above $0.36\,\mathrm{N \cdot m}$, at which point strain becomes increasingly more concentrated at the tip of the sample.

All strain experiments performed on both sized aluminum samples confirm the training structures ability to induce a tip-force load producing concentrated strain at the root as well as induce distributed strain throughout the sample via a combination of a tip-force and tip-moment type loading as applied by the training structure.

3.3 Kinematic and Parametric Studies

A kinematic study and a parametric study were conducted to assess how well the experimental setup performs. The kinematic study investigated the resulting forces introduced on the tip of a cantilevered specimen as weights are applied to the strings on one side of structure with the intention of producing a tip force. It also investigated the resulting forces introduced on the tip of a cantilevered specimen as equal weights are applied to the strings on the left and right side of the center clamp pulleys with the intention of producing a tip moment.

Figure 3.7 shows how the sample displaces as weights are applied on one side of the structure with the intention of producing a tip force. The magnitude of the string force is equal in all positions, however as is shown in part (b) of figure 3.7, as the beam deflects, the angle at which this force acts on the tip of the cantilevered specimen changes. This implies that the changing angle of the tip force leads to other resulting effects, such as tension, within the specimen.

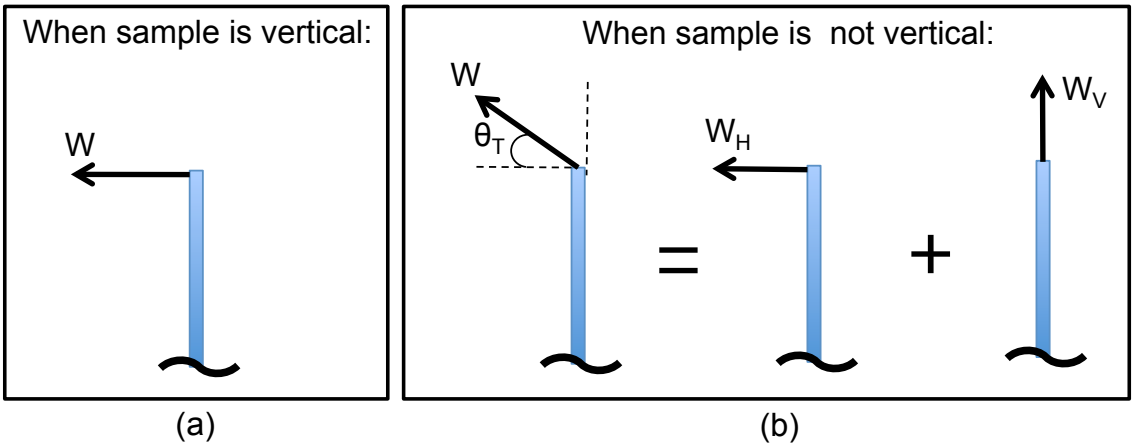

Figure 3.7: Displacement induced in cantilevered sample subjected to a tip force as produced by the training structure. (a) Sketch illustrating tip force applied on cantilevered specimen when the specimen is vertical. (b) Sketch illustrating changing direction of force acting on tip of specimen as as it deflects. The string force only produces a constant tip force when the beam is vertical.

The force applied produces a tip force perpendicular to the specimen only when the specimen is vertical. As the sample displaces, the angle at which the tip force acts on the tip of the sample changes. This tip force can be broken down into a tip force of reduced magnitude acting perpendicular to the length of the specimen and a tip force of reduced magnitude acting parallel with the length of the specimen. This is illustrated in part (b) of figure 3.7.

Although the resulting tip force is introducing additional tension along the length of the specimen, the strain studies indicated that the training structure is capable of producing a tip force that induces concentrated strain at the root of the cantilevered

specimen. For the scope of the research presented in this thesis, this type of strain distribution is comparable to the strain distribution intended.

Figure 3.8 shows how the sample displaces as equal weights are applied on either side of the structure. The magnitude of the string force on the pulleys are equal in all positions, however as is shown in part (b) of figure 3.8, as the beam deflects, the angle at which these equal forces act changes.

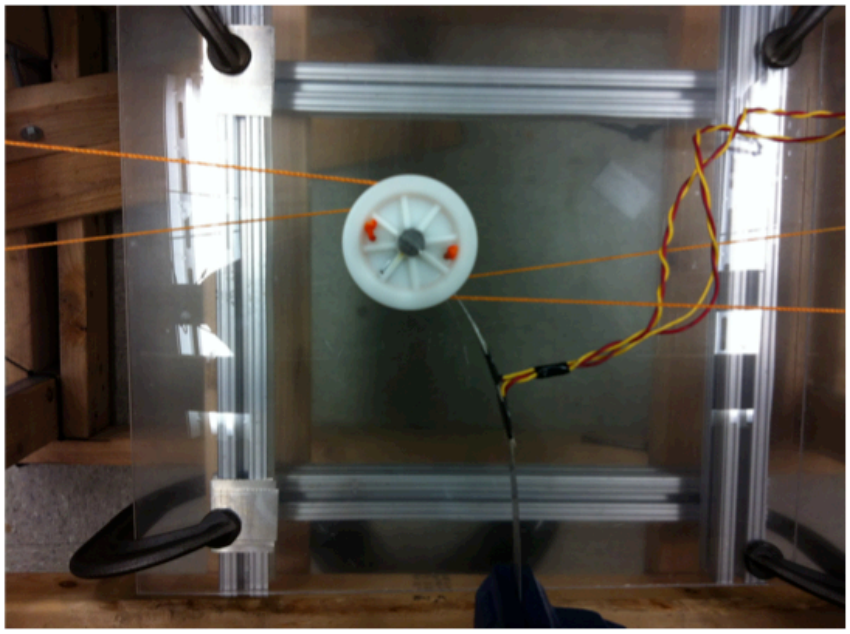

(a)

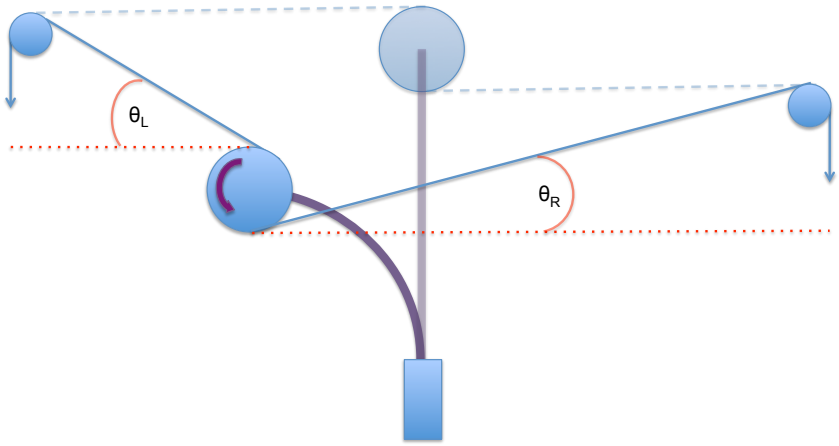

(b)

Figure 3.8: Displacement induced in cantilevered sample subjected to a tip moment as produced by the training structure. (a) Aluminum sample subject to tip moment. (b) Sketch illustrating changing direction of forces acting on center pulley as beam deflects. The string forces only produce a pure moment when the beam is vertical.

The equal forces produce a force couple, and only a moment due to the force couple, when the beam is vertical. As the beam tip deflects in response to the force couple applied when in the vertical position, the directions of the force vectors acting to the left and right of the pulleys are no longer antiparallel. This effectively results in application of a deflection dependent force couple that induces a tip moment of a reduced magnitude plus a residual force vector. This is illustrated in figure 3.9.

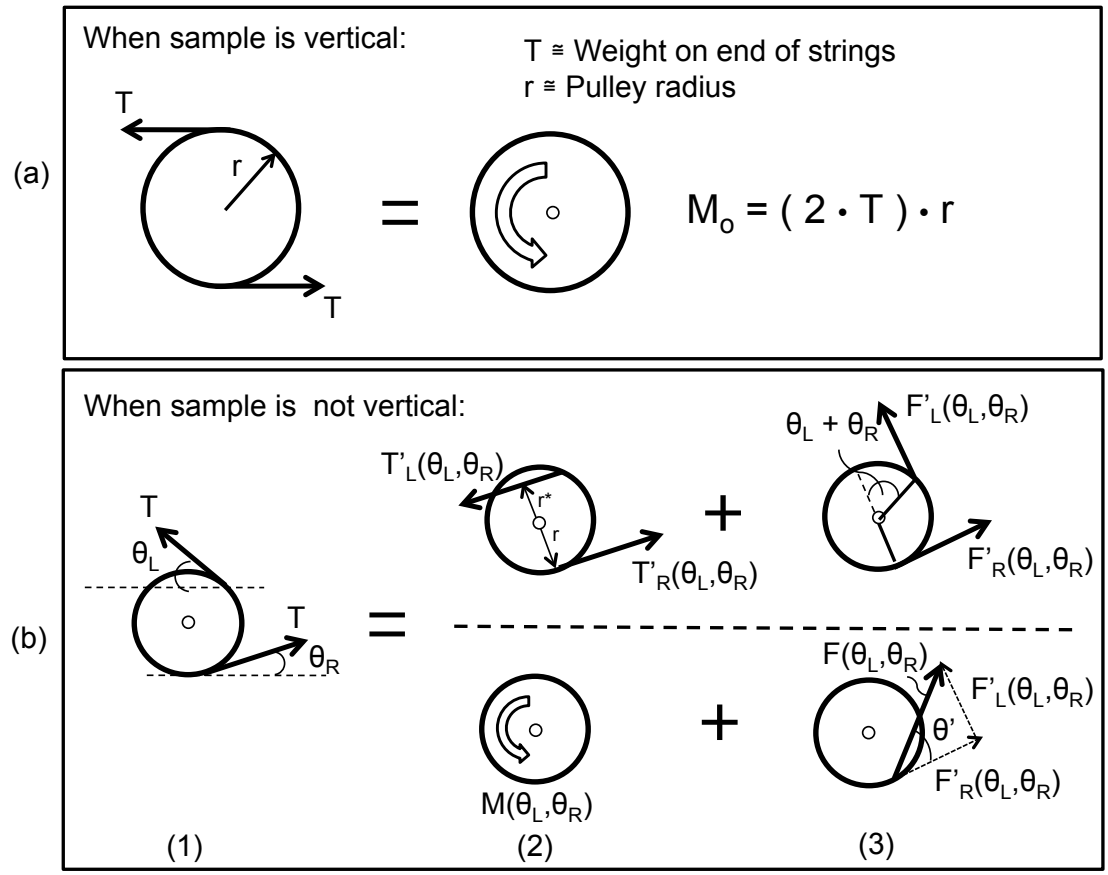

Figure 3.9: Part (a) of this figure represents the force-couple applied to the pulley when the sample is not deflected. Part (b) illustrates how the forces induced on the pulley when the sample is deflected can be broken down into a tip moment plus a residual resultant force.

When the specimen is deflected, the string to the left produces a force vector with a magnitude of T acting at an angle θ_L as shown in sketch (1) in part (b) of figure 3.9. The string to the right produces a force vector with magnitude T acting at an angle θ_R as shown.

Sketch (1) in part (b) of figure 3.9 can be broken down into the reduced tip moment plus the additional resultant force. The reduced tip moment is induced by two anti-parallel force vectors of equal magnitude

$$T'_{L,R}(\theta_L, \theta_R) = T\cos(\theta_L + \theta_R) \tag{3.1}$$

that produce a force couple. This force couple results in two tip moments of unequal magnitude (when multiplied by their respective moment arms). The sum of the two moments results in a tip moment of reduced magnitude

$$M(\theta_L, \theta_R) = [T\cos(\theta_L + \cos_R)] \cdot [r\cos(\theta_L + \theta_R)] + [T\cos(\theta_L + \theta_R)] \cdot r \tag{3.2}$$

where the second "cos" term in equation 3.2 reflects the reduced moment arm [r^* = $r\cos(\theta_L+\theta_R)$] of the top force, T'$_L$, acting on the pulley as shown in sketch (2) of figure 3.9. These force vectors have been arbitrarily selected to be parallel and antiparallel to the lower string force vectors to simplify visualization of concept.

Sketch (3) in part (b) of figure 3.9 illustrates the two orthogonal force vectors that sum to form $F(\theta_L,\theta_R)$, with a magnitude of

$$F(\theta_L, \theta_R) = \sqrt{F_L{}'(\theta_L, \theta_R)^2 + F_R{}'(\theta_L, \theta_R)^2} \tag{3.3a}$$

$$F(\theta_L, \theta_R) = \sqrt{[T\sin(\theta_L + \theta_R)]^2 + [(T - T\cos(\theta_L + \theta_R)]^2} \tag{3.3b}$$

acting at an angle of

$$\theta' = \arctan \frac{F_L'(\theta_L, \theta_R)}{F_R'(\theta_L, \theta_R)} \tag{3.4}$$

As a result of the analysis shown in figure 3.9, it is evident that it is important to minimize both θ_L and θ_R to maximize $M(\theta_L,\theta_R)$. A two dimensional rendering of the geometry relating the structure and sample was developed to assess how the training structure geometry influences θ_L and θ_R, and in turn, the line of action of the force vectors that act on the center pulleys. This drawing can be viewed in figure 3.10. An emphasis was placed on the kinematics of force vectors acting on the center pulleys. The assumptions made in the rendering of the two-deminsional sketch in figure 3.10 are listed as follows.

- The sample is pinned rather than cantilevered so that the sample does not deform as it displaces away from the initial vertical position. In reality, the sample strains and exhibits deformation as the moment is applied.
- The sample is pinned in the center of the training frame, with equal distance to the outer pulleys on either side of the sample tip pulley setup.
- The axis between the two points at which the forces are exerted on each tip pulley remains parallel with the length of the specimen at all times.
- Outer pulleys are aligned with respect to the tip pulleys such that force vectors are anti-parallel and they are perpendicular to the plane in which the specimen lies initially.

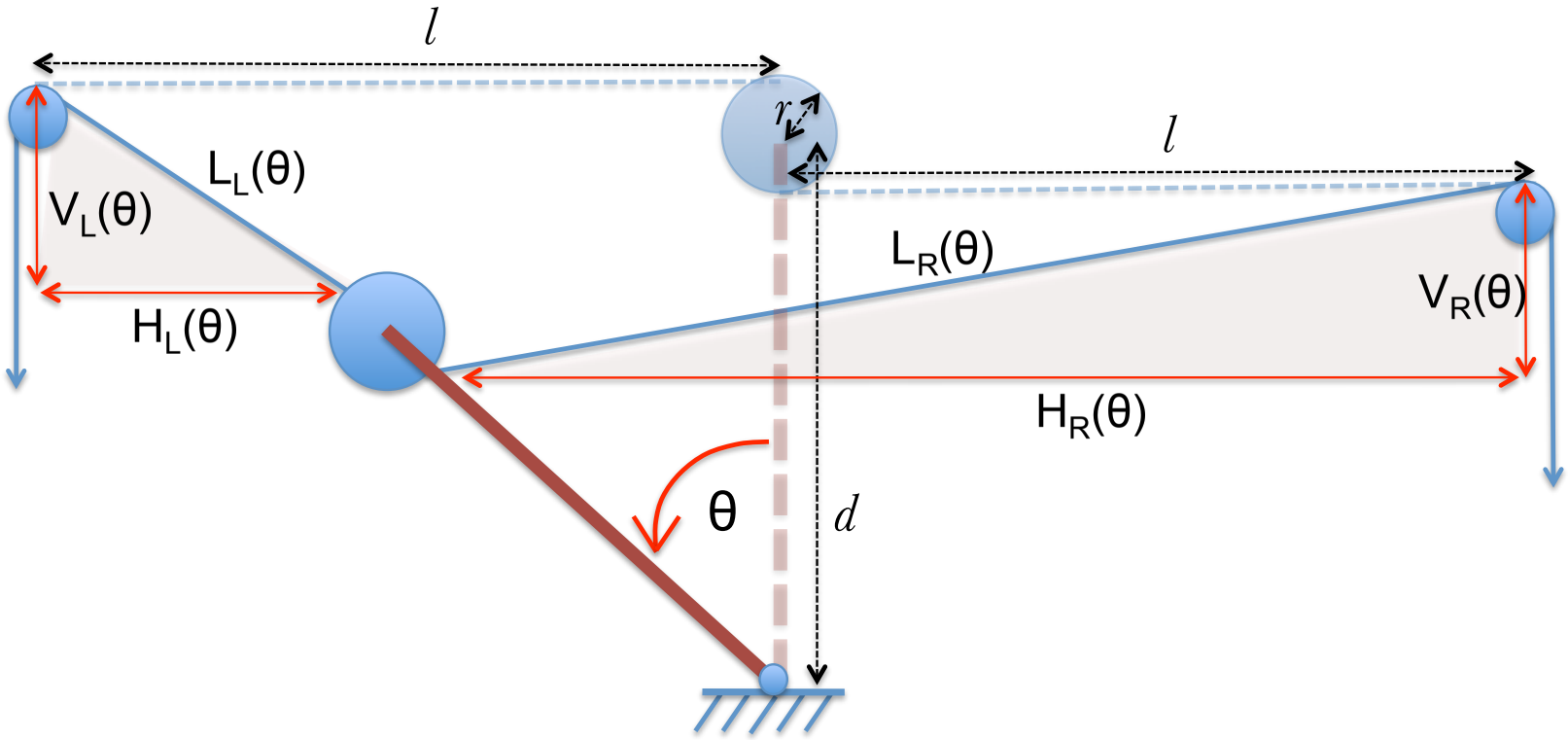

Figure 3.10: Two-dimensional sketch of training structure kinematics showing effect of a counterclockwise tip moment on a rigid pinned sample.

The parameters l, d, and r represent the distance between the axes of the center pulleys and side pulleys in the neutral position, the length of the sample, and the radius of the center pulley. The sample displaces by rotating to the counterclockwise direction from the initial vertical position. The angle of rotation is represented by θ. $L_L(\theta)$ and $L_R(\theta)$ represent the varying distances between string attachment location at the outer radius of the center pulley and upper surface of the side pulleys as the sample displaces. $H_L(\theta)$ and $H_R(\theta)$ are the horizontal components of $L_L(\theta)$ and $L_R(\theta)$, varying as $L_L(\theta)$ and $L_R(\theta)$ vary. $V_L(\theta)$ and $V_R(\theta)$ are the vertical components of $L_L(\theta)$ and $L_R(\theta)$.

From these definitions, the horizontal and vertical components of $L_L(\theta)$ and $L_R(\theta)$ can be extracted as follows:

$$\theta_L(\theta) = \arctan(\frac{V_L(\theta)}{H_L(\theta)}) \tag{3.5}$$

where

$$H_L = l - (d + r)\sin\theta \tag{3.6}$$

$$V_L = d + r - (d + r)\cos\theta = (d + r)(1 - \cos\theta) \tag{3.7}$$

$$\theta_R(\theta) = \arctan(\frac{V_R(\theta)}{H_R(\theta)}) \tag{3.8}$$

where

$$H_R = l + (d - r)\sin\theta \tag{3.9}$$

$$V_R = d - r - (d - r)(\cos\theta) = (d - r)(1 - \cos\theta) \tag{3.10}$$

This parametric study was conducted to quantify the effect of changing center pulley radius and the inner to outer pulley distance on the force vector $F(\theta_L,\theta_R)$ shown in figure 3.9 and equation 3.3a.

Using Matlab, values were calculated for the force vector $F(\theta_L,\theta_R)$ for different combinations of the variable parameters. For a fixed l distance between the center pulleys and outer pulleys, a prescribed θ rotation was applied in the Matlab code and the output for the resultant force vector was calculated. At this point, the radius, r, of the center pulleys was increased and the code was run again. The output for $F(\theta_L,\theta_R)$ was compared to that calculated previously with a smaller center pulley radius. The same process was followed with varying the initial distance between the center and side pulleys and the data was calculated and compared with the other vertical component outputs for each case of varied distance between the center and outside pulleys.

The results of this study indicated that an increase in center pulley diameter increases the magnitude of $F(\theta_L,\theta_R)$ by a small amount, therefore, producing an even more undesirable outcome. An increase in the distance between the center pulleys and side pulleys, however, decreases the magnitude of $F(\theta_L,\theta_R)$ significantly. The magnitude of the residual force vector is approximately inversely proportional to the distance. Alternately stated, doubling the distance between the side and center pulleys roughly halves the magnitude of the residual force vector. Neither

parameter change eliminated the residual force entirely, suggesting that the residual force can only be minimized, but never eliminated entirely by changing the radius of the center tip pulleys or the distance between the center and side pulleys.

Following this parametric study, altering the training structure in such a way that would completely eliminate the resultant force vector is not feasible. This confirms the use of a combination tip-moment and tip-force load as produced by the training structure as a viable option for inducing distributed strain in a cantilevered specimen.

3.4 Summary

The methods and the studies performed to support the methods by which the shape memory training of the NiTiNOL samples was conducted are described here. The test matrix used to load samples equipped with strain gauges and take intuitive strain readings is presented. The strain testing experiments provided valuable insight on the type of loading the structure is capable of producing and that insight was used to determine the type and amount of loading used to train a NiTiNOL specimen in three different ways. Strain study results are presented in this chapter.

Chapter 4

TWSM Training Methodology and Efficacy Evaluation

4.1 Overview

The aim of this research was to explore a new TWSM training load method capable of increasing work potential in a trained specimen and training it such that the specimen does work in a more efficient manner. The methods followed to induce the TWSME under the different loading protocols are described. The methodology by which the results of the TWSM training were evaluated is presented. The results of the efforts taken to characterize each training case as well as evaluate the efficacy of the training protocols used for each case are also presented and discussed in detail.

4.2 Shape Memory Training Protocol

4.2.1 One-Way Shape Memory Training

In order to exhibit the TWSME, each sample first had to be annealed in order to set the parent shape. As described in chapter 2, the annealing process is a heat treatment for NiTiNOL which allows a specimen to exhibit the OWSME and return to a trained rigid parent shape upon heating and transformation from Martensite to Austenite. For all experiments, the samples needed to be trained to return to a straight and flat configuration when heated. The heat treatment prescribed for

these particular specimens calls for a gradual heating rate of 10°C/minute up to 400°C - 600°C. The temperature is maintained at a predetermined temperature in that range for roughly 10 minutes, which is the time required for the specimen to reach the designated temperature throughout it's entirety. The specimen then undergoes a quench or rapid cooling in water. A weight was placed on top of the samples during the annealing process in order to set the parent shape in the flat configuration. The three thinner samples were annealed at 400°C. Two thicker samples required a higher temperature, closer to 600°C, as well as an additional two hours at that temperature in order to ensure that the parent shape was straight and flat. Figure 4.1 provides an image of annealed NiTiNOL strips. Although each specimen retains the straight flat configuration as the parent shape, the specimen exhibits a significant amount of post-training curvature as a result of creep.

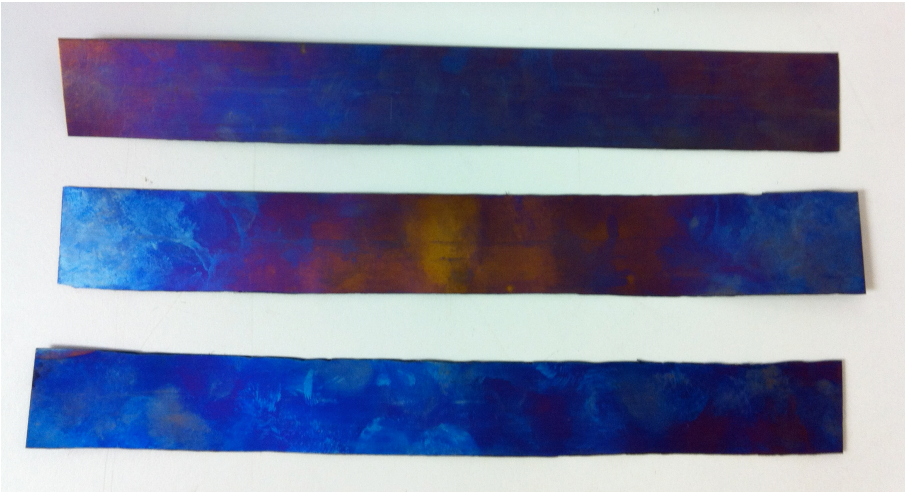

Figure 4.1: 0.2159 m×0.0254 m×0.0005 m NiTINOL samples heat treated to return to flat, straight configuration upon heating to Austenite phase.

Due to the availability of only two thicker samples for the three training protocols, one sample was trained twice. An annealing heat treatment at 600°C for 2 hours was used as a way of resetting the material to the same initial conditions for study of each TWSM training constraint protocols.

4.2.2 Two-Way Shape Memory Training

As discussed in chapter 1, there are various methods by which a SMA specimen can be trained to remember a shape in both the Austenite and Martensite phases. One variable parameter is the loading protocol used to deform a sample into the desired remembered "cold" shape. Once a type and amount of loading to be used has been specified, one can decide on a thermo-mechanical loading path that the specimen in training will be subjected to as well as the number of cycles, or iterations of that particular loading path the sample will undergo.

All thinner samples were used to test the functionality of the training system as well as investigate the maximum tolerable tip moments or tip forces applicable before the samples deform beyond recoverable strain. For the combination-type loads, an appropriate tip force compensating for the degraded integrity of the intended constant tip moment was chosen based on the collected strain data on the moment and tip force that complemented each other best in the aluminum sample strain tests presented in chapter 3.

Two thick samples were trained to exhibit the TWSME using tip force and combination tip-force and tip-moment training protocols developed from these strain

test results and investigation of different type loads on the thinner samples. One thicker sample was trained using a tip force of 1.8 N and subsequently after resetting the parent shape, using a tip force of 4.8 N. The second thicker sample was trained using a combination of a tip moment of 0.3 N· m and a tip force of 1.4 N.

The 4.8 N tip-force and 0.3 N· m tip-moment training loads were determined empirically to be the maximum tip force and tip moment that could be applied during training of a sample without causing the sample tip to start curling under itself or exhibiting excessive deformation after one cycle of training. This was based on observation of sample behavior as a load is applied. As described in chapter 1, the direction-oriented stress field induced during forward transformation (Austenite to Martensite) "plows" further in the direction of the stress applied. This means that whatever loading is used will have a much higher impact on deforming the sample at the end of the training program than after the first few training cycles. It is difficult to predict the deformation the specimen will experience towards the end of TWSM training. Therefore, the load magnitudes presumed to induce the highest possible root strain in the thicker specimens were estimated.

Although the 4.8 N tip-force and 0.3 N· m tip-moment training loads both induce assumed maximum root strain in the samples, the two types of loads can not be directly compared. A second comparison strategy was identified in which the magnitude of stress at the root of a sample was the same for the tip moment and tip force. A tip force of 1.8 N was found, using equations 4.1 and 4.2 and assumed small deflection, to produce the same root stress as that induced by the 0.3 N·m

tip-moment load. These calculations were based on a cantilevered beam with a uniform cross-section as illustrated in figure 4.2.

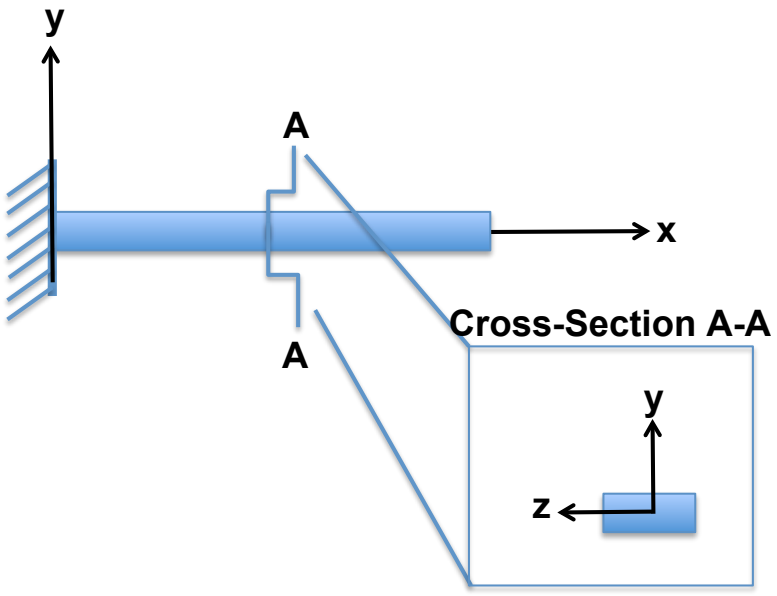

Figure 4.2: Description of coordinate system used on cantilevered beam with cross section view.

$$\sigma(d_x) = \frac{M_z(d_x) \cdot y(d_x)}{I_z} \tag{4.1}$$

$M_z(d_x)$ is the moment induced by a tip load. If the tip load was a force, F, acting perpendicular to the beam at d_x=l, where l is the length of the beam, then

$$M_z(d_x) = F \cdot d_x = F \cdot l \tag{4.2}$$

F is the tip weight applied and d_x is the moment arm which, in this case, is the length of the sample. For the loading case where a force couple is applied to two pulleys fixed at the tip of a cantilevered sample, the moment is:

$$M_z = 2 \cdot (2 \cdot F) \cdot r \tag{4.3}$$

where $(2 \cdot F) \cdot r$ is the magnitude of the force couple produced on each of the pulleys with an outer radius of r that are attached to the tip of the sample.

Based on these calculations, a tip-force load of 1.8 N has comparable root stress to that induced by a 0.3 N$\times$ m tip-moment load. Based on Hooke's Law [7] (equation 4.4), it can be assumed that the two loads also produce comparable root strain in the cantilevered specimen. The variable $\epsilon(d_x)$ in equation 4.4 represents strain along the length of the specimen and E represents Young's modulus of elasticity (constant).

$$\sigma(d_x) = E \cdot \epsilon(d_x) \tag{4.4}$$

As discussed in chapter 1, the method by which the samples in this experiment were trained to exhibit the TWSME is known as constrained thermal cycling of deformed Martensite [9]. Each sample remained constrained by the methods described in chapter 2 and the loading specified in the previous paragraph during the entire training process. Although the samples had the freedom to do work and displace under their respective load when transforming from the Martensite phase to the Austenite phase, the constraints were consistently imposed. The specimens were each forced to return to the shape induced by the type of loading used for that particular training session when returning to the Martensite phase upon cooling.

The next step in inducing the TWSME is to cycle the temperature of the constrained sample between a temperature above A_f and a temperature below M_f. For all training sessions conducted in these experiments, the samples were first heated to 120°C and then cooled to 40°C. This set of heating followed by cooling while constrained constituted one training cycle. In order to stabilize a hysteretic response and properly induce the TWSME, each specimen endured a training program consisting of 500 total cycles [9]. This number was chosen based on the training method being used and the thickness of the sample being trained. More cycles can be performed if necessary to induce the TWSME. Due to the autonomous nature of the LabView program developed to perform the SMA training as well as the extended period of time required to perform 500 thermo-mechanical loading cycles (roughly four days) on a specimen, the webcam was setup such that the entire training process was documented in a time lapse video consisting of two seconds between frames. The camera is positioned such that a birds eye view of the sample is displayed. From this viewpoint, the shape of the sample as it deforms under loading and transitions between the Austenite and Martensite phases is easily viewed.

4.2.3 Testing for Training Success

In order to see if training program worked on the various samples, a customized heating experiment was conducted after each specimen underwent training. To perform these tests, the samples were freed of all constraints at their tip, but remained cantilevered at the root in the same position as before. With all strip heaters and

thermocouples in the same locations as they occupied during training, the samples were heated to 120°C then cooled to 30°C. During this test, the movement of the specimens was monitored using the same webcam used to monitor the training procedures. The movement of the sample during phase transformation was recorded on a 1080p HD video. Each video was then post-processed and sped up 14× to clearly depict any deformation occurring within the sample during heating and cooling. These videos allowed for confirmation of successful TWSM training. All samples were able to "remember" both a hot and cold shape. Figures 4.3, 4.4, and 4.5 provide images of the TWSM trained samples for all three cases in the Martensite and Austenite case.

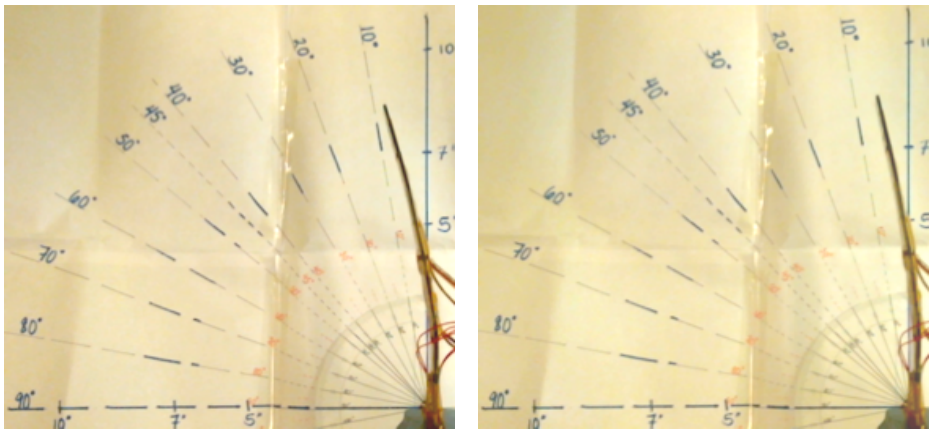

(a) (b)

Figure 4.3: 1.8 N Tip-Force TWSM Trained Sample Shape (a) Image of 1.8 N tip-force trained specimen in Martensite phase. (b) Image of 1.8 N tip-force trained specimen in Austenite phase.

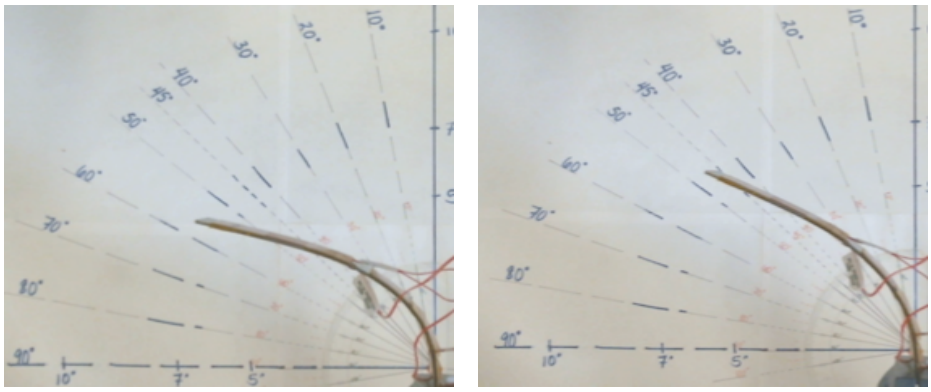

(a) (b)

Figure 4.4: 4.8 N Tip-Force TWSM Trained Sample Shape (a) Image of 4.8 N tip-force trained specimen in Martensite phase. (b) Image of 4.8 N tip-force trained specimen in Austenite phase.

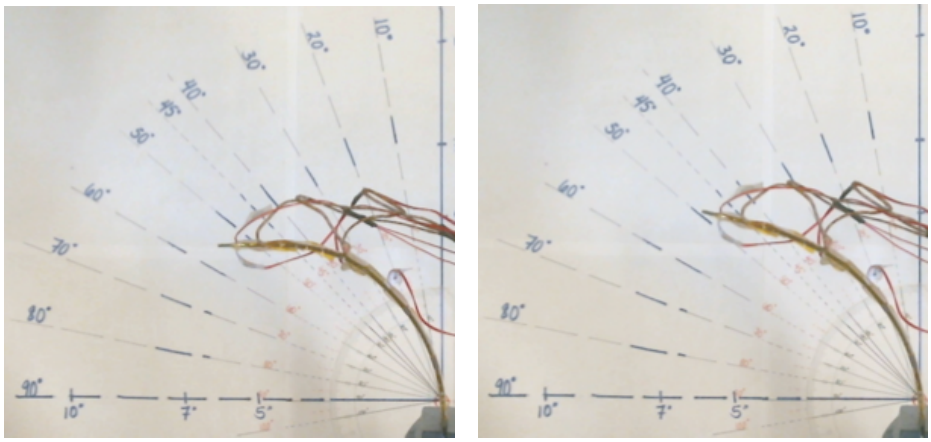

(a) (b)

Figure 4.5: 0.3 N· m Tip-Moment + 1.4 N Tip-Force TWSM Trained Sample Shape (a) Image of combination load trained specimen in Martensite phase. (b) Image of combination load trained specimen in Austenite phase.

4.3 Methods of Training Protocol Comparison

4.3.1 Evaluating Work Potential of Trained Samples

Once the thicker samples were trained, their ability to carry a load when transforming from the Martensite phase to the Austenite phase was evaluated. The structure was modified, as described in chapter 2, and the webcam was repositioned to allow for proper observation of specimen displacement between both the hot and cold phases. In order to evaluate and compare the work potential of a specimen trained under all three loading protocols implemented, a test matrix was developed which dictated the amount of weight applied at each point which the displacement was measured. The tip masses used for all three cases ranged from no mass to 420 g using the following increments which were readily achievable with the available weights (washers): 0 g, 70 g, 120 g, 165 g, 235 g, 295 g, 350 g, 385 g, and 420 g. The vertical position of the beam tip under these tip-mass loads was recorded for both the Martensite and Austenite phase.

All position measurements were done via photographs taken using the webcam. The sample was cantilevered once again at the root and positioned between the grid backdrop created for measuring the position of the tip of the sample and the line of site of the webcam. A picture was taken at that point in the Martensite state, and the vertical position of the tip of the sample being evaluated was measured against the grid backdrop, first at a no load state. The image capturing the sample trained with a 0.3 N$\cdot$ m tip moment and a tip force of 1.4 N used to document the

vertical position of the tip of the sample at no load Martensitic state is presented in figure 4.6.

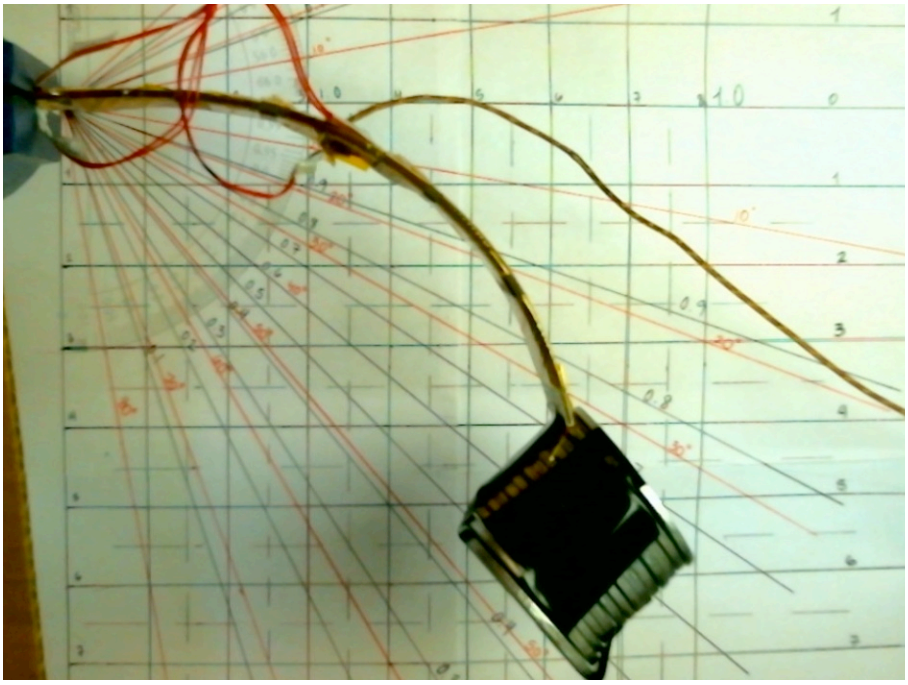

Figure 4.6: Combined tip-moment and tip-force trained NiTiNOL sample in Martensite phase.

The sample was then heated to 130°C, where another photograph was taken and used to measure the vertical position of the tip of the sample in the Austenite phase. The sample was then cooled using the fan system down to a temperature below M_f of 25°C, cool enough for the sample to be handled. The specimen was then loaded by the first predetermined tip mass and another photo was captured so that the position of the tip of the sample in the Martensite phase could be documented and any initial displacement in the sample due to the tip mass can be observed. The sample was then heated, another photo was captured, and then cooled, just as

before, prior to increasing the tip mass. This cycle was repeated until the highest tip mass was reached, at which point, the mass was removed while the sample was still Austenitic, and the sample was allowed to cool to 25°C. This entire set of increasing tip masses and position observation photo capturing was repeated twice more for a total of three trials. These three trials were conducted for each of the three load training cases. A table providing the recorded vertical displacement values for each case in all three trials is presented in appendix B.

In order to analytically compare the vertical displacement produced under the various loads by each case, the average of both the Martensite and Austenite vertical tip positions was calculated and the difference in the values of the Martensite and Austenite average vertical positions was read as the average vertical displacement. This is the vertical displacement that occurs in the sample when transforming between the Austenite and Martensite phases carrying the respective tip mass. The vertical positions of the samples in both the Martensite and Austenite phases were plotted against the respective tip force applied when those vertical positions were recorded. The vertical positions were plotted on the x axis and the tip froce magnitude on the y axis. The work potential of a sample when subject to a given tip force is the product of the force and displacement. This is proportional to the rectangular area under the line drawn from point (a) to point (b) in figure 4.7, where point (a) represents the point at which the load line meets the Austenite displacement line and point (b) represents the point at which the load line meets the Martensite displacement line. This area is proportional to the integral of

$$\int_{y_{Austenite}}^{y_{Martensite}} m \cdot g \cdot dy \tag{4.5}$$

where m is the mass used to apply a tip force and g is the acceleration due to gravity.

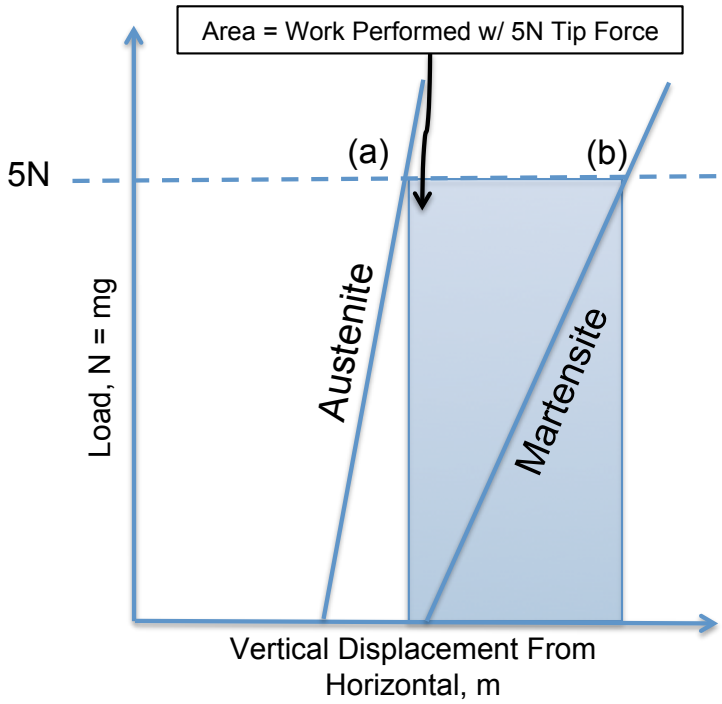

Figure 4.7: Example of how work potential is measured using the area of a rectangle drawn within the plot of sample vertical displacement when lifting a tip mass.

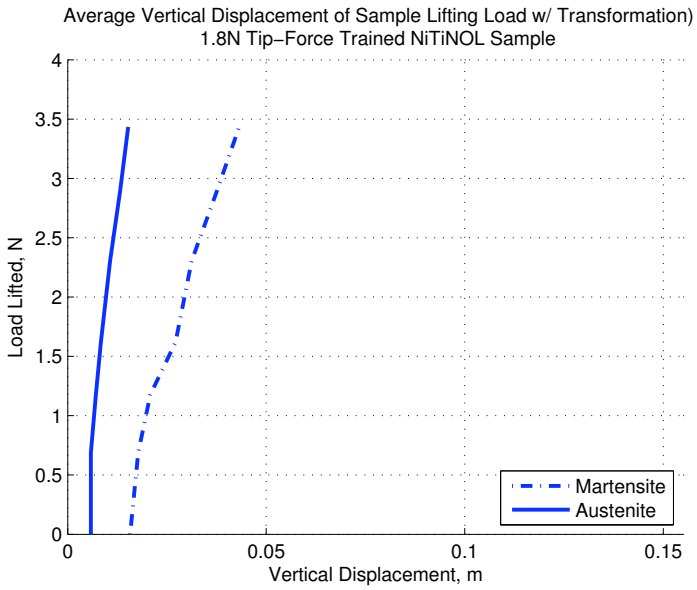

Figure 4.8: Vertical displacement of 1.8 N tip-force trained specimen measured at Austenite and Martensite phase for varying tip masses.

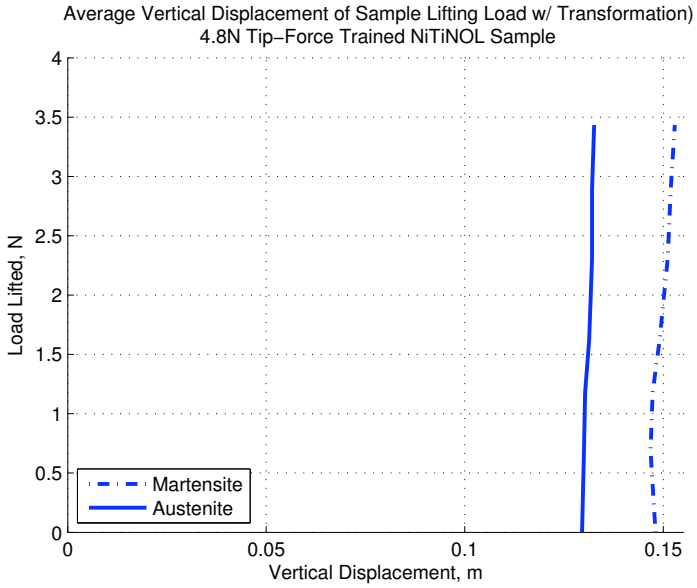

Figure 4.9: Vertical displacement of 4.8 N tip-force trained specimen measured at Austenite and Martensite phase for varying tip masses.

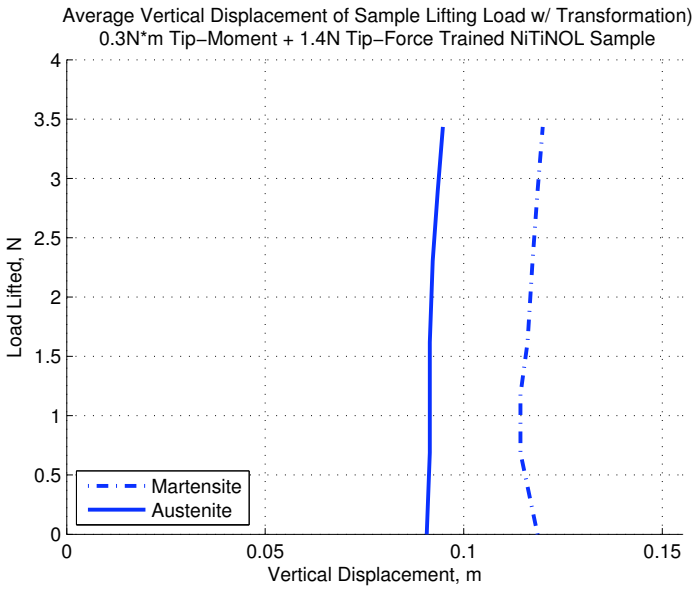

Figure 4.10: Vertical displacement of 0.3 N· m tip-moment and 1.4 N tip-force combination trained specimen measured at Austenite and Martensite phase for varying tip masses.

Examining these plots alone, the vertical displacement between the Martensite and Austenite phase in the no load state is largest with the 0.3 N· m tip-moment and 1.4 N tip-force combination trained specimen and smallest with the 1.8 N tip-force trained specimen. As described and illustrated in figure 4.7, the work performance of a sample is characterized by measuring the area created in the rectangle drawn underneath the horizontal tip-mass load line between the two phase vertical displacement lines.

Figures 4.11, 4.12, and 4.13 provide plots of the area of the work performance rectangles created for each tip mass lifted.

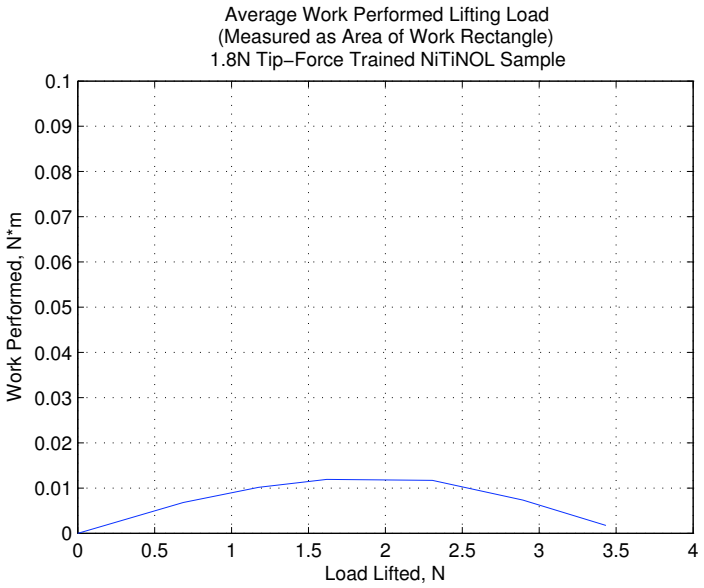

Figure 4.11: Work performed by a 1.8 N tip-force trained specimen lifting varying tip masses.

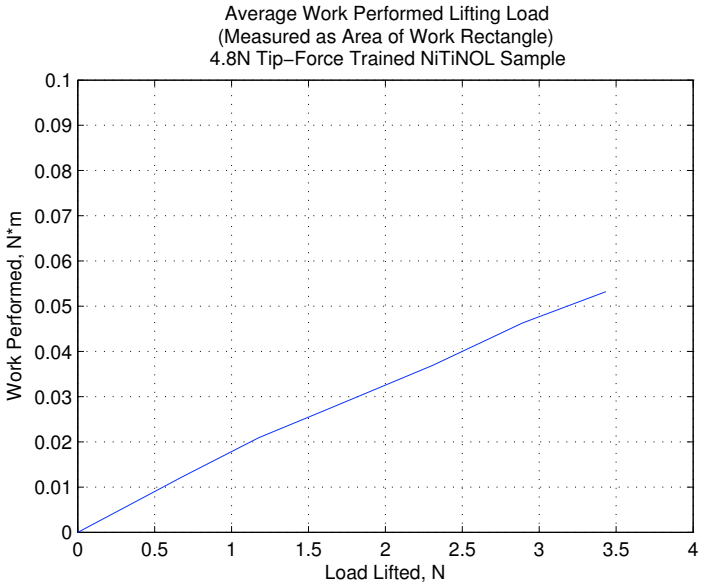

Figure 4.12: Work performed by a 4.8 N tip-force trained specimen lifting varying tip masses.

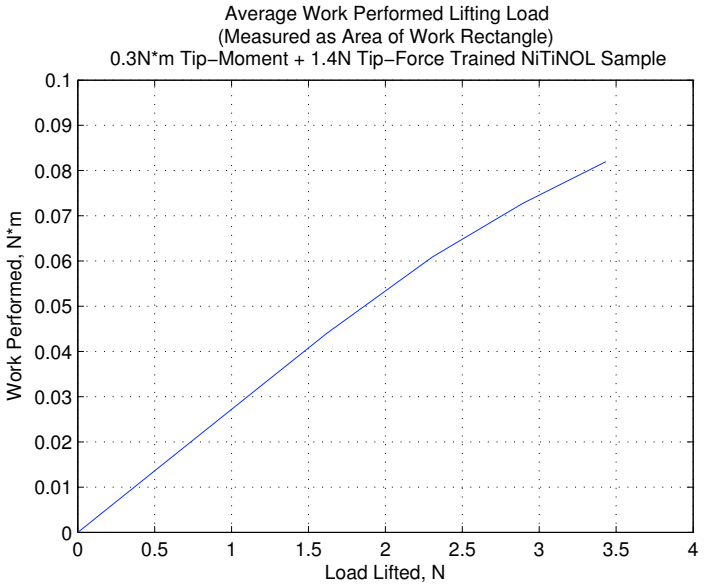

Figure 4.13: Work performed by a 0.3 N· m tip-moment and 1.4 N tip-force combination trained specimen lifting varying tip masses.

The curve representing the work performed by a 1.8 N tip-force trained specimen during TWSM transformation while lifting varying tip masses indicates that as the tip force increases beyond 2 N in magnitude, the vertical displacement begins to decrease. This implies that a 1.8 N tip-force trained sample is characterized by a limit in work potential at a tip-force load of 2 N. In comparison, the specimen trained using a 4.8 N tip force demonstrates work potential well beyond the ability to lift 2 N and continues to perform increasing work as the tip force is increased up to 3.4 N.

As explained previously, the platform of comparison between the three cases is based on root strain. The specimen trained at a 1.8 N tip force has root strain that is comparable with that of the 0.3 N$\cdot$ m tip-moment and 1.4 N tip-force combination trained specimen. Examining and comparing the work performance plots of these two training cases indicates that the combination load trained specimen, i.e. the training protocol that induces distributed strain throughout the specimen, is capable of producing more work than the tip-force trained specimen. Comparison between the combination load and the 4.8 N tip-force trained specimen indicates that training the specimen with these particular training protocols with a force that induces higher root strain does not yield higher work performance.

4.3.2 Evaluating Training Method Efficacy

The recoverable strain energy within the trained samples was also calculated and used as a way of evaluating the efficacy of a given training constraint method

and the efficiency with which a SMA specimen performs work as a result of that constraint method. Stated alternately, if a sample has a higher value of recoverable strain energy, it produces work in a more efficient manner than a sample with a lower calculated recoverable strain energy. To analytically quantify the amount of recoverable strain energy in a sample, the curvature of the trained specimens in both the Austenite and Martensite phase was plotted versus the length of the sample. A higher amount of curvature over the length of the sample indicates more strain distribution and that more of the sample is being used to perform work during the transformation process. In order to obtain the curvature of the specimen, the photos captured in the no-load state as in figures 4.3, 4.4, and 4.5 were uploaded into a software called GeoGebra [24]. In this program, a best fit polynomial or conical curve can be extracted from placing dating points along the length of the sample in the image. The points can be adjusted to achieve the best fitting curve in real time. GeoGebra [24] provides the equation for the curve chosen and using this equation, Matlab can be used to calculate the x and y coordinates representing the length of the sample. The coordinates can then be plotted in Matlab in an effort to model the actual shape and deflection of the sample. Three best fit polynomials or conical equations were extracted and averaged in an effort to best represent the final sample hot and cold shapes. Figures 4.14, 4.16, and 4.18 show the final sample shape in Martensite phase for each of the TWSM training cases. Figures 4.15, 4.17, and 4.19 show the final sample shape in Austenite phase for each of the TWSM training cases. The three separate modeled beam shapes that were averaged to create the

final model of the beam shape presented in this chapter are also plotted individually and presented in appendix C.

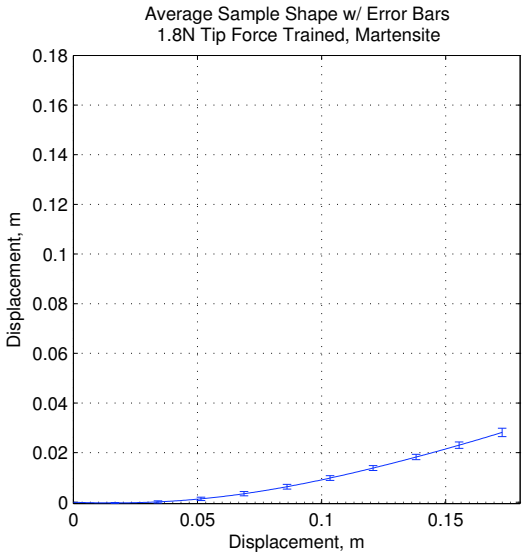

(a)

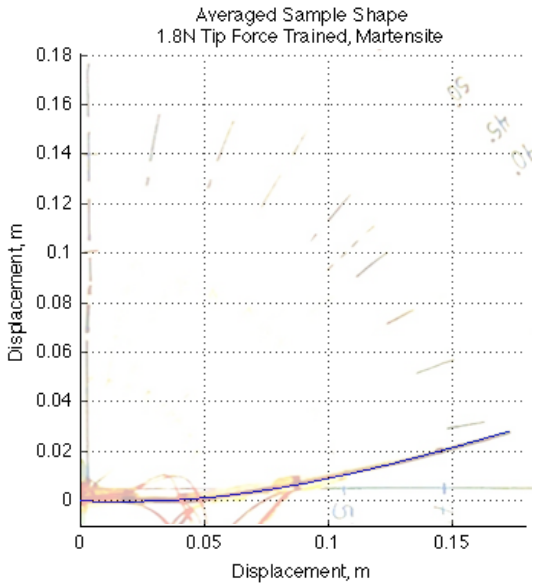

(b)

Figure 4.14: Modeled sample shape of 1.8 N tip-force trained specimen in Martensite phase: (a) Averaged sample shape. (b) Sample shape model superimposed with image of actual specimen.

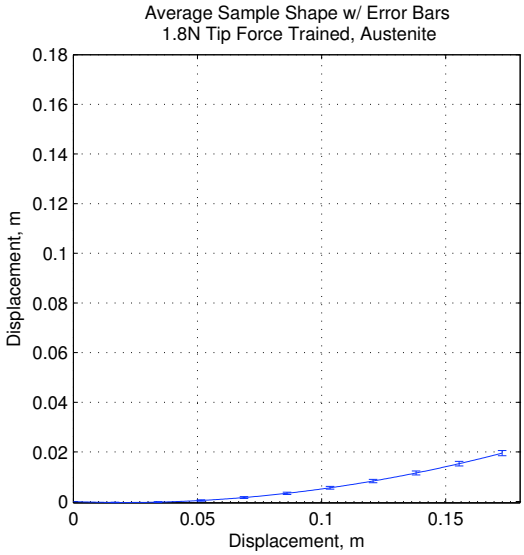

(a)

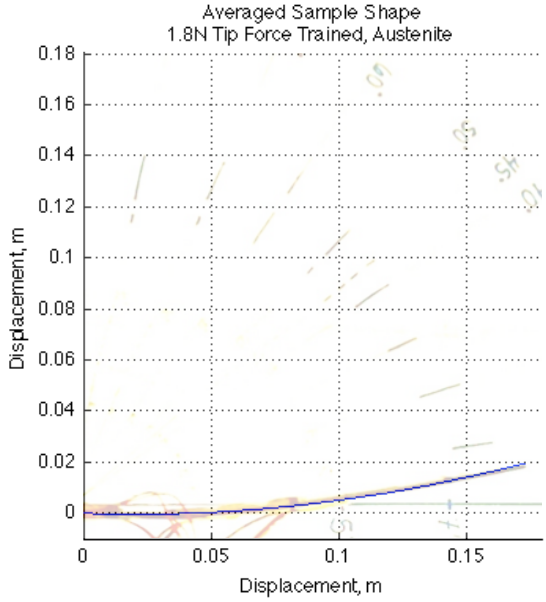

(b)

Figure 4.15: Modeled sample shape of 1.8 N tip-force trained specimen in Austenite phase: (a) Averaged sample shape. (b) Sample shape model superimposed with image of actual specimen.

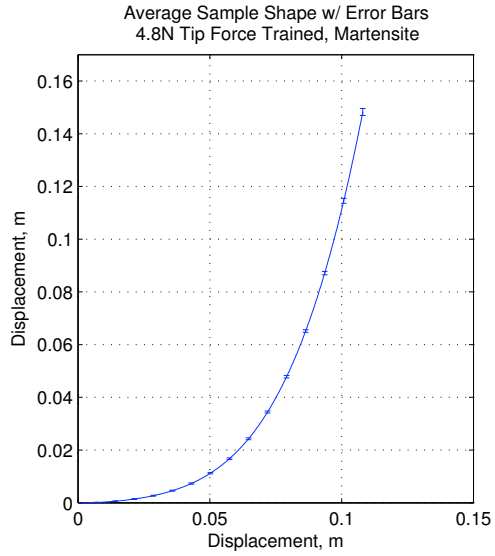

(a)

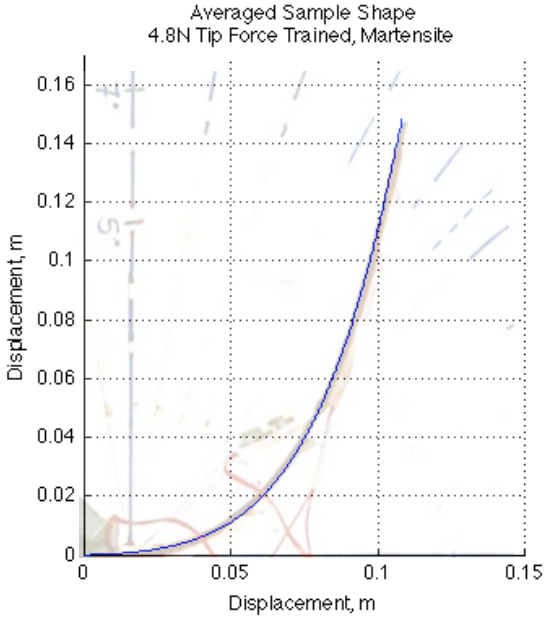

(b)

Figure 4.16: Modeled sample shape of 4.8 N tip-force trained specimen in Martensite phase: (a) Averaged sample shape. (b) Sample shape model superimposed with image of actual specimen.

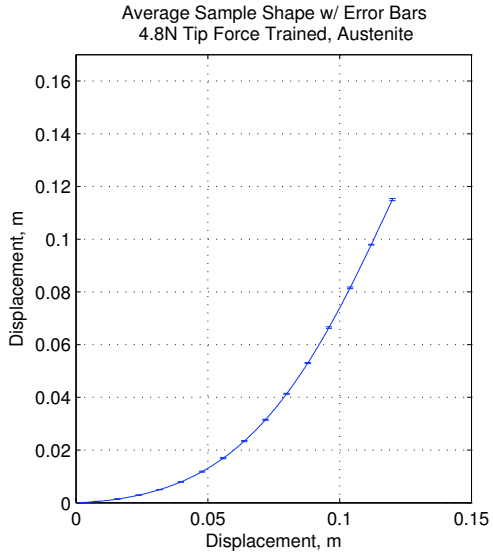

(a)

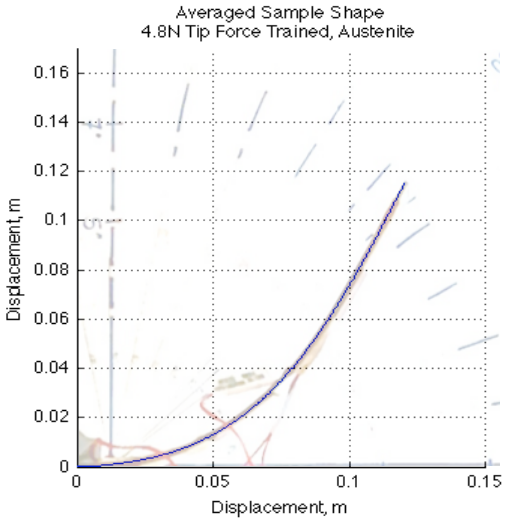

(b)

Figure 4.17: Modeled sample shape of 4.8 N tip-force trained specimen in Austenite phase: (a) Averaged sample shape. (b) Sample shape model superimposed with image of actual specimen.

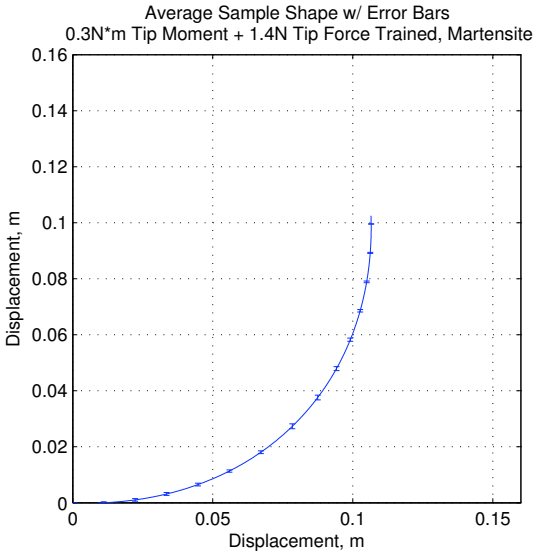

(a)

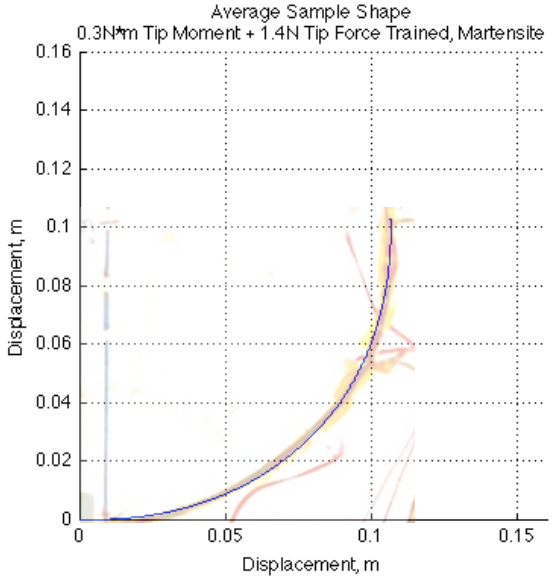

(b)

Figure 4.18: Modeled sample shape of 0.3 N· m tip-moment plus 1.4 N tip-force trained specimen in Martensite phase: (a) Averaged sample shape. (b) Sample shape model superimposed with image of actual specimen.

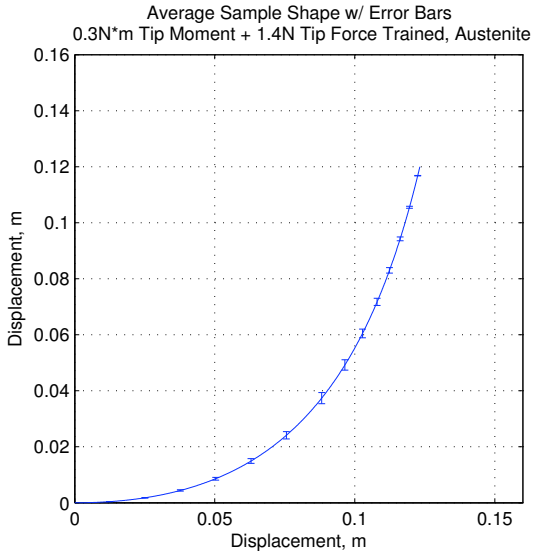

(a)

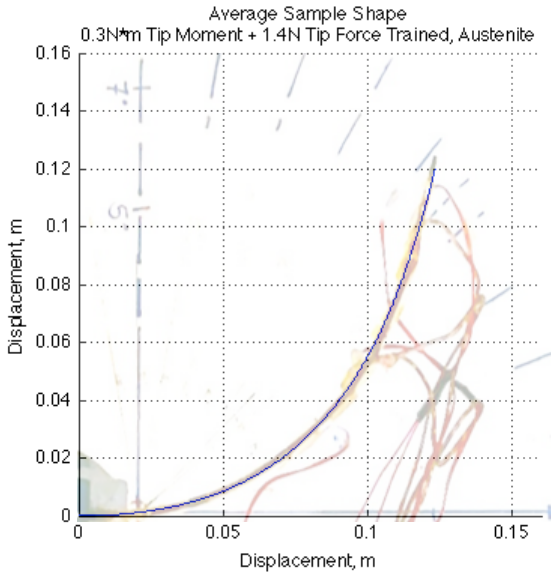

(b)

Figure 4.19: Modeled sample shape of 0.3 N· m tip-moment plus 1.4 N tip-force trained specimen in Austenite phase (a) Averaged sample shape. (b) Sample shape model superimposed with image of actual specimen.

Using these final models for the trained sample shape, the curvature can be calculated using the defined curvature equation 4.6 [25], which applies to any function that can be differentiated twice.

$$\kappa(x) = \frac{f''(x)}{[1 + (f'(x))^2]^{\frac{3}{2}}} \tag{4.6}$$

Equation 4.6 defines curvature as a function of x, which represents horizontal displacement rather than specimen length. The sketch in figure 4.20 demonstrates how the length of the sample does not match the horizontal position of the deformed sample along the x axis when the deflection is large.

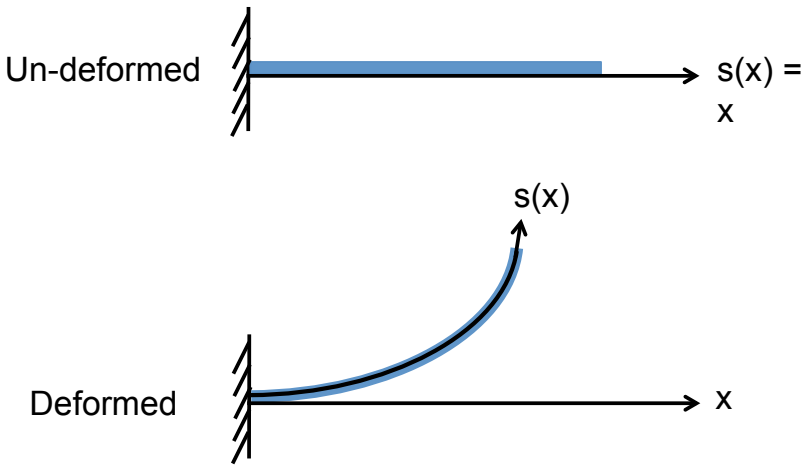

Figure 4.20: Sketch demonstrates why horizontal position of sample tip along the x axis in the deformed state does not match sample length. Definition of arclength $s(x)$ must be used to map sample length to horizontal position along x axis when sample exhibits large deflection.

To put equation 4.6 in terms of length along the sample, defined as s, the arc length formula, equation 4.7, is used to relate the x coordinate in equation 4.6 to

sample length, s, by solving equation 4.7 for x and substituting x as a function of s into equation 4.6. This equation applies to a beam of any size exhibiting any magnitude of deflection.

$$s(x) = \int_0^x \sqrt{1 + (f'(x))^2} dx \tag{4.7}$$

This procedure for obtaining curvature was done for both the Austenite and Martensite shapes of the samples with the averaged models from GeoGebra [24] for all three trained cases. After the curvature for each case was plotted with respect to sample length, the area underneath the plotted curve was calculated by numerically integrating the curvature using the mid-point rule [25]. Figures 4.21, 4.22, and 4.23 show the calculated curvature for the Martensite and Austenite phases for all three training cases. The total area under the curve is also included in the title of each plot.

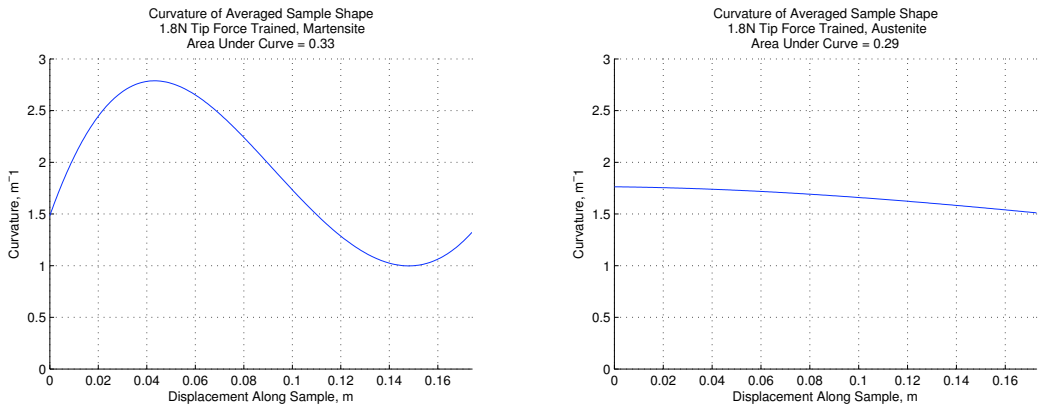

(a) (b)

Figure 4.21: Curvature of 1.8 N tip-force trained specimen modeled TWSM trained shape: (a) Curvature along length of modeled sample shape in Martensite phase. (b) Curvature along length of modeled sample shape in Austenite phase.

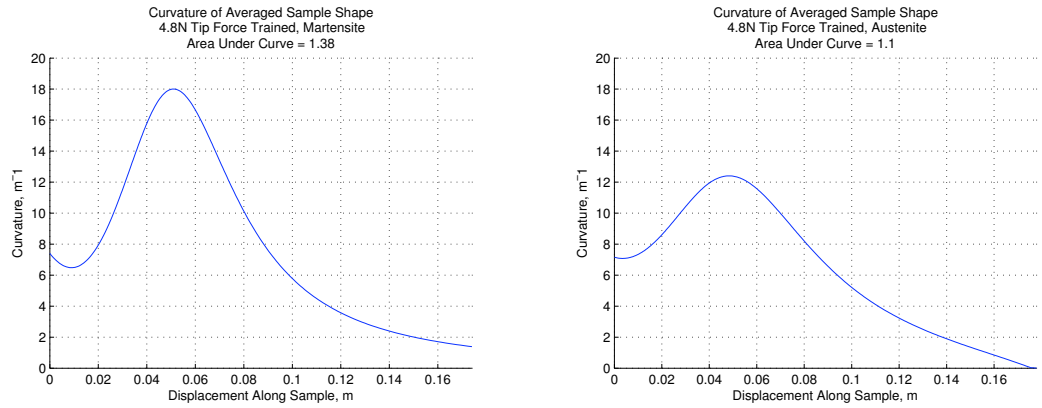

(a) (b)

Figure 4.22: Curvature of 4.8 N tip-force trained specimen modeled TWSM trained shape: (a) Curvature along length of modeled sample shape in Martensite phase. (b) Curvature along length of modeled sample shape in Austenite phase.

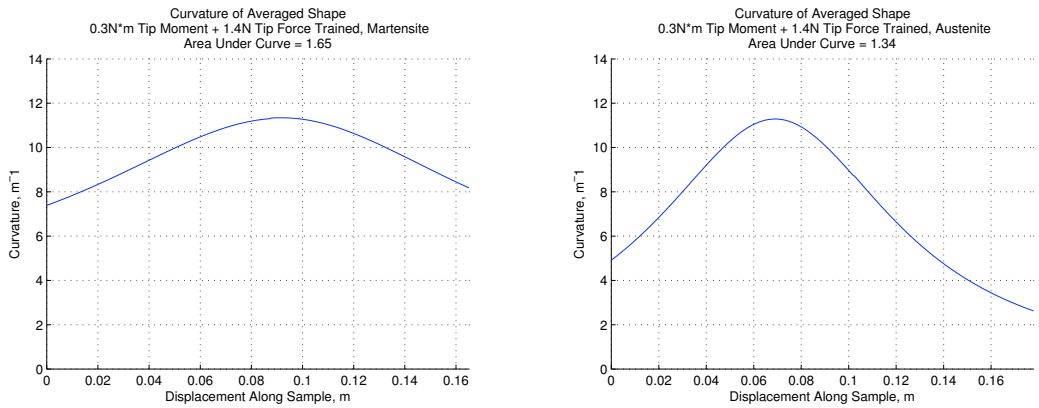

(a) (b)

Figure 4.23: Curvature of 0.3 N· m tip-moment plus 1.4 N tip-force trained specimen modeled TWSM trained shape: (A) Curvature along length of modeled sample shape in Martensite phase. (b) Curvature along length of modeled sample shape in Austenite phase.

The difference in the area under the curvature curve for the Austenite shape and that for the Martensite is comparible to the recoverable strain energy within a trained sampled. Therefore, the difference between the two phase curvature areas was calculated for each training set and compared to the strain energy of the other cases. Table 4.1 provides the calculated areas under the curvature curves for both the Martensite phase and Austenite phase as well as the difference between the two areas for all three of the training cases.

Table 4.1: Calculated Area Under Curvature Curves

	Martensite	Austenite	Difference in Phase Areas
1.8 N Tip-Force Trained	0.33	0.29	0.04
4.8 N Tip-Force Trained	1.38	1.1	0.28
0.3 N· m Tip-Moment + 1.4 N Tip-Force Trained	1.65	1.34	0.31

These calculations indicate that the amount of recoverable strain energy in the combination load trained sample is higher than that in both of the tip-force trained cases. As with the plots investigating work potential, a higher magnitude of root concentrated strain did not yield higher recoverable strain energy within the sample.

4.4 Summary

The training protocol used to induce the TWSME in each case specimen is described here. A breakdown of the number and types of samples that were trained to exhibit the TWSME is provided along with information regarding which constraint method was used. The magnitudes of the loads used for the different constraint methods and the methods by which they were chosen are described. The reasons behind choosing induced root strain as the platform for work performance comparison between the training cases are presented and discussed. The success of the TWSM training method used is confirmed. The results and a comparison of the work performance evaluation conducted on the trained sample are presented. The efficacy of the constraint methods is also evaluated and the outcome of the studies used to determine specimen efficiency in work production are discussed.

Chapter 5

Conclusions and Future Work

5.1 Overview

The work presented in this thesis investigated two different types of constraint methods for TWSM training of SMAs. Two specimens were cantilevered and subject to tip forces of 1.8 N and 4.8 N inducing concentrated root strain using the custom designed and constructed training structure. A third specimen was cantilevered and subject to a combination of a 1.4 N tip force and a 0.3 N$\cdot$ m tip moment, which induced a relatively constant strain along the length of the sample as it deflected under the load. A training system was developed to subject the specimens to cyclic thermal loading and train them to exhibit the TWSME. The three specimens were trained successfully to "remember" both a hot and cold shape. Varying tip masses were used to evaluate the work potential of each training load case by measuring their vertical displacement during phase transformation. The curvature was extracted from images taken of each case specimen in the Martensite and Austenite phase and used to characterize the efficiency with which a specimen trained under the training constraint used can perform work.

5.2 Concluding Remarks

The training structure and electrical system developed to induce the TWSME effect in SMA specimens were successfully used to conduct TWSM training via the constrained thermal cycling of deformed Martensite method. The macrostructural shape change in the specimens during both forward (Austenite to Martensite) and reverse transformation demonstrated that the chosen OWSM and TWSM training methods are effective.

The structure used to induce the training constraints can be successfully used to induce concentrated strain at the root of a cantilevered specimen but does not induce a proper tip force (force vector acting on specimen tip does not remain perpendicular with respect to specimen). The strain studies conducted confirmed that the structure could not be used to induce a pure tip moment. The results, did however, demonstrate how a tip force as induced by the training structure can be used in combination with a tip moment as induced by the training structure to subject a cantilevered specimen to evenly distributed strain throughout its entirety.

Two specimens were constrained during training using tip forces of 1.8 N and 4.8 N. The 1.8 N tip force induces root strain that is comparable to that induced by a 0.3 N$\cdot$m tip moment with assumed small deflection. The work potential of the 1.8 N tip-force trained specimen was evaluated and compared with that of a specimen trained using a combination of a 0.3 N$\cdot$m tip moment and 1.4 N tip force. The work performed by each sample was measured by the specimen's ability to lift a tip mass with reverse transformation (Martensite to Austenite). The vertical

displacement data recorded for each case lifting varying tip masses indicate that the specimen trained under the combination load is able to lift a specified load a larger total vertical distance than the samples trained under a tip-force constraint. They also demonstrated that the highest load the sample is able to lift before work performance is compromised is higher for the combination load trained sample than the tip-force trained sample. These results support the concept of training a sample to exhibit TWSM under the constraint that induces distributed strain as opposed to the constraint inducing concentrated root strain as a viable means of increasing the work potential of these TWSM trained SMA specimens.

The specimen trained at a higher tip force of 4.8 N was used to explore the potential for increased tip displacement during transformation with using a higher magnitude of the same type of training constraint. Based on these experiments, it is easier to induce a tip force such that strain remains concentrated at the root on a cantilevered sample than to induce a load which distributes strain throughout the length of the specimen. If the work potential achieved by training under a larger tip-force constraint were to exceed that of a tip-moment or combination load trained sample, the tip force constraint method would remain the most effective and favorable out of the two constraint methods for TWSM training via constrained thermal cycling of deformed Martensite of these samples. The displacement test results of the 4.8 N tip-force trained specimen, when compared with that of the lower tip-force and the combination load trained specimens, indicated that a higher tip force can increase work potential of these specimens, but not enough to match that of the specimen trained under the tip-moment and tip-force combination load. Out of all three

training cases, the sample trained with the strain distributing constraint (0.3 N· m tip-moment + 1.4 N tip force) was able to produce the most work, suggesting that training these specimen (using the training structure used for these experiments) under a constraint that induces evenly distributed strain throughout the length of the specimen can be beneficial and may yield higher overall work performance than training under a tip force, where activated strain is concentrated at the root.

The aim of the research presented in this thesis was to compare the effect of the two constraint methods explored on work performance and to also compare the efficiency with which the two constraint methods allow a trained SMA specimen to perform work. A sample that utilizes strain throughout its entirety (as induced by a combination 0.3 N· m tip moment and 1.4 N tip-force load) to perform a specified amount of work during the TWSME is producing more work than a sample that performs the same amount of work by activating strain in only a small portion of its length during transformation (as induced by a 1.8 N or 4.8 N tip force).

The recoverable strain energy stored in the specimens trained in this study was analytically determined from the change in curvature along the length of the specimens during forward and reverse transformation. The specimen with the highest amount of recoverable strain energy was trained under the combination 0.3 N· m tip-moment and 1.4 N tip-force constraint. These results indicate that a specimen trained with a specified amount of strain (as induced by the combination load used) distributed throughout its entirety can perform work more efficiently than a specimen trained with the same amount of strain concentrated at its root (as induced by the 1.8 N tip-force load). The calculated values of both work performance under

various tip forces and recoverable strain energy with transformation from Martensite to Austenite for all three training cases can be compared in table 5.1.

Table 5.1: Sample work performance and recoverable strain energy as measured per the difference in area under curvature curves for Martensite and Austenite phase for all three training cases.

	1.8 N Tip-Force Trained	4.8 N Tip-Force Trained	0.3 N· m Tip-Moment + 1.4 N Tip-Force Trained
Work Performed Lifting 235 g Tip Mass	0.01 N· m	0.03 N· m	0.06 N· m
Work Performed Lifting 295 g Tip Mass	0.007 N· m	0.046 N· m	0.07 N· m
Work Performed Lifting 350 g Tip Mass	0.02 N· m	0.05 N· m	0.08 N· m
Recoverable Strain Energy	0.04	0.28	0.31

All the studies characterizing the change in performance between the samples trained using the two types of constraints explored demonstrate how training a SMA sample to activate strain throughout its entirety when exhibiting the TWSME may potentially allow the sample to produce more work more efficiently than a specimen trained to activate strained concentrated in one portion of the sample. The extensive training structure and loading protocol modifications made in order to achieve even strain distribution in a cantilevered specimen demonstrated that inducing a constant pure tip moment is not feasible. The training structure can be used as is, however, to successfully distribute strain throughout the length of a cantilevered specimen. It can also be used to induce a tip force. Overall, the experimentation validates the idea of training a specimen to activate strain everywhere as a potential means of increasing specimen work potential and efficiency.

5.3 Recommendations for Future Work

The current work revealed the value in investigating the training of SMA specimens to exhibit TWSM by activating strain distributed throughout their entirety. The experimental methods and setup used to conduct these experiments could be used as is to train more specimens under the different tip forces and tip moments to confirm the results supporting the proposed concept for increasing work potential. The current setup could also be used to train specimens under varying combinations of tip forces and tip moments to further explore effects training constraints on TWSM performance.

An investigation of varying sample dimensions to explore varying magnitudes of root strain during training and the impact it would have on work performance could provide valuable insight as to how to optimize specimen work performance. Also the impact of varying magnitude of a load within a specific category (i.e. tip force or tip moment) should be examined to determine if increasing load magnitude continually leads to increased work performance or if exceeding a certain load magnitude causes the sample's work performance as measured by vertical displacement during transformation to decrease due to secondary effects of TWSM training, such as creep.

Although the current training structure can be used to distribute strain throughout a cantilevered sample, it is still not capable of producing a pure tip moment as the sample deflects, as originally intended. Devising and implementing structural modifications that would allow for inducing a constant tip moment on a cantilevered specimen as it deflects would contribute a signifiant advance towards optimization of TWSM training under constrained thermal cycling of deformed Martensite. Potential methods of maintaining a constant tip moment by keeping the opposing force vectors on the tip pulleys parallel to each other as the sample deflects should be investigated.

Root strain was chosen as the platform for comparison of the efficacy of the different training constraints explored. Exploring different methods of comparison between the different constraint cases may assist in understanding the magnitude by which different constraint methods can improve work potential of a SMA TWSM trained specimen.

The number of thermal cycles chosen for these experiments proved to be enough to induce the TWSME effect. However, experimentation with varying the number of cycles used to perform TWSM training should be conducted. Studies of the effects of using a different number of thermal cycles in TWSM training can possibly identify the number of thermal cycles that yields an increase in work potential due to a reduction in hysteresis effects that degrade the TWSME.

As discussed in chapter 1, a variance in stress induced on a SMA specimen can lead to changes in transformation temperature. A study on varying hot and cold temperatures used for the thermal cycling portion of training can provide insight on how the use of a tip moment or tip force affects over all SMA sample behavior.

As discussed in chapter 3, heating of the specimens is not evenly distributed using strip heaters. Alternate heating methods could be explored in an effort to evenly heat the specimens during the training process. The effect of the use of strip heaters on the mechanical properties of the specimens used could also be explored.

Appendix A

Graphical Program Case Structures

Overview

This appendix contains images of the graphical code programs used to test various components of the training electrical system. It also contains images of the user interface and graphical code used to operate the automatic and autonomous training system.

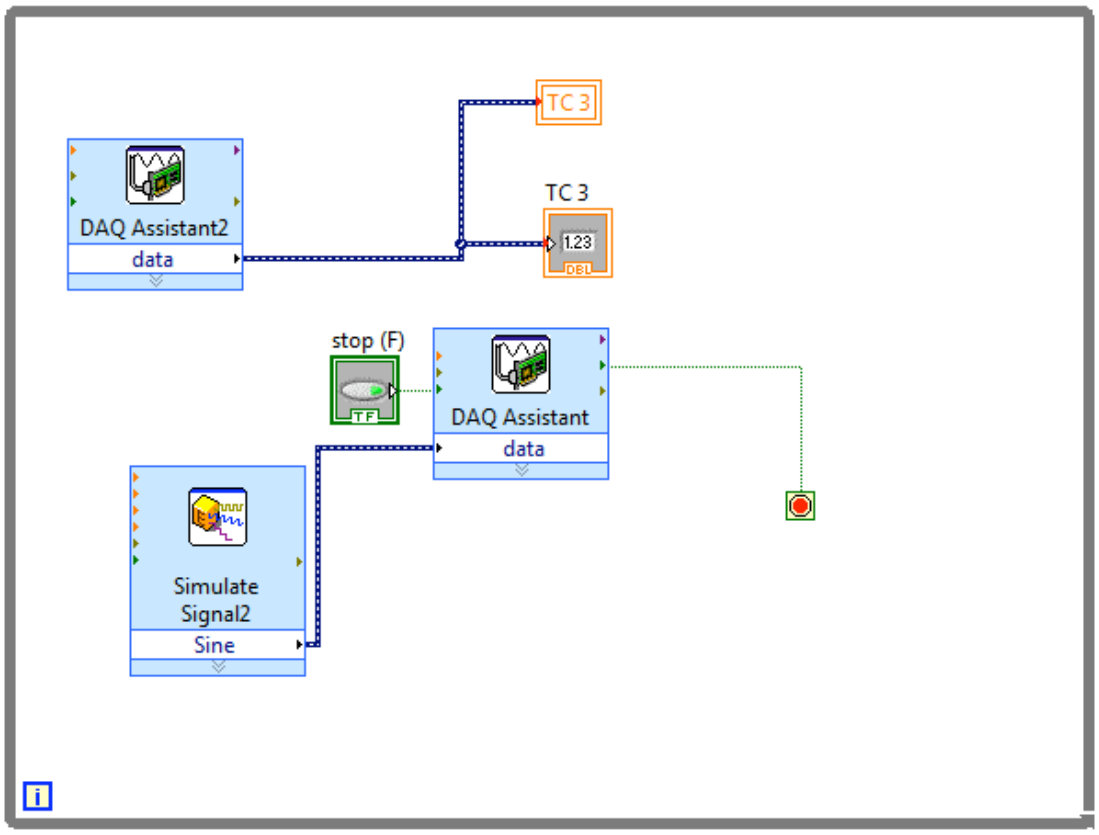

Figure A.1: Image of graphical code used to test and power strip heaters.

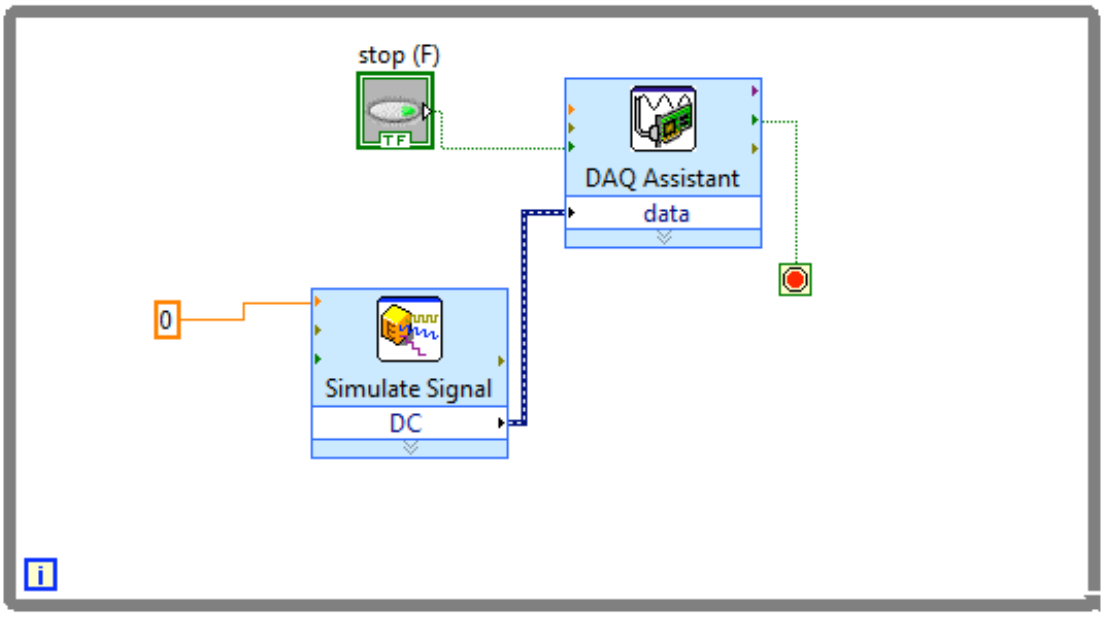

Figure A.2: Image of graphical code used to test and power relay circuit that controls the fan.

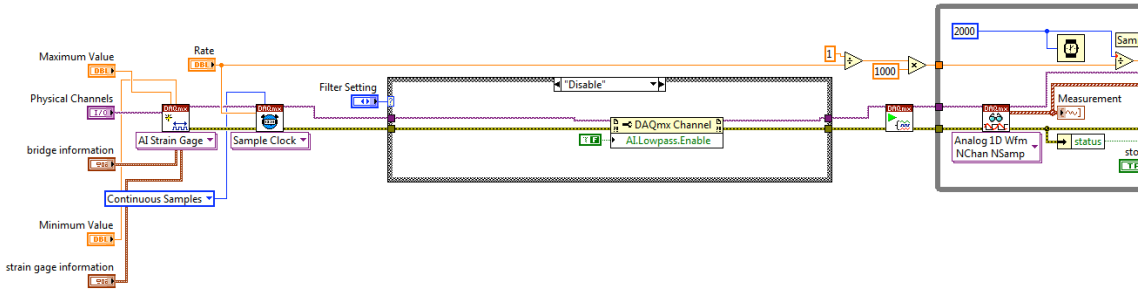

(a)

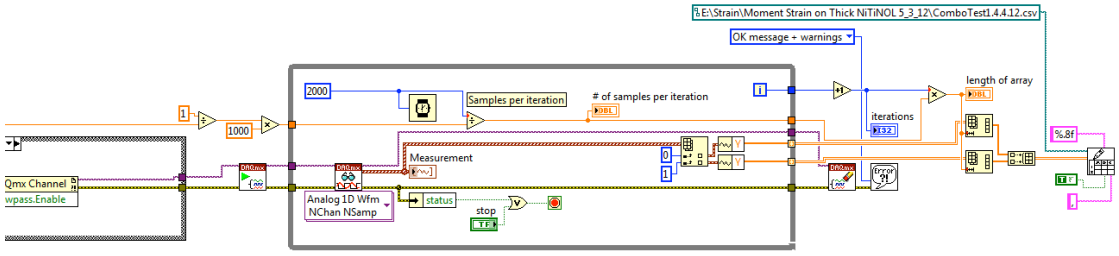

(b)

Figure A.3: Images of graphical code used for relaying strain from strain gauges. (a) Left side of graphical code. (b) Right side of graphical code.

The following figures contain images of graphical code used to autonomously train specimens with main cases displayed and sub-cases cycled.

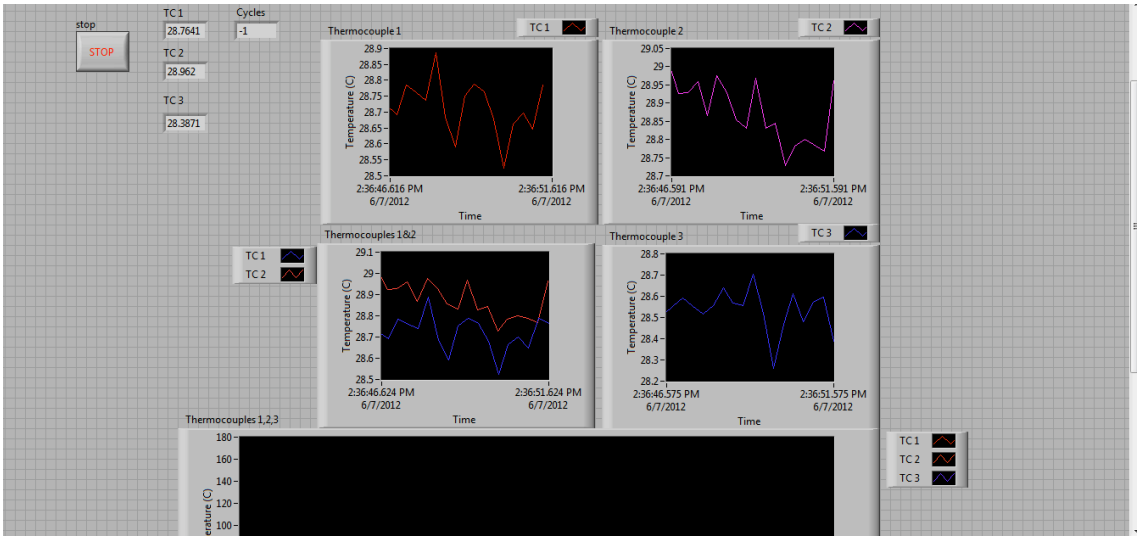

Figure A.4: Image of user interface of graphical program for operating TWSM training system..

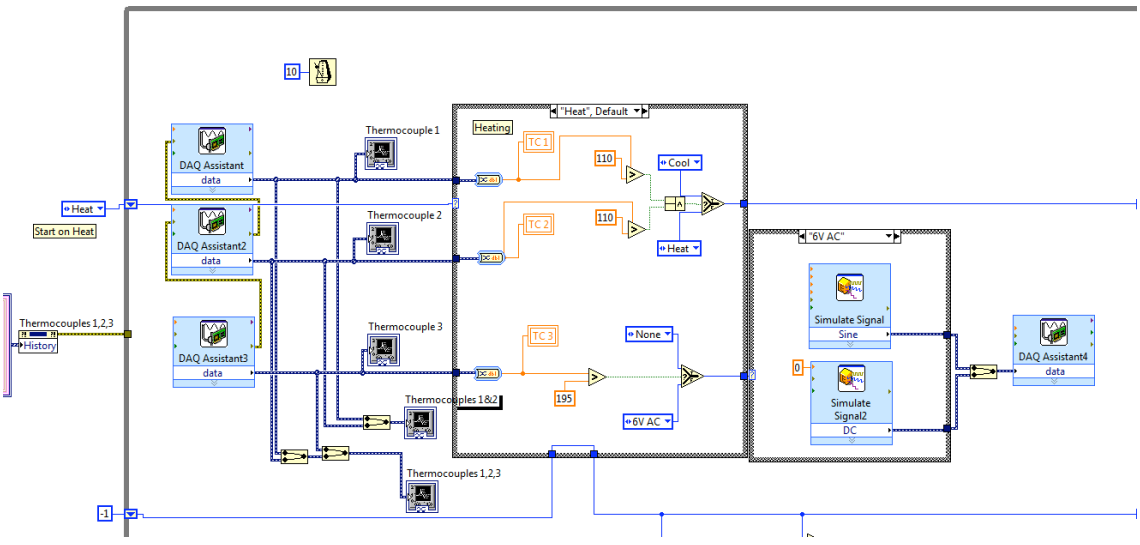

Figure A.5: Heat case structure with visible sub-case structure used to power strip heaters.

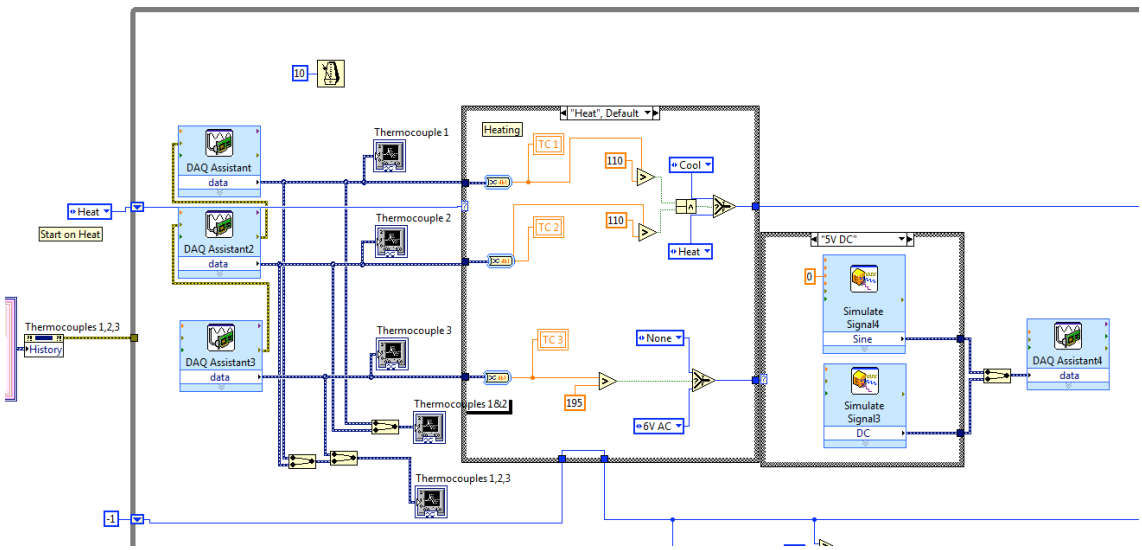

Figure A.6: Heat case structure with visible sub-case structure used to power relay system controlling fan.

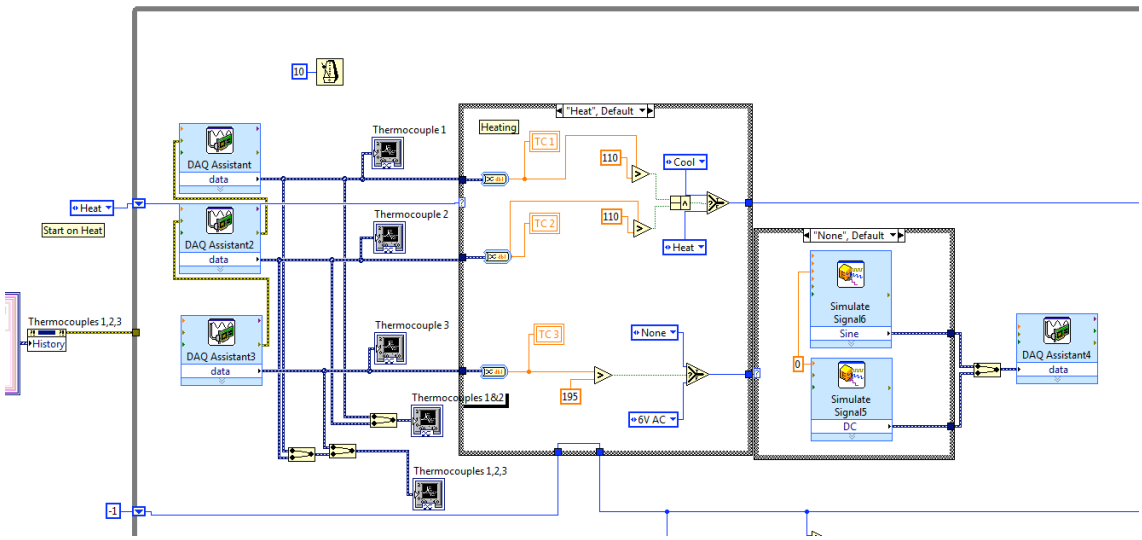

Figure A.7: Heat case structure with visible sub-case structure used to cut power to both relay system and strip heaters by sending 0V signal.

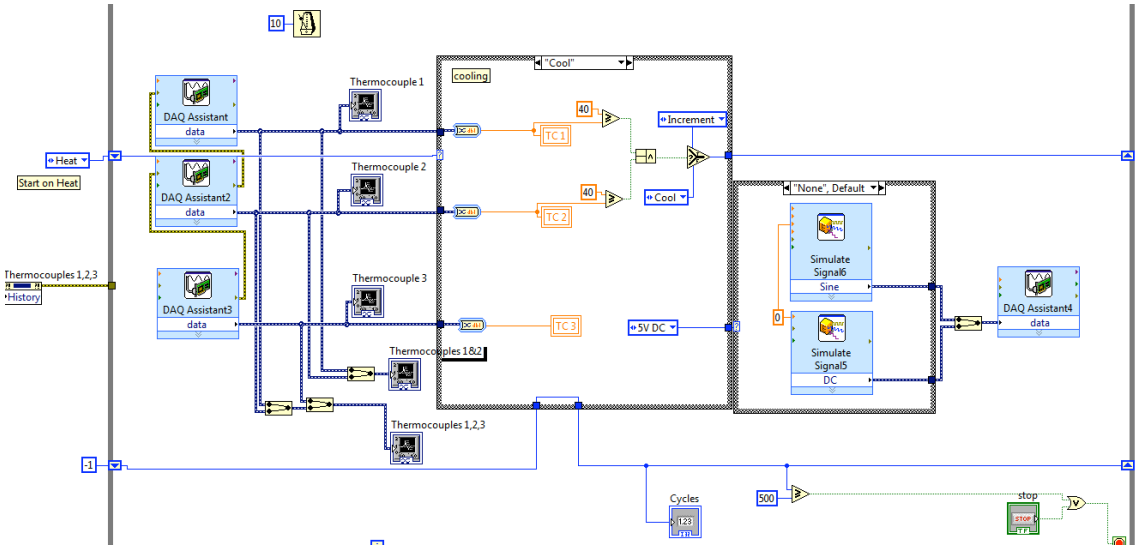

Figure A.8: Cool case structure with visible 0V sub-case structure.

Appendix B

Phase Transformation Vertical Displacement Data

Overview

This appendix contains the tables of the recorded vertical displacement values for all three trials conducted of work evaluation tests for each of the three training cases.

Table B.1: Vertical displacement data recorded during transformation for 1.8 N tip-force trained NiTiNOL specimen.

	Vertical Position, Martensite Phase			Vertical Position, Austenite Phase		
Tip Mass	Trial 1	Trial 2	Trial 3	Trial 1	Trial 2	Trial 3
0 g	-0.4	-0.7	-0.75	-0.2	-0.25	-0.25
70 g	-0.55	-0.75	-0.8	-0.2	-0.25	-0.25
120 g	-0.7	-0.85	-0.9	-0.25	-0.3	-0.3
165 g	-0.95	-1.05	-1.2	-0.3	-0.35	-0.35
235 g	-1.3	-1.2	-1.2	-0.4	-0.4	-0.45
295 g	-1.55	-1.4	-1.5	-0.5	-0.5	-0.55
350 g	-1.7	-1.7	-1.7	-0.55	-0.65	-0.6
385 g	-1.8	-1.8	-1.8	-0.65	-0.7	-0.65
420 g	-2.05	-2	-2	-0.7	-0.75	-0.7

Table B.2: Vertical displacement data recorded during transformation for 4.8 N tip-force trained NiTiNOL specimen.

	Vertical Position, Martensite Phase			Vertical Position, Austenite Phase		
Tip Mass	Trial 1	Trial 2	Trial 3	Trial 1	Trial 2	Trial 3
0 g	-5.75	-5.85	-5.9	-5	-5.15	-5.15
70 g	-5.75	-5.8	-5.8	-5.1	-5.1	-5.15
120 g	-5.8	-5.8	-5.8	-5.1	-5.15	-5.15
165 g	-5.85	-5.85	-5.9	-5.1	-5.2	-5.2
235 g	-5.9	-5.95	-6	-5.2	-5.2	-5.2
295 g	-5.95	-6	-6	-5.2	-5.2	-5.2
350 g	-6	-6.05	-6	-5.2	-5.2	-5.25
385 g	-6	-6.1	-6	-5.2	-5.3	-5.25
420 g	-6.1	-6.2	-6.1	-5.25	-5.3	-5.25

Table B.3: Vertical displacement data recorded during transformation for 0.3 N·m tip-moment plus 1.4 N tip-force trained NiTiNOL specimen.

	Vertical Position, Martensite Phase			Vertical Position, Austenite Phase		
Tip Mass	Trial 1	Trial 2	Trial 3	Trial 1	Trial 2	Trial 3
0 g	-4.5	-4.75	-4.75	-3.5	-3.6	-3.6
70 g	-4.5	-4.5	-4.5	-3.5	-3.6	-3.7
120 g	-4.5	-4.5	-4.5	-3.5	-3.6	-3.7
165 g	-4.5	-4.6	-4.6	-3.5	-3.6	-3.7
235 g	-4.5	-4.65	-4.7	-3.5	-3.7	-3.7
295 g	-4.6	-4.7	-4.7	-3.6	-3.7	-3.75
350 g	-4.7	-4.75	-4.7	-3.7	-3.75	-3.75
385 g	-4.7	-4.75	-4.75	-3.7	-3.75	-3.8
420 g	-4.8	-4.75	-4.8	-3.8	-3.8	-3.8

Table B.4: Averaged vertical displacement data recorded during transformation for all three cases.

	1.8 N Tip Force		4.8 N Tip Force		0.3 N· m tip-moment + 1.4 N Tip Force	
Tip Mass	Martensite	Austenite	Martensite	Austenite	Martensite	Austenite
0 g	-0.62	-0.23	-5.83	-5.1	-4.67	-3.57
70 g	-0.7	-0.23	-5.78	-5.12	-4.5	-3.6
120 g	-0.82	-0.28	-5.8	-5.13	-4.5	-3.6
165 g	-1.07	-0.33	-5.87	-5.17	-4.57	-3.6
235 g	-1.23	-0.42	-5.95	-5.2	-4.62	-3.63
295 g	-1.48	-0.52	-5.98	-5.2	-4.67	-3.68
350 g	-1.7	-0.6	-6.02	-5.22	-4.72	-3.73
385 g	-1.8	-0.67	-6.03	-5.25	-4.73	-3.75
420 g	-2.02	-0.72	-6.13	-5.27	-4.78	-3.8

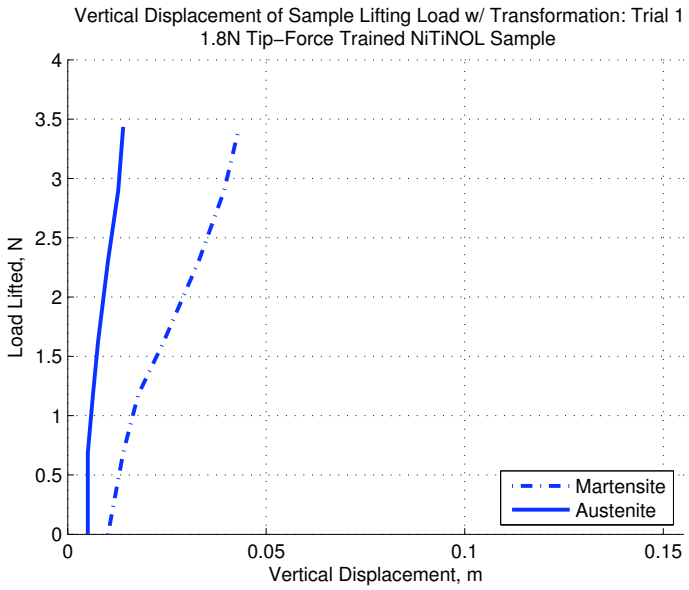

Figure B.1: Vertical displacement recorded during transformation trial 1 of 1.8 N tip-force trained specimen.

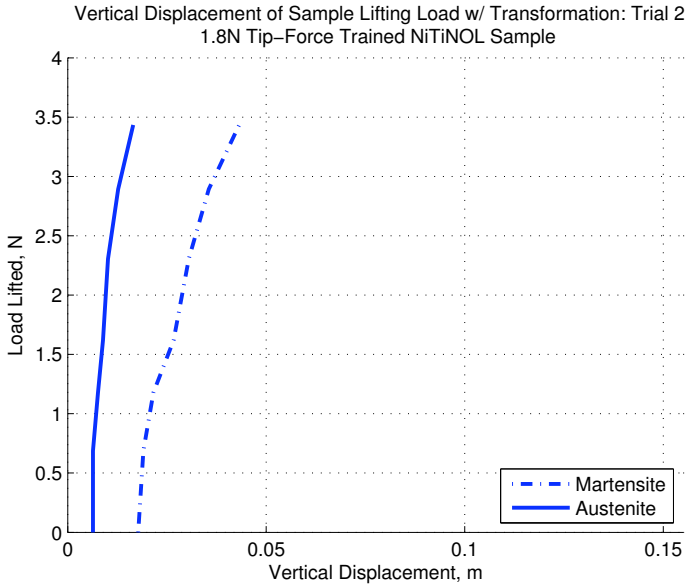

Figure B.2: Vertical displacement recorded during transformation trial 2 of 1.8 N tip-force trained specimen.

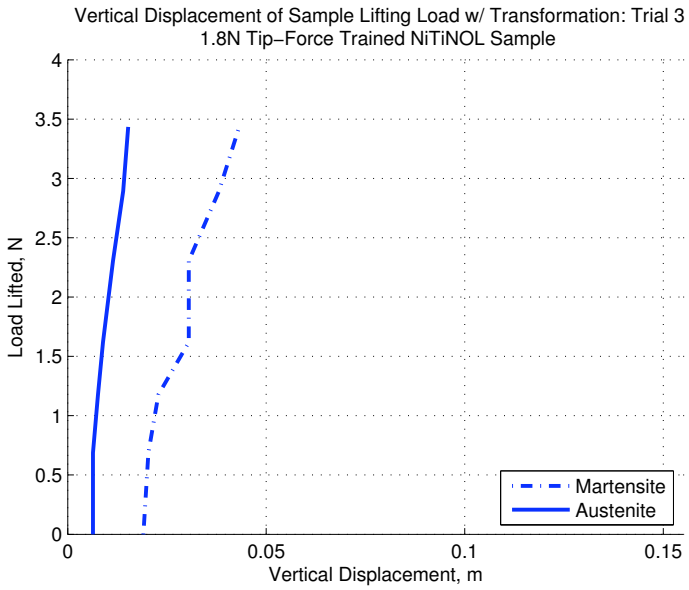

Figure B.3: Vertical displacement recorded during transformation trial 3 of 1.8 N tip-force trained specimen.

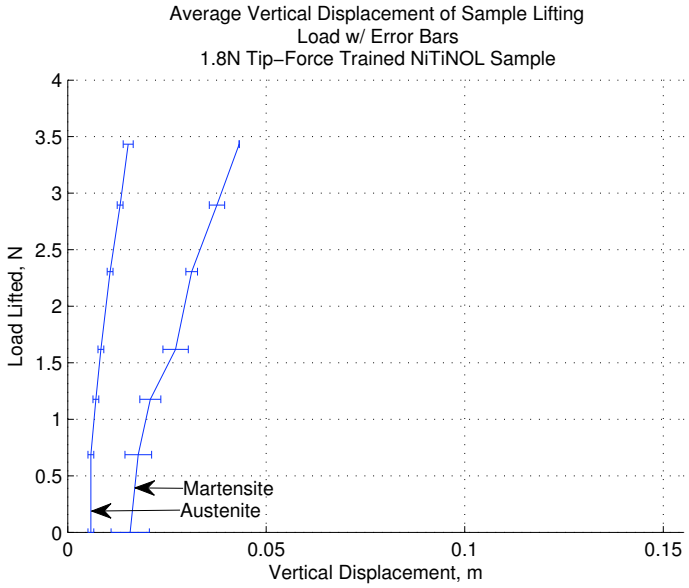

Figure B.4: Averaged vertical displacement recorded during transformation of 1.8 N tip-force trained specimen plotted with error bars.

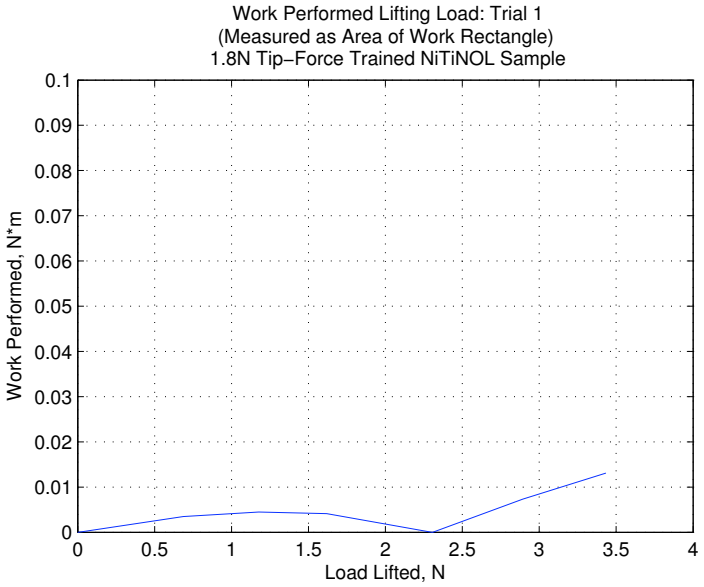

Figure B.5: Work performed calculated from vertical displacement recorded during transformation trial 1 of 1.8 N tip-force trained specimen.

Figure B.6: Work performed calculated from vertical displacement recorded during transformation trial 2 of 1.8 N tip-force trained specimen.

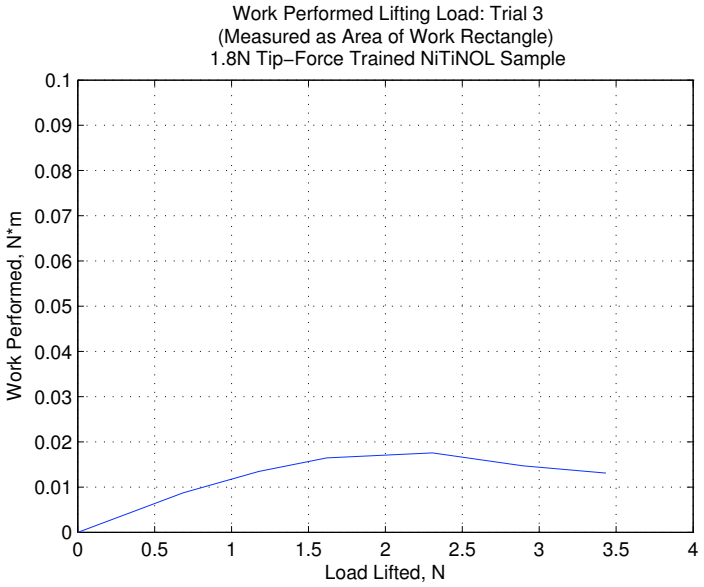

Figure B.7: Work performed calculated from vertical displacement recorded during transformation trial 3 of 1.8 N tip-force trained specimen.

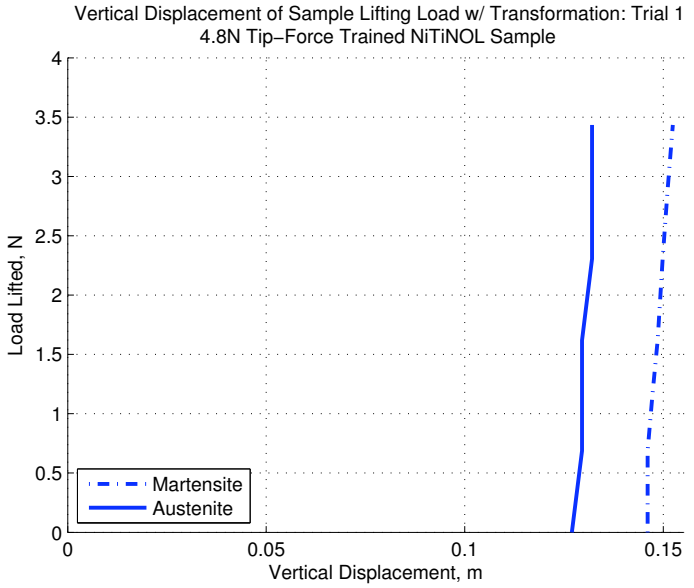

Figure B.8: Vertical displacement recorded during transformation trial 1 of 4.8 N tip-force trained specimen.

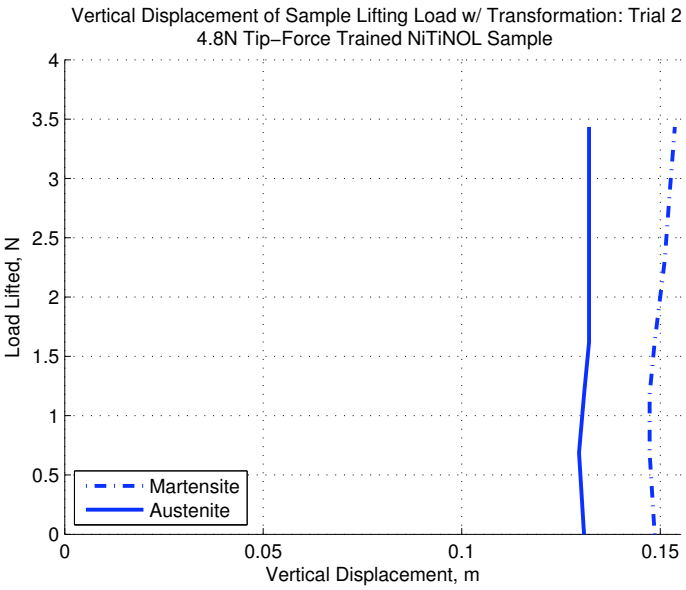

Figure B.9: Vertical displacement recorded during transformation trial 2 of 4.8 N tip-force trained specimen.

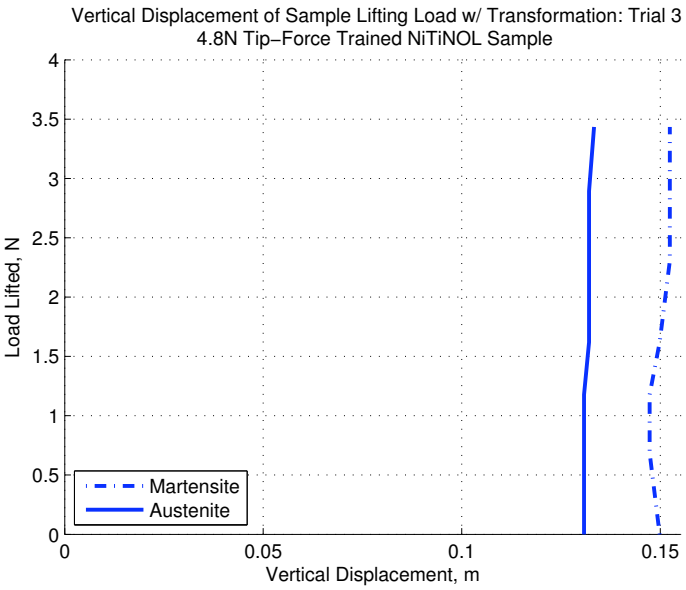

Figure B.10: Vertical displacement recorded during transformation trial 3 of 4.8 N tip-force trained specimen.

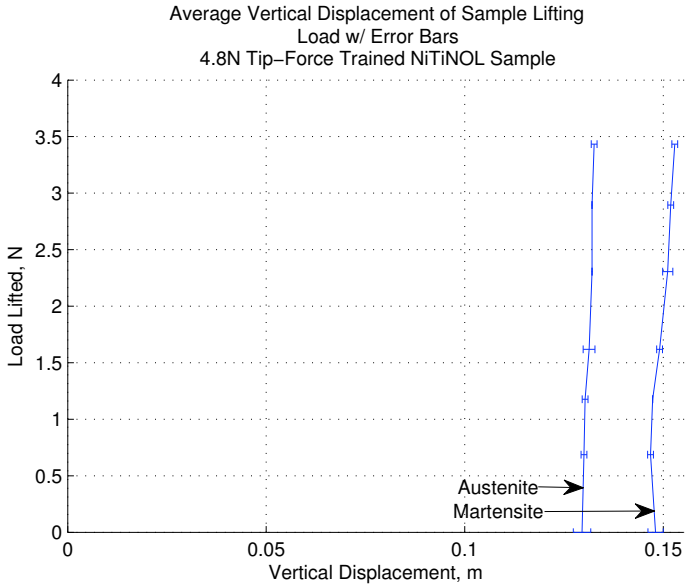

Figure B.11: Averaged vertical displacement recorded during transformation of 4.8 N tip-force trained specimen plotted with error bars.

Figure B.12: Work performed calculated from vertical displacement recorded during transformation trial 1 of 4.8 N tip-force trained specimen.

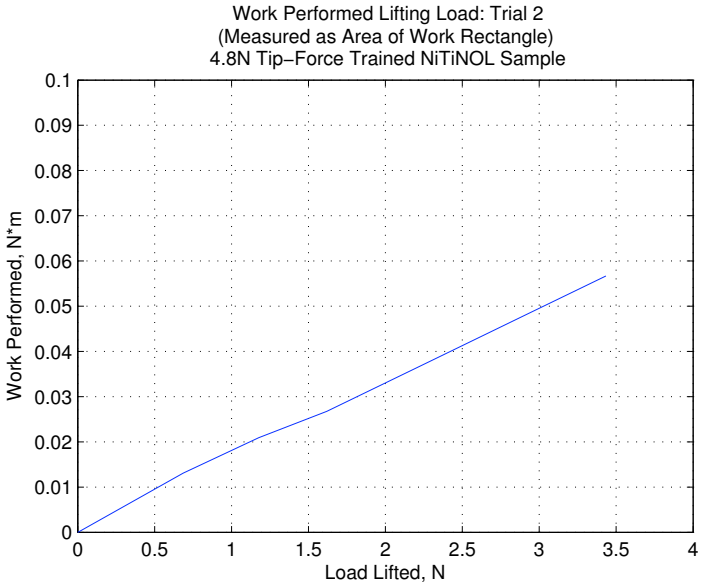

Figure B.13: Work performed calculated from vertical displacement recorded during transformation trial 2 of 4.8 N tip-force trained specimen.

Figure B.14: Work performed calculated from vertical displacement recorded during transformation trial 3 of 4.8 N tip-force trained specimen.

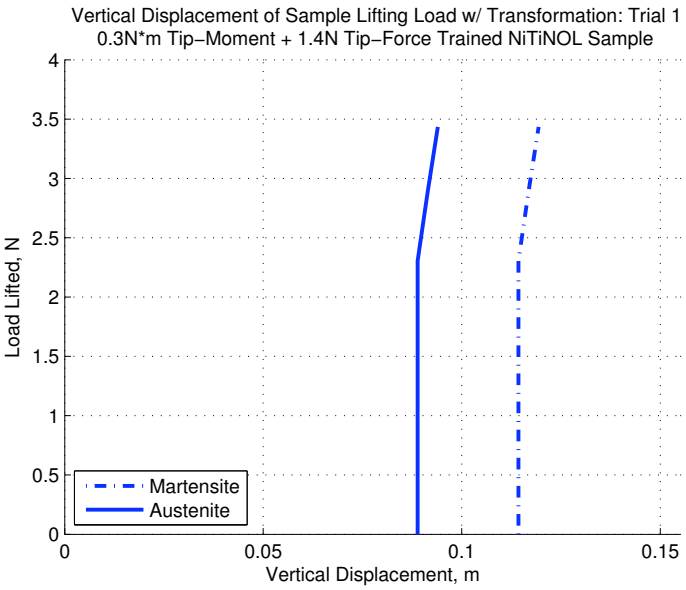

Figure B.15: Vertical displacement recorded during transformation trial 1 of 0.3 N· m tip-moment plus 1.4 N tip-force trained specimen.

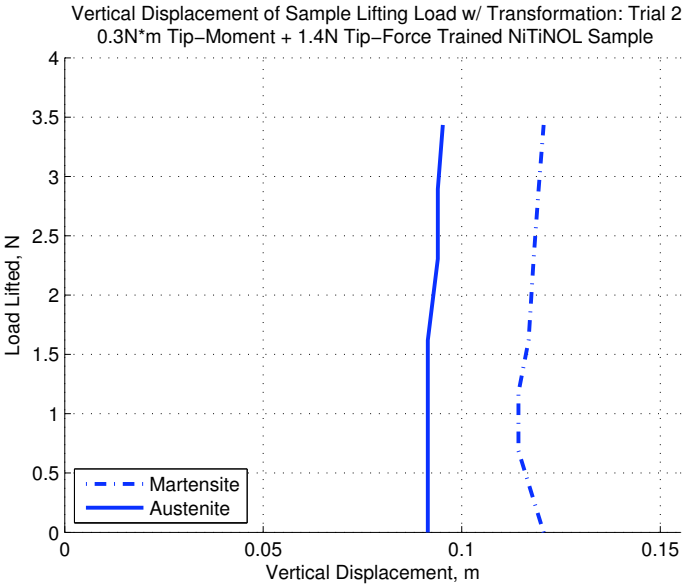

Figure B.16: Vertical displacement recorded during transformation trial 2 of 0.3 N· m tip-moment plus 1.4 N tip-force trained specimen.

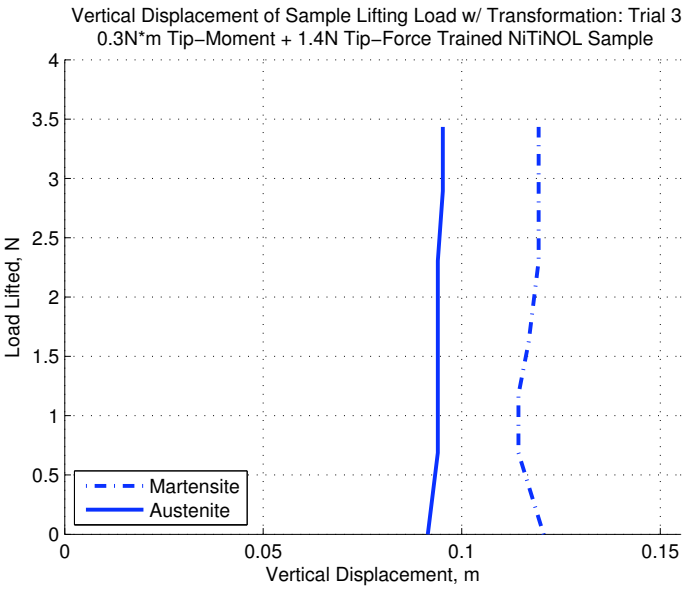

Figure B.17: Vertical displacement recorded during transformation trial 3 of 0.3 N· m tip-moment plus 1.4 N tip-force trained specimen.

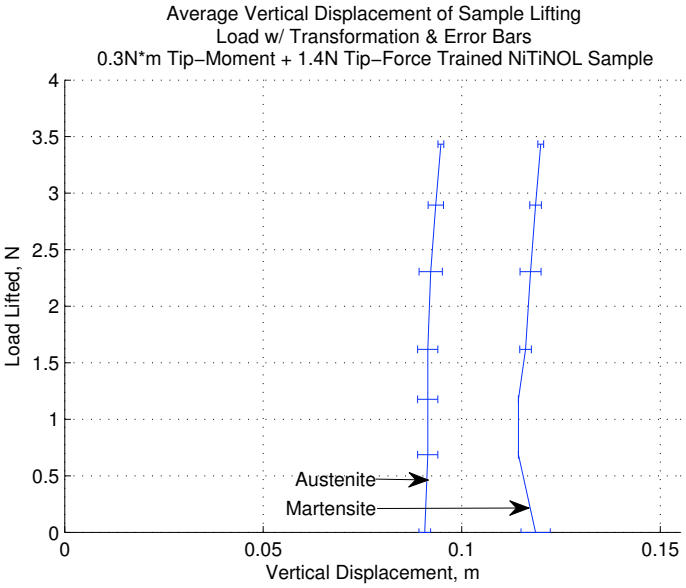

Figure B.18: Averaged vertical displacement recorded during transformation of 0.3 N· m tip-moment plus 1.4 N tip-force trained specimen plotted with error bars.

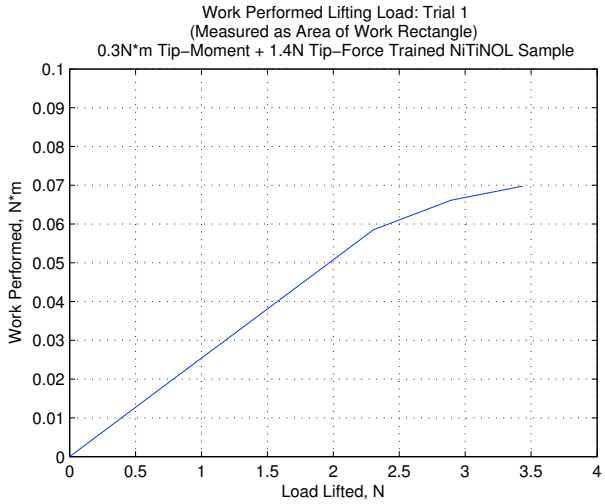

Figure B.19: Work performed calculated from vertical displacement recorded during transformation trial 1 of 0.3 N· m tip-moment plus 1.4 N tip-force trained specimen.

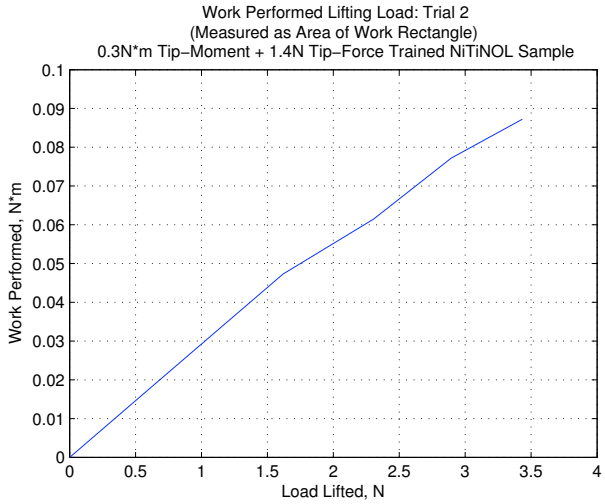

Figure B.20: Work performed calculated from vertical displacement recorded during transformation trial 2 of 0.3 N· m tip-moment plus 1.4 N tip-force trained specimen.

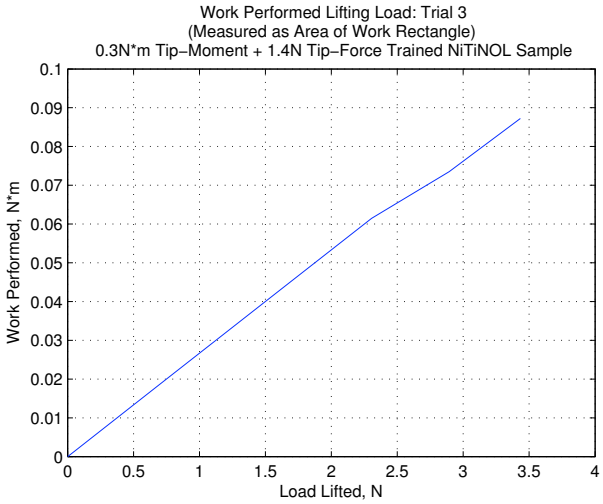

Figure B.21: Work performed calculated from vertical displacement recorded during transformation trial 3 of 0.3 N· m tip-moment plus 1.4 N tip-force trained specimen.

Appendix C

Modeling Sample Shape

Overview

This appendix contains the three modeled trained sample shapes in both the Austenite and Martensite phase used to calculate average curvature data for all three training cases.

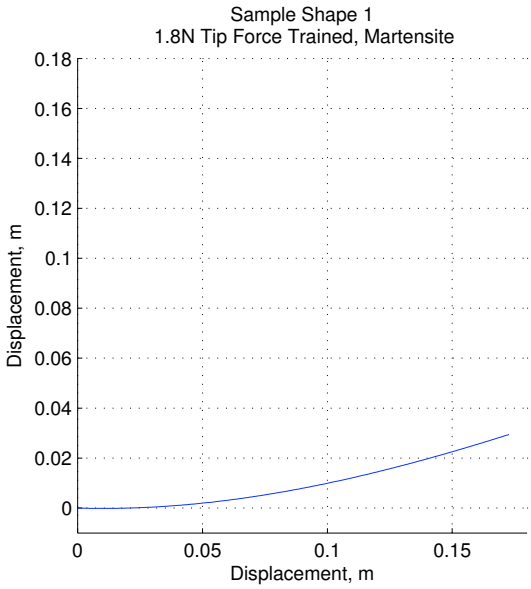

Figure C.1: Modeled Martensite sample shape 1 of 1.8 N tip-force trained specimen.

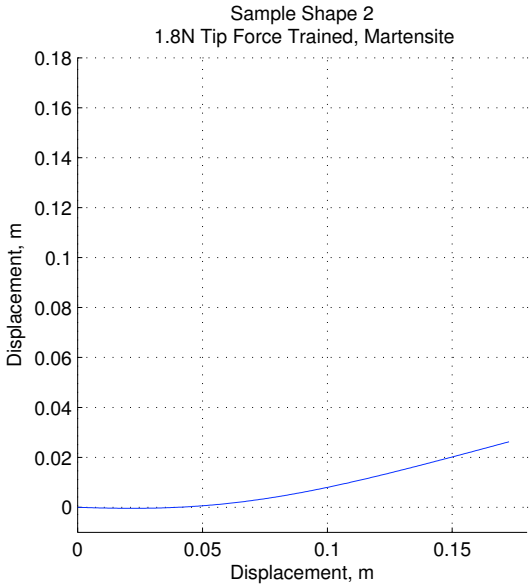

Figure C.2: Modeled Martensite sample shape 2 of 1.8 N tip-force trained specimen.

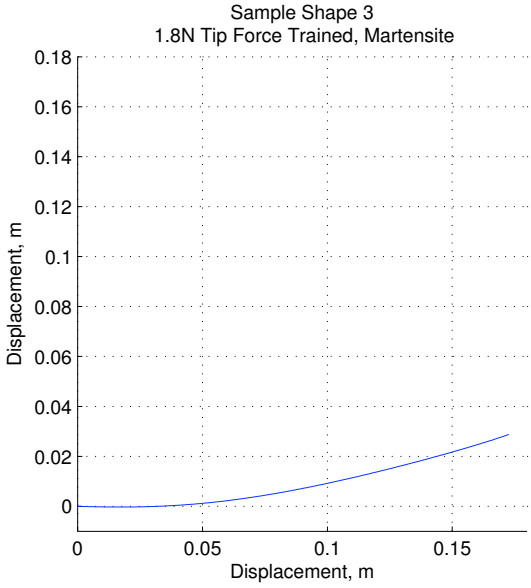

Figure C.3: Modeled Martensite sample shape 3 of 1.8 N tip-force trained specimen.

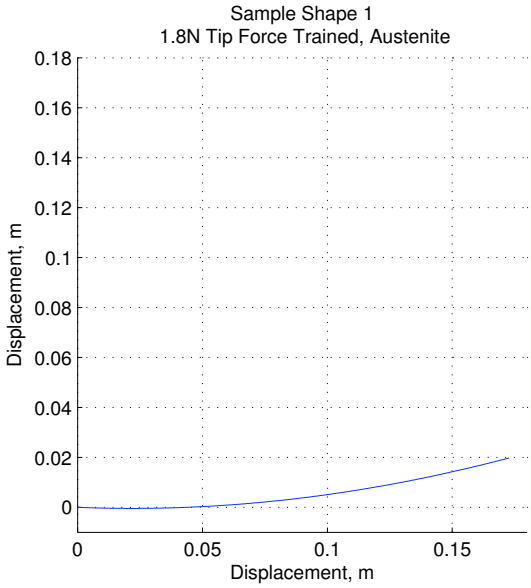

Figure C.4: Modeled Austenite sample shape 1 of 1.8 N tip-force trained specimen.

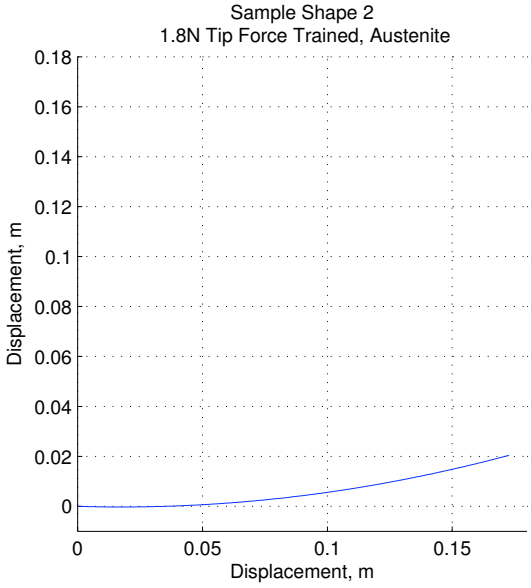

Figure C.5: Modeled Austenite sample shape 2 of 1.8 N tip-force trained specimen.

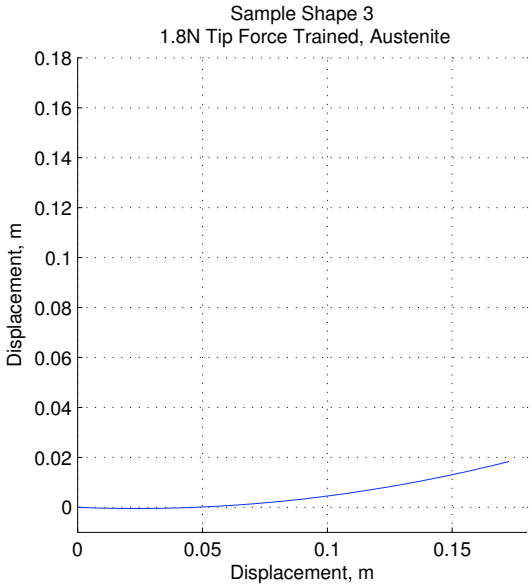

Figure C.6: Modeled Austenite sample shape 3 of 1.8 N tip-force trained specimen.

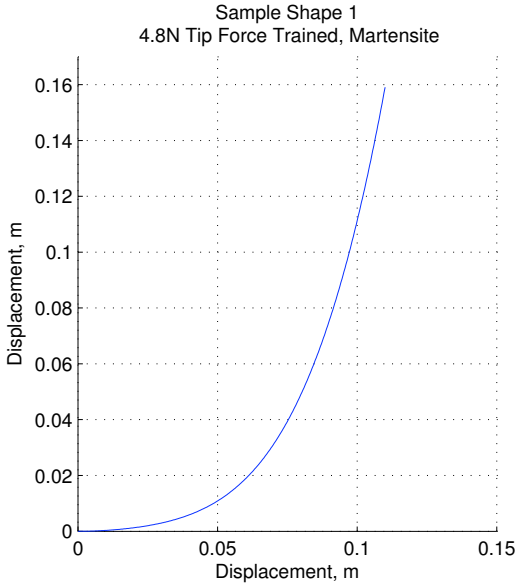

Figure C.7: Modeled Martensite sample shape 1 of 4.8 N tip-force trained specimen.

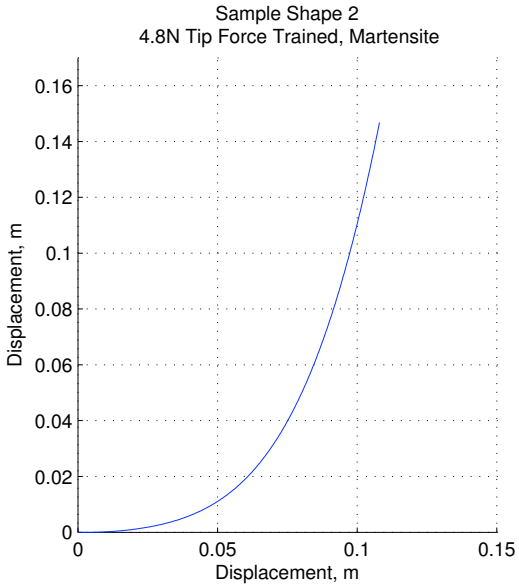

Figure C.8: Modeled Martensite sample shape 2 of 4.8 N tip-force trained specimen.

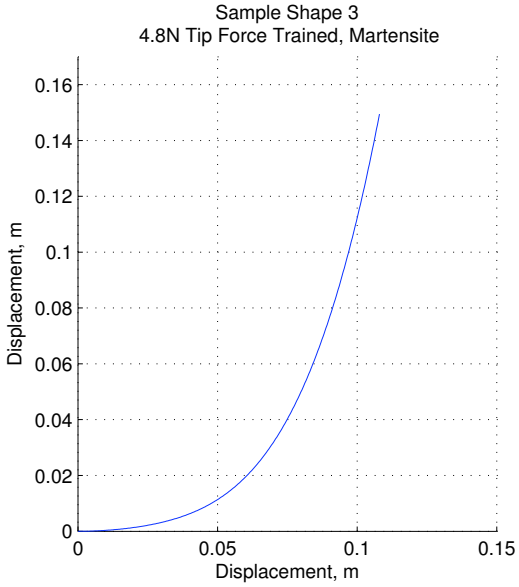

Figure C.9: Modeled Martensite sample shape 3 of 4.8 N tip-force trained specimen.

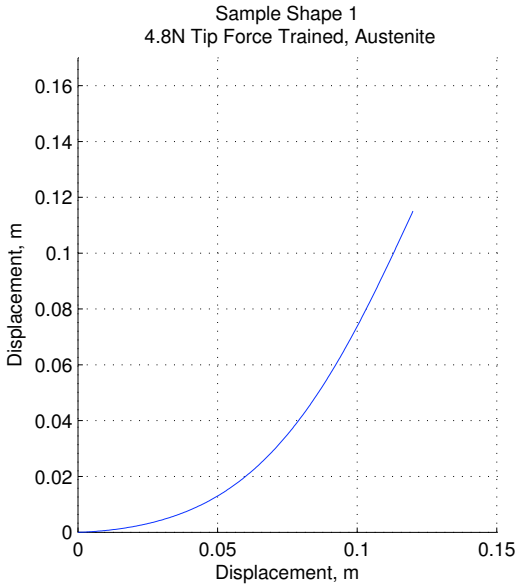

Figure C.10: Modeled Austenite sample shape 1 of 4.8 N tip-force trained specimen.

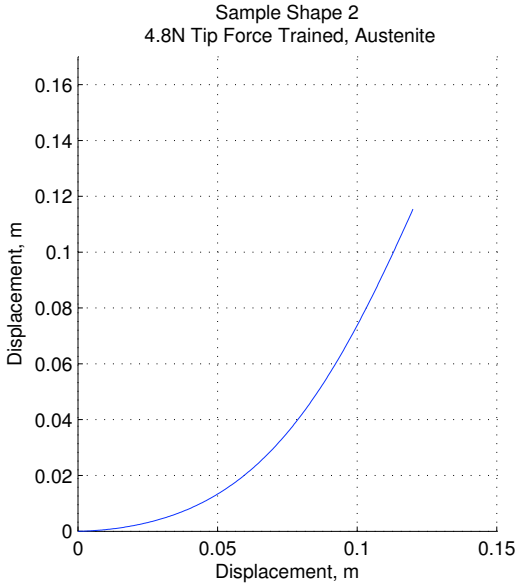

Figure C.11: Modeled Austenite sample shape 2 of 4.8 N tip-force trained specimen.

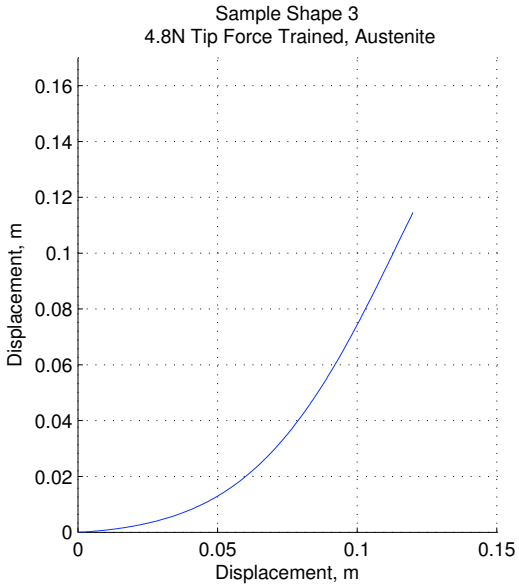

Figure C.12: Modeled Austenite sample shape 3 of 4.8 N tip-force trained specimen.

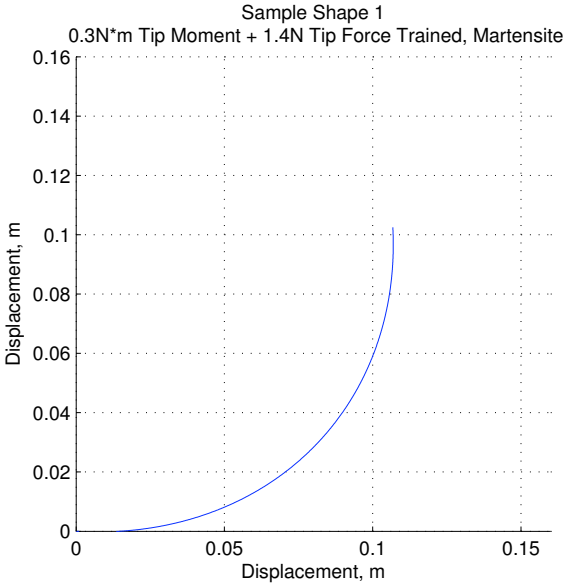

Figure C.13: Modeled Martensite sample shape 1 of 0.3 N· m tip-moment plus 1.4 N tip-force trained specimen.

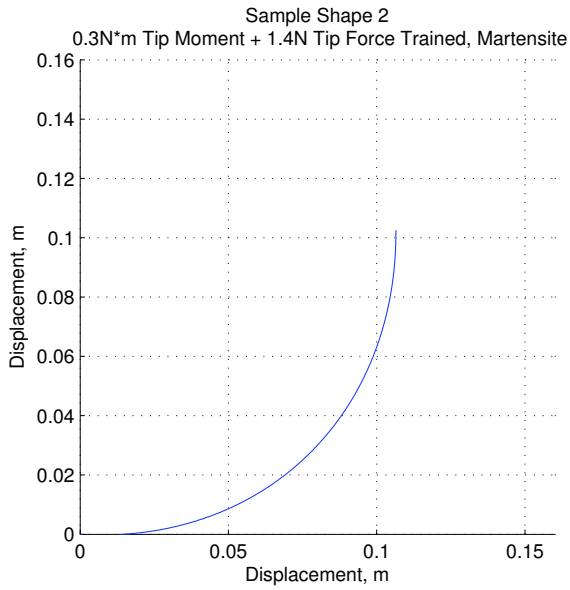

Figure C.14: Modeled Martensite sample shape 2 of 0.3 N· m tip-moment plus 1.4 N tip-force trained specimen.

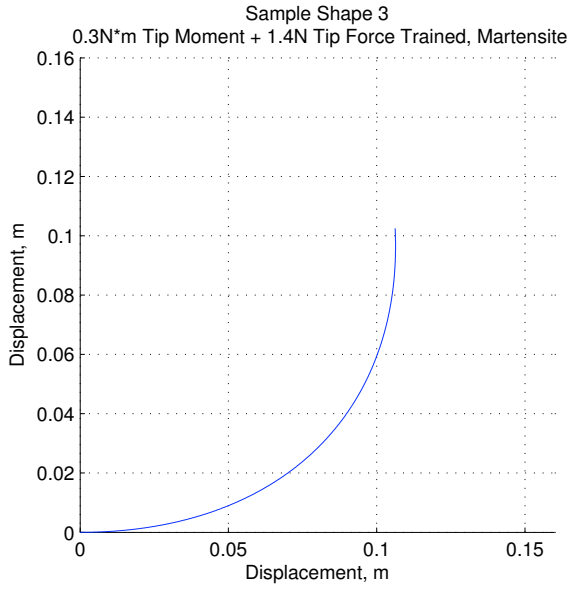

Figure C.15: Modeled Martensite sample shape 3 of 0.3 N· m tip-moment plus 1.4 N tip-force trained specimen.

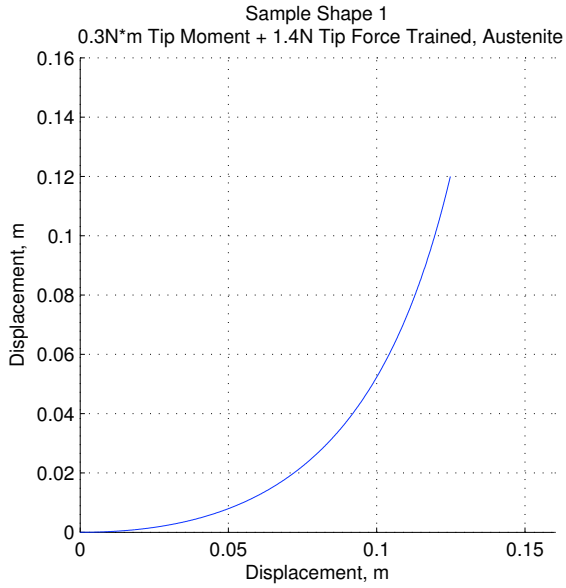

Figure C.16: Modeled Austenite sample shape 1 of 0.3 N· m tip-moment plus 1.4 N tip-force trained specimen.

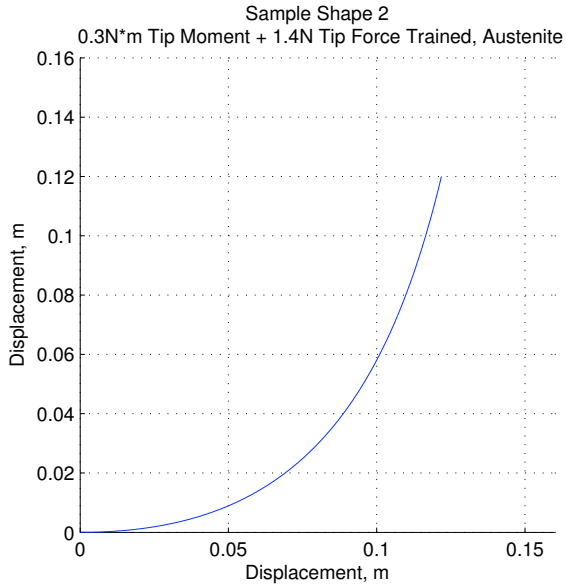

Figure C.17: Modeled Austenite sample shape 2 of 0.3 N· m tip-moment plus 1.4 N tip-force trained specimen.

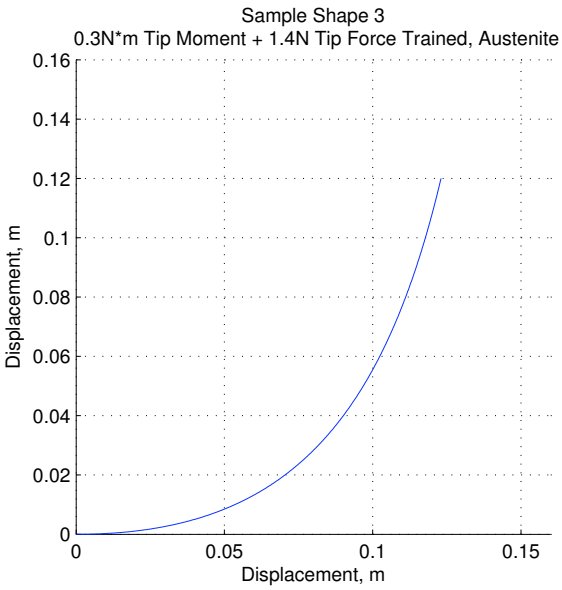

Figure C.18: Modeled Austenite sample shape 3 of 0.3 N· m tip-moment plus 1.4 N tip-force trained specimen.

Bibliography

[1] D. Hartl and D.C. Lagoudas. Aerospace applications of shape memory alloys. Technical report.

[2] E. Zanaboni. *One Way and Two WayShape Memory Effect: ThermoMechanical Characterization of NiTi wires*. PhD thesis, Universita degli Studi di Pavia, 2008.

[3] D.J. Hartl, P.K. Kumar, L.G. Machado, D.C. Lagoudas, B. Kiefer, P. Popov, P. Entchev, and M.A. Siddiq Quidwai. *Shape Memory Alloys: Modeling and Engineering Applications*. Springer Science + Business Media, Inc., 2008.

[4] J. Arghavani. *Thermo-mechanical behavior of shape memory alloys under multiaxial loadings: constitutive modeling and numerical implementation at small and*
nite strains. PhD thesis, Sharif University of Technology, 2010.

[5] T.L. Turner. Sma hybrid composites for dynamic response abatement applications. 2000.

[6] Ming H. Wu and L. McD. Schetky. Industrial applications for shape memory alloys. 2000.

[7] R.C. Hibbeler. *Mechanics of Materials*. 5th ed. Prentice Hall, 2003.

[8] Z.G. Wei, R. Sandstrom, and S. Miyazaki. Shape-memory materials and hybrid composites for smart systems part i shape-memorymaterials. *Journal of Materials Science*, 33:3743–3762, 1998.

[9] S. P. Mizar. *Thermomechanical characterization of NiTiNOL and NiTiNOL based structures using ACES methodology*. PhD thesis, Worcester Polytechnic Institute, 2005.

[10] A.J. Zak, M. P. Cartmell, W.M. Ostachowicz, and M. Wiercigroch. One-dimensional shape memory alloy models for use with reinforced composite structures. *Smart Materials and Structures*, 12:338–346, 2003.

[11] W.J. Buehler, J.V. Gilfrich, and R.C. Wiley. Effect of low-temperature phase change on the mechanical properties of alloys near composition tini. *Journal of Applied Physics*, 34:1475–1477, 1963.

[12] G. Song, N. Ma, and H.-N. Li. Applications of shape memory alloys in civil structures. *Engineering Structures*, 28:12661274, 2006.

[13] Stoeckel. Shape memory actuators for automotive applications. *Materials and Design*, 11(6):302–307, 1990.

[14] K. Otsuka and C.M. Wayman. *Shape Memory Materials*. 1. Cambridge University Press, 1998.

[15] T.J. Lim. *Behavior of a Ni-Ti Shape Memory Alloy Under Cyclic Proportional and Nonproportional Loading*. PhD thesis, Georgia Institute of Technology, 1999.

[16] D. Vokoun and V. Kafka. Mesomechanical modelling of shape memory effect.

[17] P.B. Entchev. *Micromechanical Modeling of Porous Shape Memory Alloys*. PhD thesis, Texas A&M University, 2002.

[18] M. Brocca, L.C. Brinson, and Z.P. Bazant. Three-dimensional constitutive model for shape memory alloys based on microplane model. *Journal of the Mechanics and Physics of Solids*, 50:1051 1077, 2002.

[19] A. Falvo. *Thermomechanical characterization of Nickel-Titanium Shape Memory Alloys*. PhD thesis, Universita Della Calabria.

[20] Y. Zheng, F. Jiang, L. Li, H. Yang, and Y. Liu. E?ect of ageing treatment on the transformation behaviour of ti50.9 at.

[21] Z. Wang, X. Zu, X. Feng, and J Dai. Effect of thermomechanical treatment on the two-way shape memory effect of niti alloy spring. *Materials Letters*, 54:55–61, 2002.

[22] H.J. Yu, Z.G. Wang, X.T. Zu, S.Z. Yang, and L.M. Wang. Temperature memory effect in two-way shape memory tini and tinicu springs. *Springer Science + Business Media, Inc.*, pages 1–5, 2006.

[23] J.M. McNaney, V. Imbeni, Y. Jung, P. Papadopoulos, and R.O. Ritchie. An experimental study of the superelastic effect in a shape-memory nitinol alloy under biaxial loading. *Mechanics of Materials*, 35:969986, 2003.

[24] Geogebra. *http://www.geogebra.org/*.

[25] J. Stewart. *Calculus: Early Transcendentals*. 4th ed. Brooks/Cole Publishing Company, 1999.